

***Alma Mater Studiorum – Università di Bologna***

DOTTORATO DI RICERCA IN  
**Biologia Cellulare e Molecolare**

Ciclo XXVIII

**Settore Concorsuale di afferenza: 05/E1  
Settore Scientifico disciplinare: BIO/10**

**RESPIRATORY CHAIN COMPLEXES AND SUPERCOMPLEXES  
ORGANIZATION IN CELLS WITH DEFECTIVE COMPLEX III**

Presentata da:

**Concetta Valentina Tropeano**

Coordinatore Dottorato  
**Prof. Giovanni Capranico**

Relatore  
**Prof.ssa Michela Rugolo**

Correlatore  
**Dott.ssa Anna Maria Ghelli**

Esame finale: **Bologna, Aprile 2016**

# Index

---

|  |           |
|--|-----------|
| <b>Abstract</b> .....  | <b>1</b>  |
| <b>Introduction</b> .....  | <b>3</b>  |
| 1.1 Mitochondria .....   | 3         |
| 1.1.1 Mitochondrial structure .....  | 4         |
| 1.1.2 Mitochondrial genome.....  | 5         |
| 1.1.2.1 <i>Replication, transcription and translation</i> .....                | 6         |
| 1.1.3 Mitochondrial genetics.....  | 7         |
| 1.2 The OXPHOS.....  | 8         |
| 1.2.1 The ATP synthase .....   | 10        |
| 1.3 The respiratory chain.....   | 11        |
| 1.3.1 Complex I.....   | 12        |
| 1.3.2 Complex II.....  | 17        |
| 1.3.3 Complex III.....   | 20        |
| 1.3.3.1 <i>Cytochrome b</i> .....  | 24        |
| 1.3.4 Complex IV .....   | 26        |
| 1.4 Reactive oxygen species production by respiratory complexes .....          | 30        |
| 1.5 The respiratory supercomplexes.....  | 33        |
| 1.5.1 Structural organization of SCs .....                                     | 34        |
| 1.5.2 Advantages of SCs organization.....                                      | 35        |
| 1.5.3 SCs assembly and their assembly factors .....                            | 36        |
| 1.6 Mitochondrial diseases .....   | 38        |
| 1.6.1 Mitochondrial diseases associated with CIII .....                        | 39        |
| 1.6.1.1 <i>Pathogenic mutations in cytochrome b</i> .....                      | 40        |
| <b>Aims</b> .....  | <b>43</b> |
| <b>Experimental Procedures</b> .....   | <b>45</b> |
| 3.1 Cell Lines and Culture Conditions .....                                    | 45        |
| 3.2 Heteroplasmy Evaluation .....  | 47        |
| 3.3 Mitochondria isolation from cybrid cells .....                             | 47        |
| 3.4 Cellular lysates .....   | 48        |
| 3.5 Solubilization of mitochondrial membranes.....                             | 48        |
| 3.6 Cell viability assay.....  | 48        |
| 3.7 Mitochondrial ATP synthesis.....   | 49        |
| 3.8 Citrate synthase activity.....   | 50        |
| 3.9 Respiratory complexes activities.....                                      | 50        |
| 3.10 Determination of GSH/GSSG content.....                                    | 50        |
| 3.11 Hydrogen peroxide production analysis.....                                | 51        |
| 3.12 SDS-PAGE.....   | 52        |
| 3.13 Respiratory complexes analysis by Blue Native- and Clear Native-PAGE..... | 52        |
| 3.14 Supercomplexes analysis by BN-PAGE.....                                   | 53        |
| 3.15 Complex I In-Gel activity.....  | 53        |
| 3.16 Two dimensional blue native/SDS-PAGE.....                                 | 53        |
| 3.17 Super-supercomplex band SDS-PAGE .....                                    | 53        |
| 3.18 Western Blotting.....   | 54        |
| 3.19 <i>In Vitro</i> mitochondrial translation assay .....                     | 55        |
| 3.20 <i>In silico</i> dynamic simulation for $\Delta$ I300-P305 mutation ..... | 55        |
| 3.21 Statistics.....   | 56        |

---

|   |           |
|---|-----------|
| <b>Results</b> .....  | <b>60</b> |
| 4.1 Viability of cybrids bearing the <i>MTCYB</i> mutations after metabolic stress .....                      | 62        |
| 4.2 Expression level of respiratory complex subunits .....  | 64        |
| 4.3 Molecular dynamic simulation of $\Delta I300$ -P305 mutation.....   | 65        |
| 4.4 Analysis of respiratory complexes assembly and activity.....  | 67        |
| 4.5 Analysis of the respiratory complexes supramolecular organization .....                                   | 69        |
| 4.6 Combined redox activities and ATP synthesis .....   | 72        |
| 4.7 Oxidative damage associated with p.278Y>C mutation.....   | 75        |
| 4.8 Hydrogen peroxide production and CII activation in cell bearing the $\Delta I300$ -P305<br>deletion ..... | 78        |
| 4.9 Phosphorylation of the SDHA subunit of CII.....   | 80        |
| 4.10 Effect of treatment of $\Delta I300$ -P305 cybrids with NAC.....   | 81        |
| <b>Discussion and Conclusions</b> .....   | <b>84</b> |
| <b>References</b> .....   | <b>91</b> |

# Abstract

---

Cytochrome *b* is the only subunit of complex III (CIII, ubiquinol:cytochrome *c* oxidoreductase) encoded by the mitochondrial DNA (mtDNA). Constituting the central core of CIII, this protein is essential for both assembly and catalytic activity of the complex. CIII is a dimer (CIII<sub>2</sub>) in its native form and can closely associate in varying proportions with complex I (CI) and complex IV (CIV) to form supramolecular structures, referred to as supercomplexes (SCs). Defects in CIII are relatively rare and mostly associated with mutations in the *MTCYB* gene encoding cytochrome *b*. *MTCYB* mutations can affect CIII only or both CI and CIII, likely as a consequence of the critical role of this latter complex on the stability of CI within the SCs.

In this study, we have investigated the effects of two pathogenic mutations affecting *MTCYB*: the p.278Y>C missense mutation, causing the substitution of the highly conserved Tyr<sup>278</sup> close to the Q<sub>o</sub> site, and the ΔI300-P305 microdeletion, producing the loss of six aminoacids in the sixth transmembrane helix, but leaving the remaining of the *MTCYB* coding region in frame. The biochemical analysis has been carried out taking advantage of a cell model specifically developed to investigate the mtDNA mutations, the cybrids, derived from fusion of enucleated patient's fibroblasts with 143B-osteosarcoma cells devoid of their own mtDNA. We were able to generate cybrids bearing each of the two pathogenic mutations in homoplasmic and heteroplasmic conditions. We have demonstrated that both homoplasmic *MTCYB* mutations severely impaired the activity of CIII: the missense mutation produced an oxidative damage of CIII due to increased superoxide production, whereas in cells bearing the ΔI300-P305 microdeletion, CIII was not detected, with consequent derangement also of CI. The detailed analysis of SCs organization revealed in both cases a strong perturbation of the CIII<sub>2</sub>+IV SC, together with an attempt to preserve the respirasome stability. Indeed, in p.278Y>C cells, the CI+III<sub>2</sub>+IV SC was slightly increased, whereas in ΔI300-P305 a minimal amount of the CI+III<sub>2</sub> SC was maintained despite the almost complete disassembly of CI and CIII. These results favor the hypothesis that SCs not only preserve the structure and stability of respiratory complexes, but become crucial for attenuating the mitochondrial dysfunction due to the occurrence of pathogenic mutations affecting the enzymes.

Moreover, in cells bearing the  $\Delta I300$ -P305 deletion, analysis of SCs also evidenced the presence of a high molecular weight SC, containing CI, CIII and CIV, mostly associated to heteroplasmic clones. This unusual high molecular weight SC, which was not detected in controls, might derive from the presence of both wild-type and mutant cytochrome *b* in the same cells, a situation similar to that occurring in many patient's tissues.

Finally, in cells with the homoplasmic  $\Delta I300$ -P305 deletion only, we described a marked increase in complex II (CII) redox activity, which was associated with significant hydrogen peroxide production. In addition, analysis by western blotting revealed that the band corresponding to SDHA-CII subunit only was positive to anti P-tyrosine antibody, suggesting the involvement of a tyrosine kinase-dependent mechanism in CII activation. Interestingly, prolonged treatment with the antioxidant N-acetylcysteine dampened both hydrogen peroxide production and CII activity stimulation, and caused the disappearance of the P-tyrosine positive band of SDHA subunit. It is noteworthy that CII activity was not detected in cells with the p.278Y>C missense mutation, despite the complete inhibition of CIII. Enhanced CII activity is a rather general phenomenon in cell adaptation to respiratory chain dysfunction, being detected also in CIII-deficient cells provided that hydrogen peroxide production is increased.

# Introduction

---

## 1.1 Mitochondria

Mitochondria are cytoplasmatic organelles present within eukaryotic cells. The number of mitochondria differs depending on the tissues energy request, such as skeletal muscle or kidney, which are tissues with a high energy requirement, have a larger number of mitochondria. They are the descendants of endosymbiotic  $\alpha$ -proteobacteria adapted to an increasingly oxygen-rich atmosphere that invaded progenitors of contemporary eukaryotes approximately 1.5–2 billion years ago [Margulis, 1970]. The organelles still maintain some characteristics of their ancestor bacteria, as, in particular, their own genome, the presence of a double membrane, the ability to synthesize adenosine triphosphate (ATP) and an independent protein synthesis apparatus.

Mitochondria are often referred as the “powerhouses” of the cells because of their main role in the cellular energy production, in the form of ATP, via the oxidative phosphorylation (OXPHOS) system. However, in addition to ATP generation, mitochondria are involved in other important pathways, such as the Krebs cycle, fatty acid oxidation, and metabolism of amino acid and hormones [Shadel and Horvath, 2015]. Moreover, they play a critical role in generation of cellular signals, such as reactive oxygen species (ROS) [Dan Dunn *et al.*, 2015], control of cytosolic calcium ( $\text{Ca}^{2+}$ ) concentration [Finkel *et al.*, 2015], modulation of oxidation–reduction (redox) status through the assembly of iron-sulfur clusters [Stehling *et al.*, 2014], apoptosis [Lopez and Tait, 2015] and innate immunity [Weinberg *et al.*, 2015].

Mitochondria were described for the first time in 1890 by Richard Altmann. He called them “bioblasts” [ $\beta\iota\acute{o}\varsigma$  (bios), life;  $\beta\lambda\alpha\sigma\tau\acute{o}\varsigma$  (blastos), germ] to indicate that these cytoplasmic ubiquitous structures existing in the cells were “elementary organisms” carrying out vital functions and resembling bacteria [Altmann, 1980]. The term mitochondrion [from the Greek  $\mu\iota\tau\omicron\varsigma$  (mitos), thread and  $\chi\omicron\nu\delta\rho\iota\omicron\nu$  (kondrion), granule] was coined by Carl Benda in 1898, referring to the structure appearance of the organelle [Benda, 1898].

### 1.1.1 Mitochondrial structure

Mitochondria are about 0.5–1  $\mu\text{m}$  in diameter and up to 7  $\mu\text{m}$  long organelles. They are separated from the cytoplasm by the outer and the inner membrane, which are different in appearance and in physicochemical properties. The two membranes are characterized by different phospholipid compositions and protein-to-lipids ratio, 50:50 for the outer membrane and 80:20 for the inner membrane. The outer membrane is porous and freely permeable to ions and small, uncharged molecules through the pore-forming membrane proteins porins. The larger molecules, such as proteins, are imported in by translocases. On the other hand, the inner membrane cannot be freely traversed, thus ions and larger molecules can cross this membrane through specific membrane transport proteins or carriers, which are highly selective. In particular, the proton selectivity of the inner membrane causes the formation of a proton electrochemical potential ( $\Delta\mu_{\text{H}^+}$ ), where the electrical component ( $\Delta\psi_{\text{m}}$ ), negative inside, is about 180 mV. The presence of the inner and outer membranes creates four compartments within the mitochondrion. The first one is the mitochondrial matrix, enclosed by the inner membrane. The matrix has a high pH ( $\sim 7.9\text{-}8$ ), due to the  $\Delta\mu_{\text{H}^+}$ , and is the site of organellar DNA replication, transcription, protein biosynthesis and numerous enzymatic reactions. Between the matrix and the intra-membrane space, the inner membrane is located. It contains several carrier proteins shuttling ions, ATP, ADP and small metabolites between the cytoplasm and the matrix. Actually, the inner membrane can be divided into two sub-compartments: the inner boundary membrane, facing the outer membrane, and the cristae membrane. Cristae are formed by inner membrane invaginations into the matrix, greatly increasing the surface of the inner membrane compared to the outer membrane. Cristae are continuous with the inner boundary membrane through the crista junctions, whose components only start to be known, which are also connected with the outer membrane [Harner *et al.*, 2011]. Cristae contain most of the complexes of the electron transport chain and the ATP synthase, thus becoming the main site of energy production (Figure 1.1) [Kühlbrandt, 2015].

Initially, mitochondria were believed to be single static entities. Today, it is well known mitochondria form a highly dynamic network which continuously moves and fuses, undergoing membrane remodeling through cycles of fusion (two mitochondria joining to form a single mitochondrion) and fission (a single mitochondrion dividing into two fragments) [Lackner, 2014]. The balance between fusion and fission controls the

mitochondrial structure, shifting the numerous separate mitochondria in single or interconnected membranous structures [Mishra and Chan, 2014].

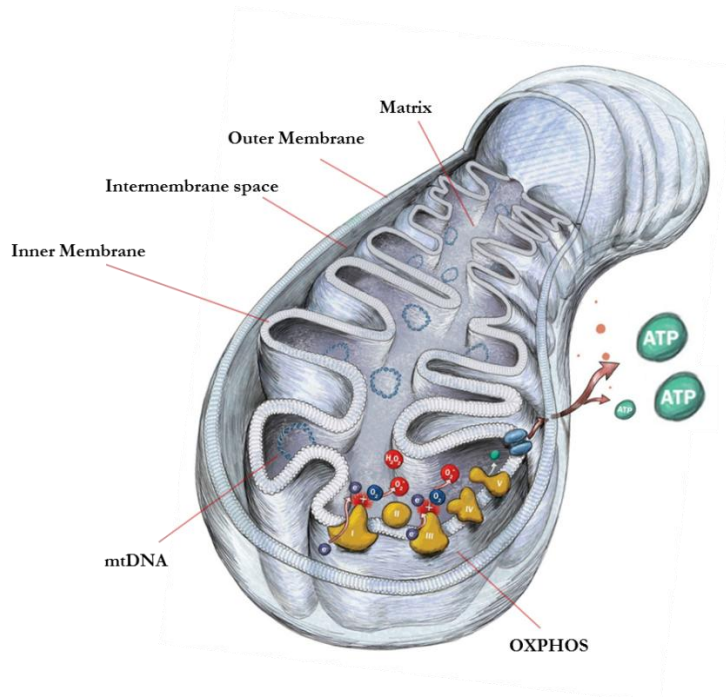


**Figure 1.1** A schematic picture of a mitochondrion. The red lines indicate the mitochondrial membranes and compartments. The mtDNA and the OXPHOS complexes in the inner membrane are also indicated.

### 1.1.2 Mitochondrial genome

As result of bacteria endosymbiosis, mitochondria have their own genome. In humans mitochondrial DNA (mtDNA) is a circular double-stranded molecule long approximately 16.569 base pairs. The two strands are referred to as the heavy strand (H-strand, rich in guanine) and the light strand (L-strand, rich in cytosine). The mtDNA is highly compact, indeed, there are no introns or intergenic noncoding sequences, with the exception of the 1.1 kb displacement loop (D-loop), forming a triple-stranded structure, and a 30 nucleotides sequence containing the origin of replication for the L-strand (OriL). D-loop contains one transcription promoter for each strand (light strand promoter, LSP; heavy strand promoter, HSP) and the origin of replication for the H-strand (OriH). Furthermore, mitochondrial genome has some of the coding regions overlapping each other (Figure 1.2) [Anderson *et al.*, 1981; Uhler and Falkenberg, 2015]. MtDNA is organized into DNA-protein complexes called nucleoids, which are believed to be associated with the inner mitochondria membrane, exchanged between mitochondria. Each nucleoid was shown to frequently contain only a single copy of mtDNA, packed with



ligase [Ferreira *et al.*, 2015]. The replication mechanism is still debated, three different models have been proposed: (i) in the asynchronous mechanism, the replication starts at the origin of the H-strand, proceeds around two-thirds of the mitochondrial genome, until the L-strand origin is exposed, initiating the replication in the opposite direction [Clayton, 1982]; (ii) in the strand-coupled model, the replication of H-strand and L-strand starts simultaneously [Holt *et al.*, 2000]; (iii) in the RITOLS model (RNA Incorporated Through Out the Lagging Strand), the replication proceeds unidirectionally from the D-loop region, with RNA replication intermediates which are subsequently matured into DNA [McKinney and Oliveira, 2013; Yasukawa *et al.*, 2006].

The transcription of mitochondrial genes starts from promoters on both H-strand (HSP1 and HSP2) and L-strand (LSP). It requires the mitochondrial RNA polymerase (POLRMT), the TFAM and the mitochondrial transcription factor B1 or B2. The termination of mature transcripts is carried out by mitochondrial termination factor 1 (MTERF1). The mitochondrial transcription generates polycistronic transcripts, which produce, after processing, individual mRNA, rRNA and tRNA molecules [Ferreira *et al.*, 2015].

The translation of mitochondrial proteins is still an unclear process. The mitochondrial protein synthesis machinery is independent from the cytosolic ribosome and takes place within the matrix. The mito-ribosomes (the mitochondrial ribosome) are assembled by the two mitochondrial rRNAs and nuclear encoded proteins. Translation requires the two mitochondrial initiation factors, mtIF1 and mtIF3, this later causing the dissociation of the mitoribosomes and consequently the assembly of the initiation complex. Then, mRNA is bound the small subunit, aligning the start codon to the peptidyl site of the mito-ribosome. Peptide elongation is controlled by a number of nuclear-encoded genes, including mitochondrial elongation factor Tu (mtEFTu), which binds the tRNA to the mito-ribosome and mitochondrial elongation factor G1 (mtEFG1), required to move the newly added amino acid along one position and allowing amino acid inclusion. Translation termination is carried out solely by mitochondrial release factor 1a (mtRF1a), which recognizes the stop codons (UAA and UAG) and triggers hydrolysis of the bond between the terminal tRNA and the nascent peptide [Chinnery and Hudson, 2013].

### 1.1.3 Mitochondrial genetics

Mitochondrial genetics is deeply different from the Mendelian genetics at least in four main aspects. First, mtDNA is exclusively inherited through the maternal lineage.

After fertilization of the oocyte, sperm mtDNA is ubiquitinated and consequently removed. Therefore, the mtDNA content of the zygote is determined exclusively by the previously unfertilized egg. The lack of paternal inheritance is still debated, three mechanisms are suggested: (i) a dilution effect (sperm contain only 100 copies of mtDNA, compared with 100 000 in the unfertilized egg), (ii) selective ubiquitination of paternal mtDNA or (iii) the “mtDNA bottleneck” excludes the “minor” paternal alleles [Sutovsky, 2003]. Second, the genome of the organelle has a genetic code which is different from the nuclear code; for instance, unlike the nuclear genetic code, “UGA” is not a stop codon but it encodes tryptophan or “AUA” encodes methionine and not isoleucine [Tuppen *et al.*, 2010]. Third, mitochondrial genome is polyploid with multiple copies of mtDNA per mitochondrion (2-10 copies) and 1000–10.000 copies within cells. This latter feature gives rise to the concept of heteroplasmy and homoplasmy of mtDNA. Heteroplasmy is referred to the situation where different mitochondrial genotypes coexist within the same cell, tissue or organism, whereas homoplasmy is referred to the situation where all copies of mtDNA are identical [Keogh and Chinnery, 2015]. Finally, mtDNA follows mitotic segregation, indeed during mitosis, mitochondria are randomly segregated, and in heteroplasmic cells, the proportion of mutant mtDNA in the daughter cells can thus shift, causing accumulation or loss of one of the mtDNA copies [Park and Larsson, 2011].

## 1.2 The OXPHOS

Mitochondria are referred as “the powerhouses” of the cell because of their role in energy production, in the form of ATP, through the metabolic process known as OXPHOS. The ATP production is fueled by metabolites derived from glycolysis,  $\beta$ -oxidation and Krebs cycle. Briefly, pyruvate, derived from glucose via glycolysis, is transported into mitochondria and metabolized by the pyruvate dehydrogenase complex resulting in acetyl-CoA. Fatty acids are activated to acyl-CoAs which are transferred into mitochondria and oxidized by  $\beta$ -oxidation to acetyl-CoA. Acetyl-CoA then enters the Krebs cycle where it is oxidized generating  $\text{CO}_2$ , succinate and reduced coenzymes such as NADH and  $\text{FADH}_2$ . Reducing equivalents are produced also during glycolysis and  $\beta$ -oxidation [Lenaz and Genova, 2010; Szalárdy *et al.*, 2015; Wallace and Fan, 2010].

NADH and  $\text{FADH}_2$  act as electron donors to the complexes of the respiratory chain embedded within the inner mitochondrial membrane. NADH provides electrons to complex I (CI, NADH:ubiquinone oxidoreductase),  $\text{FADH}_2$  to complex II (CII,

succinate:ubiquinone oxidoreductase). The electrons are then transported to complex III (CIII, ubiquinol:cytochrome  $c$  oxidoreductase) via the lipophilic mobile redox-active molecule coenzyme Q (ubiquinone; CoQ; quinone) and flow through cytochrome  $c$  to complex IV (CIV, cytochrome  $c$  oxidase) where  $O_2$ , the final electrons acceptor, is reduced to  $H_2O$ . During the electron transport, CI, CIII and CIV pump out protons from the matrix across the inner membrane, generating the electrochemical gradient ( $\Delta\mu_{H^+}$ ), consisting of a proton gradient ( $\Delta pH$ , alkaline in the matrix side) and an electrical potential ( $\Delta\Psi_m$ :  $\sim -180$  mV; negative in the matrix) across the membrane [Mitchell, 1961]. The three complexes catalyze the translocation of 10 protons from the matrix to the inter-membrane space for each NADH molecule oxidized. The electrochemical gradient (also called proton motive force) drives back the protons into matrix via ATP synthase (complex V, CV) inducing conformational changes in the active site of the enzyme and consequently promoting the phosphorylation of ADP to ATP (Figure 1.3) [Nath and Villadsen, 2015; Sazanov, 2015; Szalárdy *et al.*, 2015; Wallace and Fan, 2010].

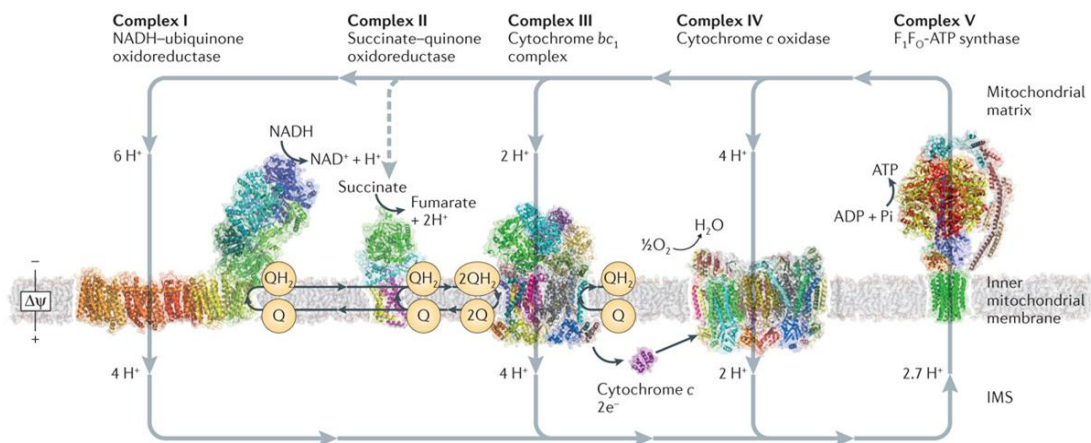


**Figure 1.3** The OXPHOS system consisting in CI, CII, CIII and CIV and the ATP synthase [modified from Sazanov, 2015].

In addition to ATP synthesis,  $\Delta\mu_{H^+}$  is used for other important mitochondrial functions such as the import of nucleus-encoded proteins in the matrix, the uptake of inorganic phosphate, the ADP/ATP exchange, the maintenance of ion homeostasis, in particular of  $Ca^{2+}$  ions [Bernardi, 1999; Bernardi *et al.*, 2015; Rizzuto *et al.*, 2012].

### 1.2.1 The ATP synthase

Mitochondrial ATP synthase or CV is a large protein complex which works as a molecular motor to generate and hydrolyze ATP in cells. ATP synthase generates ATP from ADP and  $P_i$  using the driving force of the  $\Delta\mu_{H^+}$  built up across the inner membrane by the respiratory CI, CIII and CIV. On the other hand, ATP synthase can hydrolyze ATP to pump protons back to the inter-membrane space to maintain membrane potential at the expenses of glycolytic ATP [Bernardi *et al.*, 2015; Futai *et al.*, 2012; Long *et al.*, 2015; Walker, 2013].

As illustrated in Figure 1.4, ATP synthase consists of two distinct subcomplexes with complementary functions: the  $F_0$  complex containing the rotatory trans-membrane subunits that transport protons from the inter-membrane space to the matrix, and the  $F_1$  complex, protruding into the matrix, which catalyzes nucleotide binding and ATP synthesis.  $F_0$  and  $F_1$  are connected through two stalk-like subunits: a central rotor shaft and a peripheral stator [Abrahams *et al.*, 1994; Chen *et al.*, 2004; van Raaij *et al.*, 1996]. In the mammalian enzyme,  $F_1$  is composed of three copies each of nucleotide-binding subunits  $\alpha$  and  $\beta$ , and one each of subunits  $\gamma$ ,  $\delta$  and  $\epsilon$ . Subunit  $\gamma$ , together with  $\delta$  and  $\epsilon$  subunits, forms the central stalk which connect  $F_1$  with  $F_0$ .  $F_0$  consists of a c-ring, constituted by 10-14 copies of the subunit c, and one copy each of subunits a, b, d, h ( $F_0$ ) and the O subunit or oligomycin sensitivity conferring protein (OSCP). A number of additional subunits (e, f, g, i/j, k and A6L) are associated with  $F_0$ , although their precise location within the complex remains unknown. All subunits of ATP synthase are encoded by nuclear genome, except for ATP6 and ATP8 which are encoded by mtDNA [Chen *et al.*, 2006; Gibbons *et al.*, 2000; Karrasch and Walker, 1999; Rubinstein *et al.*, 2003]. Protons accumulated in the inter-membrane space are driven through a semi-channel in  $F_0$ , which causes rotation of the c-ring along with the attached central stalk. Subsequently, rotation of subunit  $\gamma$ , within the  $F_1$ - $\alpha_3\beta_3$  hexamer provides energy for ATP synthesis at the catalytic sites (located in each of the three  $\beta$  subunits, at the interface with an adjacent  $\alpha$  subunit) [Bernardi *et al.*, 2015; Long *et al.*, 2015; Noji *et al.*, 1997; Walker, 2013].

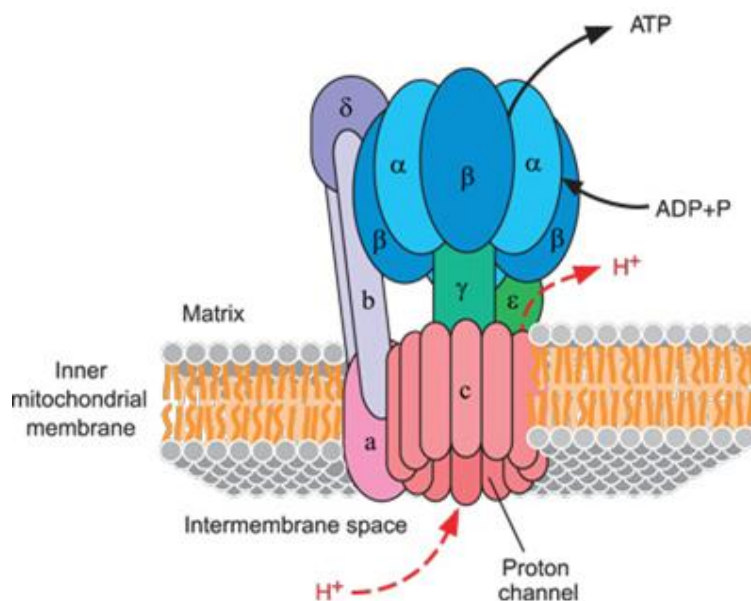


**Figure 1.4** Schematic representation of the ATP synthase.

The ATP synthase is present in the inner membrane as a dimer or a monomer. The F<sub>0</sub> subunits e, g, k and i were identified to be essential for the dimerization [Arnold *et al.*, 1998; Davies *et al.*, 2014; Dudkina *et al.*, 2005b, 2006; Giorgio *et al.*, 2013]. The presence of ATP synthase dimer was shown to be essential for the cristae structure formation and maintenance and consequently for the normal mitochondrial energetic function [Chaban *et al.*, 2014; Dudkina *et al.*, 2005b; Seelert and Dencher, 2011; Velours *et al.*, 2009].

### 1.3 The respiratory chain

As introduced in 1.2 paragraph and summarized in Figure 1.3, the respiratory chain is constituted by four large protein complexes embedded within the inner membrane transferring electrons from NADH or FADH<sub>2</sub> to oxygen. CI, CIII and CIV, but not CII, are able to promote the efflux of protons into the inter-membrane space generating the  $\Delta\mu_{H^+}$  [Lenaz and Genova, 2010; Szalárdy *et al.*, 2015; Wallace and Fan, 2010]. These complexes contain multiple redox cofactors to facilitate intra-complex electron transfer [prosthetic group such as flavin mononucleotide (FMN) and Fe-S clusters] and are connected each other by two mobile redox-active molecules: coenzyme Q, embedded in the inner membrane, and cytochrome c, outside the inner membrane [Lenaz and Genova, 2010]. By using a combination of spectrophotometry-based enzymatic assays, 2D/SDS-PAGE complex separation and Coomassie blue-staining, a ratio of one CI to 1.3 CII to

three CIII to 6.7 CIV in beef heart mitochondria was determined [Schägger and Pfeiffer, 2001].

Auxiliary enzymes of the respiratory chain are the mitochondrial glycerol-3-phosphate dehydrogenase (mtGPDH), the electron-transfer flavoprotein (ETF):ubiquinone oxidoreductase, the choline dehydrogenase, the dihydroorotate dehydrogenase and the alternative NADH dehydrogenases which transfer electrons to CoQ. Another auxiliary enzyme which feed electrons to CoQ is the malate:quinone oxidoreductase which is found only in some eukaryotes. In addition to CIII, all eukaryotic mitochondria possess the sulfite oxidase which feeds electrons to cytochrome *c*. Moreover, within mitochondria of plants, some yeasts and fungi an alternative quinol oxidases is found, catalyzing the aerobic oxidation of ubiquinol in addition to the cytochrome pathway. Unlike the above indicated respiratory complexes, the auxiliary enzymes are not involved in generation of the protonmotive force [Lenaz and Genova, 2010].

### 1.3.1 Complex I

Mitochondrial CI (NADH:ubiquinone oxidoreductase; EC 1.6.5.3) is the largest complex of the respiratory chain. In mammals, the enzyme comprises 44 subunits, seven of which are encoded by mitochondrial genome [Carroll *et al.*, 2006]. Our knowledge of the structure and function of this complex derives from the bacterial enzymes, constituted of 14 conserved subunits necessary and sufficient for the catalytic activity. The 14 subunits are defined as core subunits and classified into three distinct modules: the N-, Q- and P-module, that together form the typical L-shaped structure.

The first intact CI structure was recently solved in the *T. thermophilus* enzyme to 3.3 Å resolution completing the model of the core subunits [Baradaran *et al.*, 2013]. Figure 1.5A shows that the NADH-dehydrogenase N-module, which provides electron input into the chain of Fe–S clusters, and the connecting Q-module, which conducts electrons to the quinone-binding site, compose the peripheral arm of CI. It contains seven conserved core subunits: Nqo1, Nqo2, Nqo3, Nqo4, Nqo5, Nqo6, Nqo9 and cofactors including 8-9 Fe-S clusters and the FMN molecule. Seven of the Fe-S clusters form a 95 Å-long redox chain connecting FMN to the quinone-binding site at the interface with the membrane domain (Figure1.5B). Nqo1 coordinates the FMN in a solvent-exposed cavity which contains also the NADH binding site. The peripheral arm of *T. thermophilus* CI contains two additional subunits Nqo15 and Nqo16, as possible chaperon [Baradaran *et al.*, 2013; Efremov and

Sazanov, 2012; Letts and Sazanov, 2015; Sazanov, 2015]. The proton pumping P-module is part of the membrane-arm of CI containing the core subunits Nqo7, Nqo10, Nqo11, Nqo14, Nqo13 and Nqo12. The membrane-arm also contains the highly conserved core subunit Nqo8 which is not included in the P-module. Nqo8 plays a key role in the Q binding site, the proton translocation pathway and the junction the peripheral- and membrane-arm. All of membrane-arm subunits contain 14 trans-membrane helices each. Nqo12 contains a C-terminal extension comprising two trans-membrane helices connected by a 110 Å-long  $\alpha$ -helix that runs along the cytoplasmic membrane surface, linking the Nqo12, Nqo13 and Nqo14 subunits. The 14 common trans-membrane helices of Nqo12, Nqo13 and Nqo14 are divided in the 10-trans-membrane helices core (containing the helices from 4 to 13) and the less conserved 1-3-14 trans-membrane helices. Nqo7, Nqo10, Nqo11 and Nqo8 are connected to Nqo12, Nqo13 and Nqo14 through a 11-trans-membrane helices bundle. On the periplasmic side of the membrane arm a series of connected  $\beta$ -hairpins and helices form the element  $\beta$ H. The total molecular weight of the bacterial CI is ~550 kDa (Figure 1.5A) [Baradaran *et al.*, 2013; Efremov *et al.*, 2010; Efremov and Sazanov, 2011; Letts and Sazanov, 2015; Sazanov, 2015].

The complete structure of mitochondrial CI is not available yet. The cryo-EM map of bovine CI at 5Å resolution [Vinothkumar *et al.*, 2014] and the electron density map of CI from the yeast *Yarrowia lipolytica* obtained at ~3.8 Å resolution [Zickermann *et al.*, 2015] were recently published. These studies showed that the core is very similar to the bacterial enzyme, except for small variation in C- and N-termini length of subunits, and the presence of ~30 supernumerary subunits forming a shell around the 14 conserved core subunits, predominantly in the membrane- and lower peripheral-arm (Figure 1.6). These accessory subunits increases the molecular weight of enzyme to ~1 MDa. Currently, only 14 accessory subunits are identified and with an assigned structure position [Vinothkumar *et al.*, 2014]. The function of these supernumerary subunits is still unclear, it has been suggested they can assist the assembly, regulation and stability of the complex [Letts and Sazanov, 2015; Vinothkumar *et al.*, 2014].

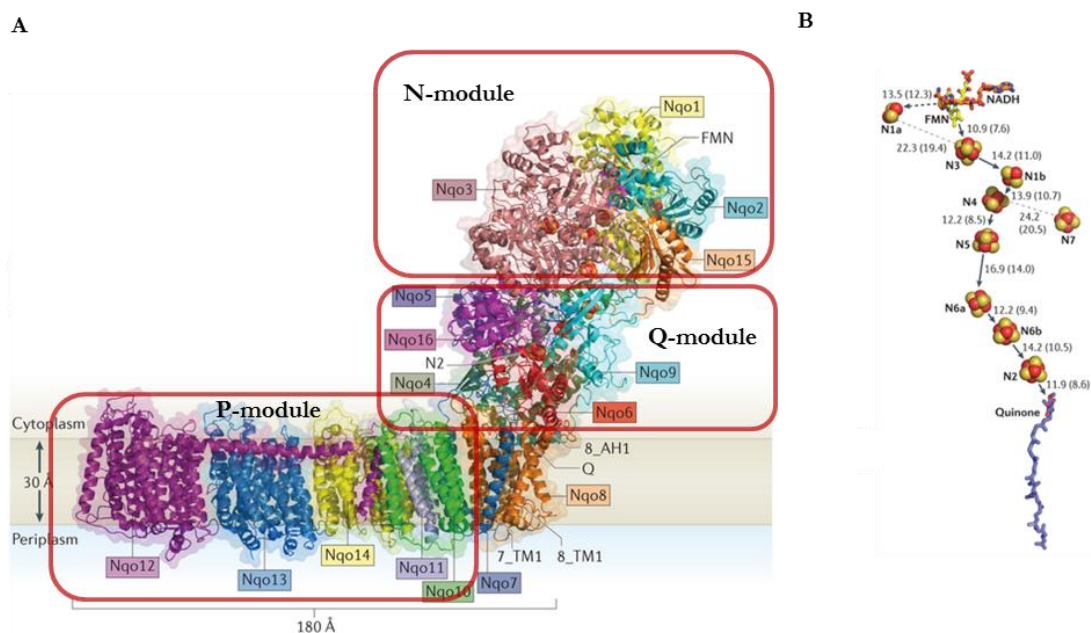


**Figure 1.5** (A) Structural model of *T. thermophilus* CI. The subunits are represented with different colors each and labeled with text in the same colors. The N-, Q- and P-module are shown [modified from Baradaran *et al.*, 2013]; (B) Electron transfer pathway from FMN to quinone through Fe-S clusters [from Sazanov, 2015].

Treatment of purified bovine CI with a mild detergent such as lauryldimethylamine oxide (LDAO) revealed that the enzyme dissociates in four sub-complexes named  $I\alpha$ ,  $I\beta$ ,  $I\gamma$  and  $I\lambda$ . Subcomplex  $I\lambda$  corresponds to peripheral arm, containing 14 subunits (7 core subunits and 7 supernumerary subunits), the redox cofactors and the NADH binding site.  $I\alpha$  subcomplex is composed by  $I\lambda$  subcomplex plus 9 additional subunits, such as ND1. The  $I\beta$  subcomplex is composed of the core subunits ND4 and ND5 and an additional 12 supernumerary subunits. Finally, subcomplex  $I\gamma$  is formed by ND2 and three supernumerary subunits.  $I\beta$  and  $I\gamma$  subcomplexes provide the membrane arm (Figure 1.7) [Letts and Sazanov, 2015; Vinothkumar *et al.*, 2014; Zickermann *et al.*, 2015].

The entry-point of the subunits encoded by mitochondrial genome involved in the assembly of mammalian CI has been recently identified [Perales-Clemente *et al.*, 2010]. ND1 and ND2 define two different sub-complexes which progress separately. ND1 joins peripheral-arm subunits, forming an  $\sim 400$ -kDa intermediate that is anchored to the inner mitochondrial membrane. ND2 is placed in  $\sim 460$ -kDa membrane sub-complex which joins the ND1 subassembly building the complete CI. Thus, ND1 is the first mtDNA-encoded subunit which enters in the  $\sim 400$  kDa-subcomplex, the second step is

represented by ND2, ND3 and ND4L in the  $\sim 460$  kDa-subcomplex. Finally, ND4, ND6 and ND5 are incorporated into complete CI as third, fourth and fifth entry points, respectively [Perales-Clemente *et al.*, 2010].

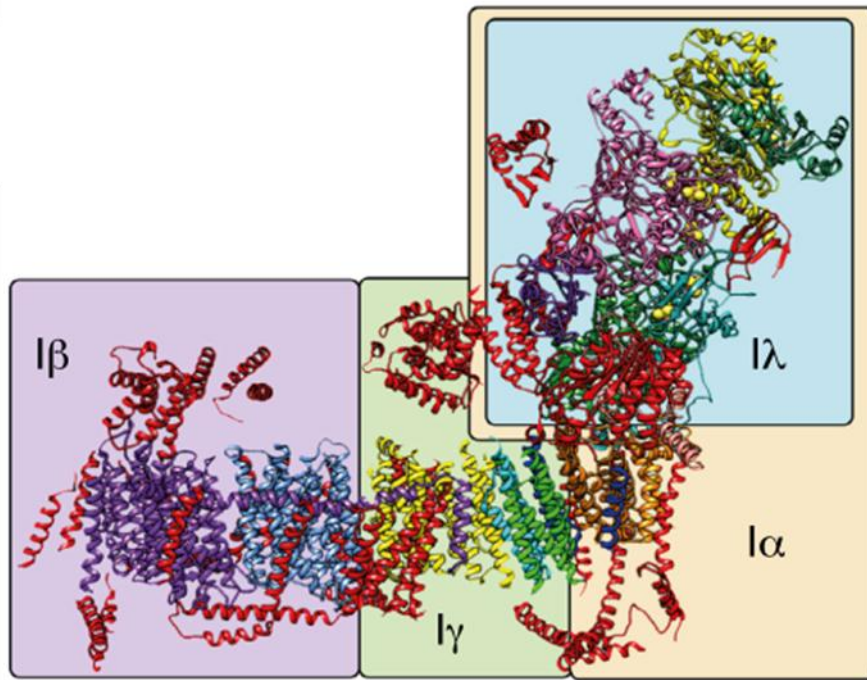


**Figure 1.7** 5 Å resolution structure of CI from *Bos taurus* heart mitochondria determined by single-particle electron cryo-microscopy. I $\alpha$ , I $\beta$ , I $\gamma$  and I $\lambda$  domains are highlighted [from Letts and Sazanov, 2015].

Other studies carried out in hamster chinese and human cells helped to clarify how the mammalian CI is assembled. As illustrated in Figure 1.8, the core subunits NDUFS2 and NDUFS3 form a small hydrophilic assembly complex. Then, NDUFS7, NDUFS8 and later NDUF9 are incorporated forming the early peripheral complex. This complex forms a  $\sim 400$  kDa assembly intermediate, together with a small membrane complex containing ND1. This  $\sim 400$  kDa complex incorporates with a  $\sim 460$  kDa membrane complex containing ND3, ND6, ND2, ND4L and NDUF6 to form a  $\sim 650$  kDa complex. Another membrane complex containing ND4, ND5 and probably NDUF2, is associated to  $\sim 650$  kDa complex, forming an  $\sim 830$  kDa complex. Meanwhile, the N-module is assembled by some nDNA-encoded subunits directly or indirectly involved in binding and oxidizing NADH. With the addition of the N-module and remaining subunits (such as the inter-membrane space subunits NDUF8 and

NDUFS5), mature CI is assembled [Letts and Sazanov, 2015; McKenzie and Ryan, 2010; Mimaki *et al.*, 2012].

The catalytic mechanism of CI can be simply described as the NADH oxidation by FMN with the consequent transfer of two electrons along the Fe-S clusters to the ubiquinone binding site where quinone is reduced to quinol [Hirst, 2013]. The pathway starts with NADH binding to its site in the NDUFV1 subunit on the top part of the peripheral arm. The nicotinamide ring of NADH is juxtaposed over FMN isoalloxazine system, allowing the electron transfer and reduction of FMN [Berrisford and Sazanov, 2009]. Seven of the Fe-S clusters form a chain to carry electrons from the FMN to quinone bound into its site (Figure 1.5B) [Baradaran *et al.*, 2013]. The FMN reduction and the quinone reduction in the chain involve the transfer of two electrons, whereas Fe-S clusters transfer one electron at a time [Sazanov, 2015]. Electron transfer along the seven clusters chain is generally considered fast [Page *et al.*, 1999], indeed each catalytic cycle would take ~5 milliseconds [Vinogradov, 1998]. The electron transfer pathway ends in the quinone-binding site formed by subunits NDUFS2, NDUFS7, ND3 and ND1 [Sazanov, 2015]. The size of this site is large enough to accommodate an entire quinone molecule. The quinone binding site is mostly constituted by hydrophilic residues which guide the head of the quinone to bind in the deep end of the cavity, about 15 Å out from the membrane surface [Baradaran *et al.*, 2013].

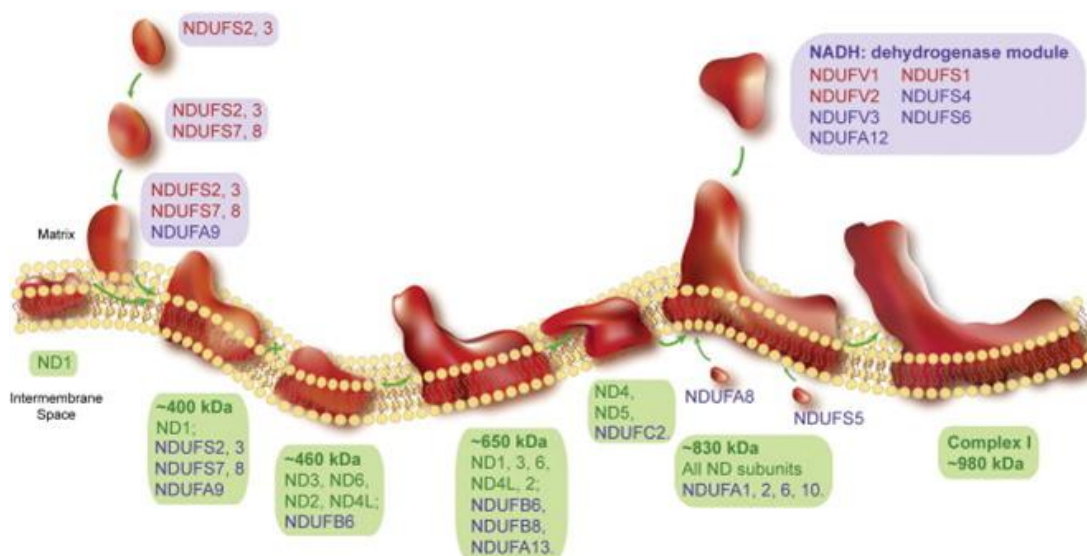


**Figure 1.8** Schematic human CI assembly [Mimaki *et al.*, 2012].

| Table 1.1 Complex I core subunits nomenclature |                             |                   |                     |
|--|-----------------------------|-------------------|---------------------|
| Module   | <i>Thermus thermophilus</i> | <i>Bos taurus</i> | <i>Homo sapiens</i> |
| Peripheral arm                                 |                             |                   |                     |
| N  | Nqo1                        | 51 kDa            | NDUFV1              |
|  | Nqo2                        | 24 kDa            | NDUFV2              |
|  | Nqo3                        | 75 kDa            | NDUFS1              |
| Q  | Nqo4                        | 49 kDa            | NDUFS2              |
|  | Nqo5                        | 30 kDa            | NDFUS3              |
|  | Nqo9                        | TYKY              | NDUFS8              |
|  | Nqo6                        | PSSI              | NDUFS7              |
| Membrane arm                                   |                             |                   |                     |
|  | Nqo8                        | ND1               | ND1                 |
| P  | Nqo7                        | ND3               | ND3                 |
|  | Nqo10                       | ND6               | ND6                 |
|  | Nqo11                       | ND4L              | ND4L                |
|  | Nqo14                       | ND2               | ND2                 |
|  | Nqo13                       | ND4               | ND4                 |
|  | Nqo12                       | ND5               | ND5                 |

**Table 1.1** CI core subunits nomenclature.

For each molecule of oxidized NADH, four protons are transported across the membrane to the inter-membrane space [Hirst, 2013]. Two set of five helices in ND2, ND3 and ND5 subunits of the membrane-arm have been proposed to form channels for proton translocation. The channels are constituted by conserved polar residues and polar cavities containing water molecules [Baradaran *et al.*, 2013]. The key residues involved in proton translocation are the conserved Lys and Glu residues of the helices 5, 7, 8 and 12 [Sazanov, 2015]. The electron transport from the FMN through the Fe-S cluster chain causes a cascade of conformational changes in the peripheral-arm which are propagated into membrane-arm where the key residues of ND2, ND3 and ND5 are protonated. When the quinone is totally reduced and the conformational changes are completed, the key residues eject a proton across the membrane [Baradaran *et al.*, 2013; Hirst, 2013; Sazanov, 2015].

### 1.3.2 Complex II

Mitochondrial CII (succinate:ubiquinone oxidoreductase or succinate dehydrogenase, SDH; EC 1.3.5.1) is the only respiratory complex totally encoded by nuclear DNA [Her and Maher, 2015; Sun *et al.*, 2005]. CII is also the only membrane

complex of the Krebs cycle, catalyzing the oxidation of succinate to fumarate in the mitochondrial matrix and producing one molecule of FADH<sub>2</sub>. Succinate oxidation is coupled to reduction of quinone to quinol at the inner membrane as one part of the respiration electron transfer chain. Electrons are transferred from succinate to quinone through the prosthetic groups flavin-adenine dinucleotide (FAD), the [2Fe-2S], [4Fe-4S], and [3Fe-4S] clusters, and a *b*-type heme, which form an integral part of the complex [Her and Maher, 2015].

CII was crystallized from porcine heart in 2005 by Sun and colleagues [Sun *et al.*, 2005]. SDH is a 124 kDa complex which consists of a soluble catalytic heterodimer and an integral membrane region, resembling a Q-shaped structure (Figure 1.9) [Sun *et al.*, 2005]. The hydrophobic domain is composed by SDHC and SDHD subunits which anchor the complex to the inner membrane. The hydrophilic domain, protruding into the matrix, is formed by SDHA and SDHB subunits. SDHA contains the binding site for succinate and a FAD prosthetic group covalently bound. Succinate is juxtaposed with the isoalloxazine ring of FAD, where oxidation to fumarate is catalyzed. SDHB connects SDHA to SDHC and SDHD. SDHB contains three Fe-S clusters: [2Fe-2S], [4Fe-4S], and [3Fe-4S], which mediate electron transfer from succinate to ubiquinone. The complex has two quinone-binding sites: i) the high-affinity site (Q<sub>p</sub>), formed by residues from SDHB, SDHC, and SDHD subunits and located near the matrix side of the inner mitochondrial membrane; ii) and the low-affinity site (Q<sub>d</sub>), formed by SDHC and SDHD subunits and located on the inter-membrane space side. Both the quinone binding pockets are constituted by a long hydrophobic channel formed by helices of the involved subunits. Between four bound helices of SDHC and SDHD subunits, a *b* heme group is found. It is stabilized by hydrophobic interaction between the porphyrin group and the four helices [Her and Maher, 2015; Sun *et al.*, 2005].

Despite being formed by 4 subunits only, CII assembly is very intricate and several chaperones are needed to help the protein folding and the factor insertion [Her and Maher, 2015]. The SDHA assembly process requires the insertion of FAD. FAD is imported in mitochondria from cytosol through Flx1 protein at the inner membrane, being a member of the superfamily of mitochondrial carriers that exchange substrates between the cytosol and the matrix [Robinson and Kunji, 2006]. SDHAF2 is necessary for the covalent insertion of FAD into the catalytic SDHA subunit [Hao *et al.*, 2009]. SDHAF1 and SDHAF3 allow the insertion of Fe-S clusters into SDHB subunits [Ghezzi *et al.*, 2009];

Na *et al.*, 2014]. SDHAF4 is required for the association of SDHA to SDHB and the consequent assembly of CII holocomplex [Van Vranken *et al.*, 2014]. The *tom62* gene encodes a mitochondrial membrane protein that was shown to directly interact with three SDH subunits helping the folding of CII [Dibrov *et al.*, 1998].

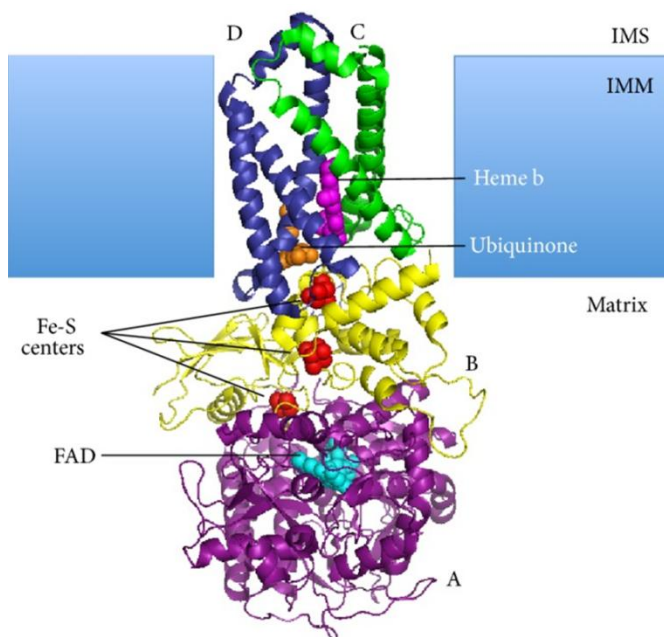


**Figure 1.9** Structure of porcine CII. SDHA-B-C-D subunits, Fe-S clusters, FAD, *b* heme group and the quinone are indicated [from Her and Maher, 2015].

The catalytic mechanism of SDH starts at the binding site of the succinate. The  $\alpha$ -carbon of succinate is deprotonated by basic residues or cofactors, FAD accepts hydride from the  $\beta$ -carbon and the succinate is oxidized to fumarate. Oxidized fumarate is free to exit the protein and a  $\text{FADH}_2$  molecule is released. The electrons derived from the succinate oxidation are carried along the Fe-S clusters until [3Fe-4S] center where they are transferred to quinone bound in its site. The reduction pathway of the quinone requires two electrons to fully reduce quinone to quinol. The first electron forms a quinone intermediate, a semiquinone radical specie, the second electron from the [3Fe-4S] center provides to reduce the semiquinone to ubiquinol [Sun *et al.*, 2005].

The activity of SDH is highly regulated by succinate competitors, ubiquinone inhibitors, or post-translational modifications [Her and Maher, 2015]. Malonate, malate, and oxaloacetate are succinate competitors, being similar in structure. Carboxin and thenoyltrifluoroacetone are synthetic ubiquinone inhibitors that block electron transfer

from the SDH complex to ubiquinone [Her and Maher, 2015]. The catalytic activity of the complex is also modulated by post-translational modifications such as phosphorylation and acetylation of SDHA lysine residues. The acetylation of SDHA lysine decreases the activity of CII [Cimen *et al.*, 2010; Finley *et al.*, 2011]. Phosphorylation of SDHA lysine residues has similar effects of the acetylation on SDH activity [Tomitsuka *et al.*, 2009]. Recently, Acín-Pérez and colleagues found that the tyrosine 604 phosphorylation of SDHA subunit strongly increases the CII activity [Acín-Pérez *et al.*, 2014]. Moreover, succinylation of SDHA lysine residues has been reported, this modification possibly modulating the SDH activity [Park *et al.*, 2013].

### 1.3.3 Complex III

Respiratory CIII (ubiquinol:cytochrome *c* oxidoreductase, cytochrome *bc*<sub>1</sub> complex; EC 1.10.2.2) is the central component of the mitochondrial respiratory chain, coupling the transfer of electrons from quinol to cytochrome *c* with the generation of a proton gradient across the inner membrane [Bénil *et al.*, 2009].

The mammalian CIII is an homodimeric enzyme (CIII)<sub>2</sub>, with each monomer consisting of 11 polypeptide subunits, one encoded by mitochondrial genome and ten encoded by nuclear genes. The catalytic center is formed by three redox essential subunits: cytochrome *b*, cytochrome *c*<sub>1</sub> and the Fe-S protein (Rieske protein, ISP). Cytochrome *b* contains two *b*-type hemes, a low potential heme *b*<sub>L</sub> ( $E_{m7} = -30$  mV) and a high potential heme *b*<sub>H</sub> ( $E_{m7} = +100$  mV); cytochrome *c*<sub>1</sub> has a globular domain which binds a *c*-type heme group ( $E_{m7} = +230$  mV for bovine CIII) and the Rieske protein also contains a globular domain with two *2Fe-2S* iron-sulfur cluster whose iron atoms are ligated by two cysteine and two histidine residues. The exact function of the other eight supernumerary subunits (UQCRC1, UQCRC2, UQCRH, UQCRB, UQCRQ, Subunit 9, UQCR10 and UQCR11) remains to be established, their possible functions include structural stability and regulation of coordinated activity of the dimeric enzyme [Xia *et al.*, 2013].

Structures of CIII from several organism are available, including the bovine heart mitochondria, which was the first obtained [Iwata *et al.*, 1998; Xia *et al.*, 1997]. CIII structure can be divided into three regions: the membrane spanning, the inter-membrane and the matrix region. Each monomer of CIII is composed by 13 trans-membrane helices: eight from cytochrome *b* and one each from cytochrome *c*<sub>1</sub>, the ISP, subunits 7, 10, and 11. Accessory subunits 1, 2, 6 and 9 are exclusively present in the matrix region, while subunit

8 is associated with cytochrome  $c_1$  at the inter-membrane space side [Iwata *et al.*, 1998; Xia *et al.*, 1997]. The two  $b$ -type hemes of cytochrome  $b$  are part of the active sites that catalyze opposite reactions: the  $Q_P$  ( $Q_O$  near  $b_L$  heme; O, outer; P, positive) site, located near the inter-membrane space, provides access to lipid-soluble  $QH_2$  for oxidation, and the  $Q_N$  ( $Q_I$  near  $b_H$  heme; I, inner; N, negative) site, situated close to the matrix, is involved in the reduction of ubiquinone. Both the cytochrome  $c_1$  and ISP subunits are anchored to the membrane by trans-membrane helices with their respective extra membrane domains localized on the inter-membrane space. The globular domain of the Rieske protein is attached to a membrane-spanning helix and appears to be able to rotate so that its Fe–S centre can contact either the quinone-binding site or the  $c$ -type heme of cytochrome  $c_1$  (Figure 1.10) [Xia *et al.*, 2013].

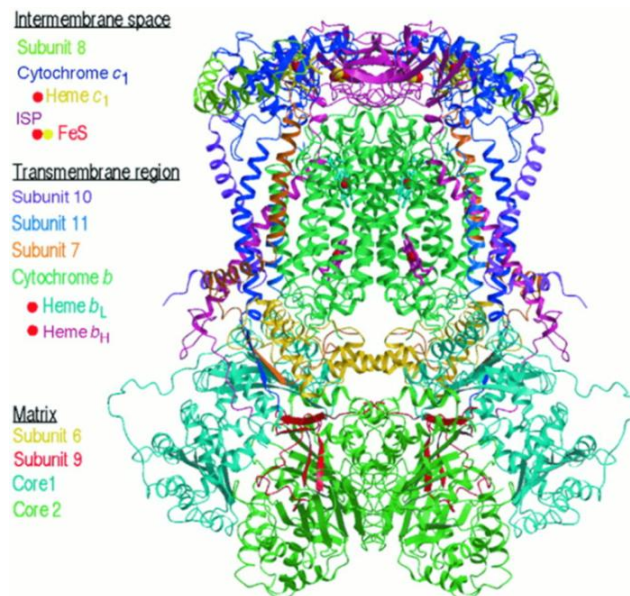


**Figure 1.10** Crystallographic structure of bovine CIII. The three regions with their subunits are indicated [from Iwata *et al.*, 1998].

The proton extrusion mechanism at CIII is quite unique, since ubiquinol is used to shuttle protons across the membrane via the so called Q-cycle [Mitchell, 1976]. The Q-cycle requires a quinol oxidation site and a quinone reduction site and the oxidation of two quinol molecules to complete one cycle. In the first half of the Q-cycle, a  $QH_2$  moves into the  $Q_P$  site, formed when the globular domain of the ISP rotates allowing the binding of  $QH_2$  by bridging residues of both proteins.  $QH_2$  undergoes oxidation with one electron arriving to cytochrome  $c$  via the ISP and cytochrome  $c_1$  and the other going to hemes  $b_L$ .

The electron on  $b_L$  moves across the membrane to reduce the second heme  $b_H$  and finally the quinone bound in the  $Q_N$  site, forming a semiquinone radical ( $Q^{\cdot-}$ ). This pathway releases two protons in the inter-membrane space. In the second half of the Q-cycle, a second  $QH_2$  is oxidized in the same way at the  $Q_P$  site, reducing completely the  $Q^{\cdot-}$  at  $Q_N$  site. The fully reduced  $QH_2$ , upon taking up two protons from the matrix, moves through the membrane to the  $Q_P$  site to be oxidized. Thus, as a result of the Q-cycle, four protons are transferred to the inter-membrane space, two protons are taken up from the matrix, two quinol molecules are oxidized and one quinone is reduced (Figure 1.11) [Xia *et al.*, 2013].

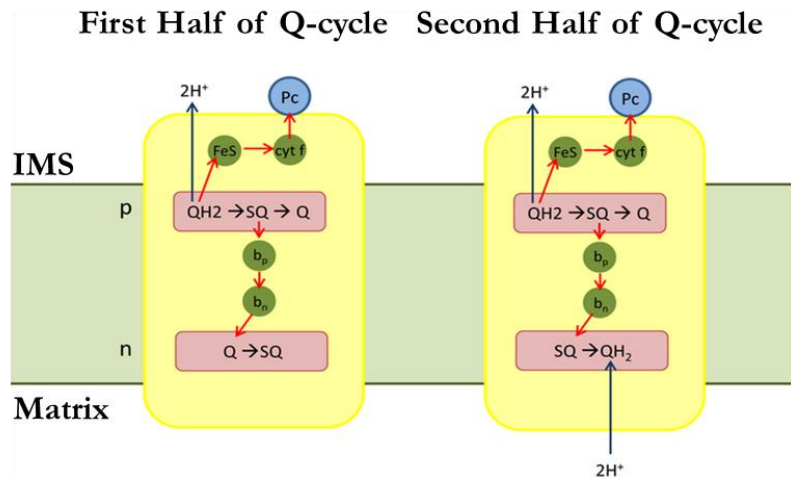


**Figure 1.11** Representative scheme of the Q-cycle.

| Table 1.2 The bovine and yeast CIII subunits |                   |                      |                                 |                |
|--|-------------------|----------------------|---------------------------------|----------------|
| Subunit                                      | <i>Bos taurus</i> |                      | <i>Saccharomyces cerevisiae</i> |                |
|  | Gene              | Protein              | Gene                            | Protein        |
| 1  | <i>UQCRC1</i>     | Core I               | <i>QCR1</i>                     | Cor1           |
| 2  | <i>UQCRC2</i>     | Core II              | <i>QCR2</i>                     | Cor2           |
| 3  | <i>MTCYB</i>      | Cytochrome <i>b</i>  | <i>COB</i>                      | COB            |
| 4  | <i>CYC1</i>       | Cytochrome <i>c1</i> | <i>CTC1</i>                     | Cyt1p          |
| 5  | <i>UQCRFS1</i>    | ISP-Rieske Protein   | <i>RIP1</i>                     | Rip1p          |
| 6  | <i>UQCRB</i>      | SU8                  | <i>QCR7</i>                     | Q $\alpha$ 7p  |
| 7  | <i>UQCRQ</i>      | SU7                  | <i>QCR8</i>                     | Q $\alpha$ 8p  |
| 8  | <i>UQCRH</i>      | SU8                  | <i>QCR6</i>                     | Q $\alpha$ 6p  |
| 9  | <i>UQCR10</i>     | SU10                 | <i>QCR9</i>                     | Q $\alpha$ 9p  |
| 10   | <i>UQCR11</i>     | SU11                 | <i>QCR10</i>                    | Q $\alpha$ 10p |
| 11   | -                 | SU9*                 | -                               | -              |

SU9\* Mitochondrial targeting presequence deaved from UQCRFS1

**Table 1.2** Nomenclature of the bovine and yeast CIII subunits.

CIII assembly has been mainly studied in the yeast *Saccharomyces cerevisiae* [Atkinson *et al.*, 2010; Cui *et al.*, 2012; Gruschke *et al.*, 2011, 2012; Hildenbeutel *et al.*, 2014; Smith *et al.*, 2012; Zara *et al.*, 2007, 2009a, 2009b]. A model of the human CIII assembly, based on the data obtained from yeast, has been recently proposed by Fernández-Vizarra and Zeviani (Figure 1.12) [Fernández-Vizarra and Zeviani, 2015]. The initial step is the release of cytochrome *b* from the mito-ribosome and its insertion into the inner membrane, a process that requires the two assembly factors, UQCC1 and UQCC2. The UQCC1-UQCC2 complex remains bound to cytochrome *b* once it is completely synthesized and incorporated into the inner membrane. Once  $b_L$  type heme is inserted into the catalytic center of cytochrome *b*, UQCC3 binds followed by  $b_H$  type heme incorporation. The UQCC1-UQCC2 dimer is released when UQCRB and UQCRQ bind to cytochrome *b*, to form the early-stage CIII intermediary. Additional subunits, i.e., UQCRC1, UQCRC2, and CYC1 are then incorporated, followed by UQCRH and later UQCR10, to form pre-CIII<sub>2</sub>. At this point, the complex is already dimeric, but the precise stage at which dimerization occurs is currently unknown. Finally, UQCRFS1 (Rieske protein) is translocated from the matrix into the inner membrane and is incorporated into pre-CIII<sub>2</sub>, operated by the assembly factor, BCS1L. In the matrix, UQCRFS1 is bound and stabilized by MZM1L. Finally the last subunit (UQCR11) joins the nascent complex, so that assembly is completed. TTC19 is also necessary for the correct biogenesis of CIII<sub>2</sub> in human mitochondria, although the step in which it intervenes is not known yet. The nomenclature used is for the human/bovine, for the yeast nomenclature see the Table 1.2 [Fernández-Vizarra and Zeviani, 2015].

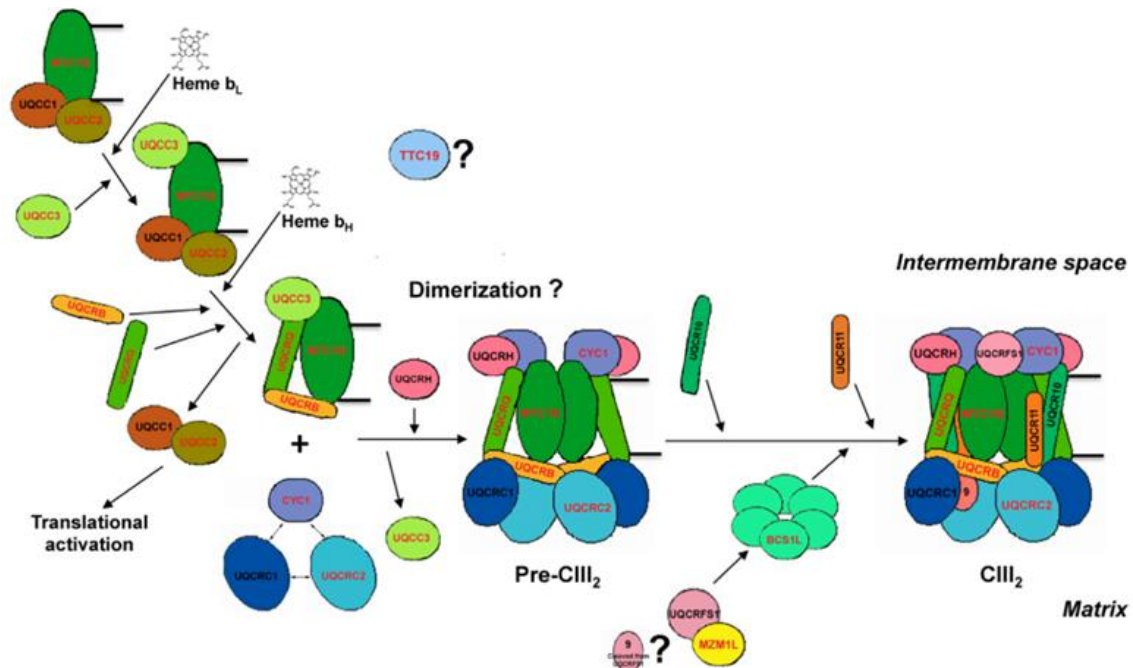


Figure 1.12 Human CIII assembly model [from Fernández-Vizarra and Zeviani, 2015].

### 1.3.3.1 Cytochrome *b*

The cytochrome *b* is the only CIII subunits encoded by mtDNA. It is a highly conserved membrane protein 380 amino acid residues long in human CIII [Iwata *et al.*, 1998; Xia *et al.*, 1997]. The *MTCYB* gene encompasses 1140 nps of mtDNA and encodes a single polypeptide. The mRNA has a 4-np, 5-prime noncoding region followed by the AUG start codon, and ends with the U of the UAA termination codon. It is transcribed as a part of the polycistronic H-strand transcript, flanked by the tRNAGlu and tRNAThr transcripts. These tRNAs are clove out at the transcript freeing transcript 11, the cytochrome *b* mRNA. The mRNA is then polyadenylated completing the termination codon [Wallace, 1989]. The translation of the mitochondrial genome encoded subunit was first studied by Gruschke and colleagues in yeast. Cytochrome *b* pre-mRNA is processed by matrix protein Cbp2, then translation is activated by the mitochondrial proteins Cbs1 and Cbs2, that interact with 5' untranslated region, allowing the transcript to begin its translation by mito-ribosomes. The newly synthesized protein binds to a complex formed by the translational activator Cpb6 (UQCC1 in human) and the matrix assembly protein Cpb3. This assembly complex recruits another assembly factor Cpb4 (UQCC2 in human),

altogether stabilize the newborn subunit while it receives its cofactors and forms interactions with additional CIII subunits [Gruschke *et al.*, 2011].

When folded, the protein is formed by eight trans-membrane helices named A-H with both of the N- and the C-terminus located in the matrix. The trans-membrane helices are linked by seven extra-membrane loops, five of which are prominent: the AB, CD, DE, and EF protrude into the inter-membrane space, while the DE loop projects towards the matrix side. These loops are the primary participants in the formation of the Q<sub>O</sub> and Q<sub>I</sub> site, thus, they are crucial for the function of cytochrome *b*. The AB, CD and EF loop have secondary structure: AB and EF loop contain one helix each, ab helix for AB loop and ef helix for EF; the CD loop is formed by two helices, cd1 and cd2, arranged as hairpin. Between the helices E and F, in the EF loop, the PEWY sequence is located. This sequence is highly conserved, containing P<sup>270</sup>-E<sup>271</sup>-W<sup>272</sup>-Y<sup>273</sup> in the bovine, and it seems to be important for electron transfer and quinol binding at the Q<sub>O</sub> site. The eight helices form two helical bundles, one consisting of helices A–E and the other of helices F–H. The *b<sub>L</sub>* and *b<sub>H</sub>* hemes are incorporated into the first helical bundle, bound to conserved histidine residues (H<sup>83</sup> and H<sup>182</sup> for *b<sub>L</sub>*, H<sup>97</sup> and H<sup>196</sup> for *b<sub>H</sub>*). The two helical bundles are separated from each other near the inter-membrane space side of the membrane, thus creating the so-called Q<sub>O</sub> pocket between the *b<sub>L</sub>* heme and the 2Fe–2S cluster of the Rieske protein. Near the *b<sub>H</sub>* another hydrophobic pocket is formed, the Q<sub>I</sub> site (Figure 1.13). The two bundles contact each other on the negative side of the membrane, but separate on the positive side, creating a gap that is bridged by the cd helices (cd1 and cd2) and by the EF loop [Gao *et al.*, 2003; Iwata *et al.*, 1998; Xia *et al.*, 1997].

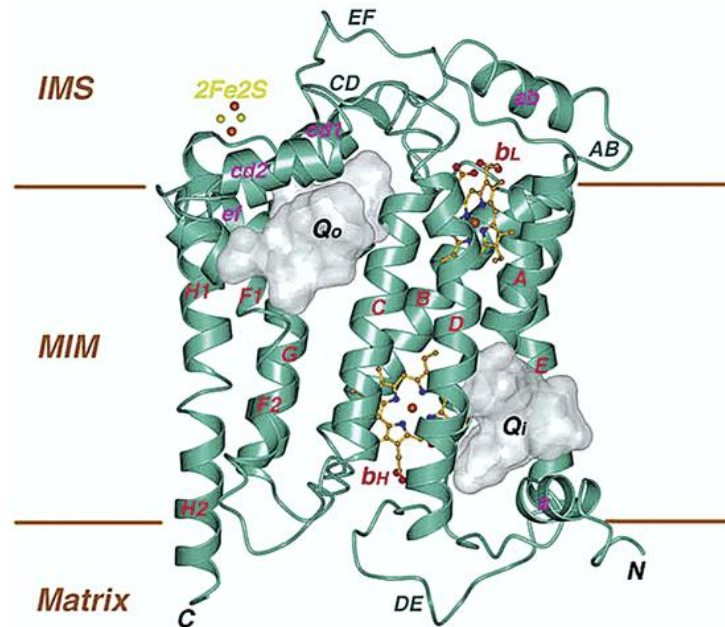


**Figure 1.13** Schematic representation of cytochrome *b*. The quinone binding sites ( $Q_I$  and  $Q_O$ ) and the  $b_H$  and  $b_L$  are indicated. The trans-membrane helices are indicated A-H [from Gao *et al.*, 2003].

### 1.3.4 Complex IV

CIV (cytochrome *c* oxidase, COX; EC.1.9.3.1) catalyzes the electron transport from cytochrome *c* to oxygen coupled to proton pumping across the mitochondrial membrane. In mammals CIV is a homodimer, each half comprising 13 subunits. Three of these subunits (I-III) form the catalytic core and are encoded by mtDNA, whereas the remaining ten subunits (IV, Va, Vb, VIa, VIb, VIc, VIIa, VIIb, VIIc, VIII) encoded in the nucleus, are tightly bound to I-III subunits. The nuclear-coded subunits are essentially involved in the regulation of oxygen consumption and proton translocation by CIV [Kadenbach and Hüttemann, 2015].

The CIV structure from bacteria [Iwata *et al.*, 1995] and bovine [Tsukihara *et al.*, 1996] is known. Subunit II has two membrane-spanning  $\alpha$ -helices and a large globular hydrophilic domain forming a docking surface for cytochrome *c*. It also contains a bimetallic copper center,  $Cu_A$ , providing the entry point for the electrons. Subunit I is the largest of the catalytic core subunits. It is composed of 12 trans-membrane helices arranged in groups of four around three cavities. The first of these cavities contains an  $\alpha$ -type heme, heme  $a$ , bound to two histidine residues. In the second cavity, the oxygen reduction site is present, formed by a second  $\alpha$ -type heme, heme  $a_3$ , and the histidine-bound copper,  $Cu_B$ . The heme  $a_3$  iron is bound to a histidine residue on its proximal side, whereas on the distal

side the iron faces the  $\text{Cu}_b$ . This site is often called binuclear centre (BNC), due to the presence of two metals. The histidine bound to  $\text{Cu}_b$  and a close tyrosine residue, involved in the catalysis, create a covalent link, producing a pentameric ring with the highly conserved sequence HPEVY. The crystal structure revealed three possible proton-transfer pathways. One of these, named the “K” channel from a conserved lysine residue,  $\text{Lys}^{319}$ , leads from the matrix towards the BNC. A second, named the “D” channel from an aspartate residue,  $\text{Asp}^{91}$ , near its entrance, leads from the matrix to a conserved glutamic acid residue ( $\text{Glu}^{242}$ ) that is in the middle of the pentameric HPE<sup>242</sup>VY ring sequence. An additional possible proton channel, the “H” channel, has been described in the bovine structure leading from the matrix towards heme *a* (Figure 1.14) [Kadenbach and Hüttemann, 2015; Rich and Maréchal, 2010; Tsukihara *et al.*, 1996].

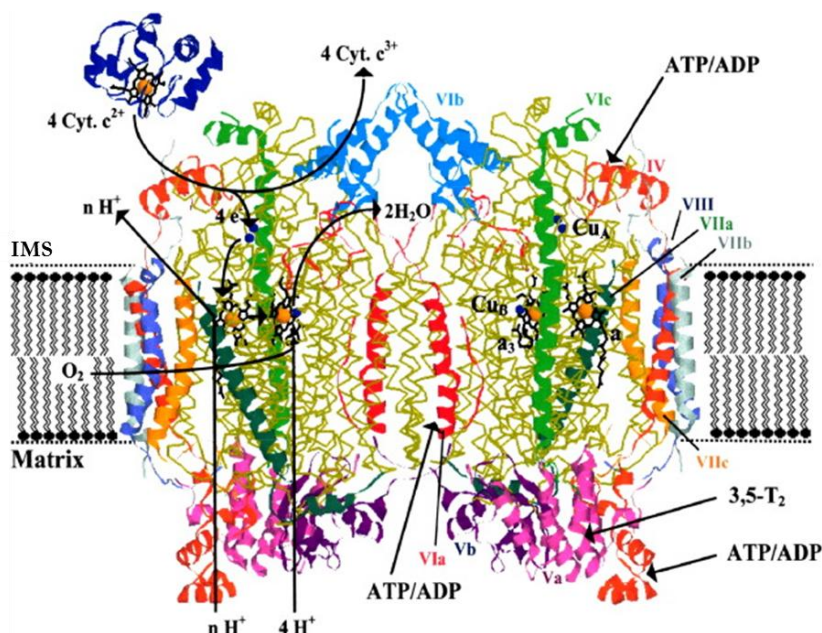


**Figure 1.14** Crystal structure of dimeric CIV from bovine heart [modified from Tsukihara *et al.*, 1996]. The mtDNA-coded subunit I, II and III are in yellow, the other subunits are in colors.

CIV reduces molecular oxygen to water in the  $\text{O}_2$ -reduction site composed of  $\text{Fe}_{a_3}$  and  $\text{Cu}_b$ . This mechanism requires the sequential arrival of four electrons and four protons.  $\text{O}_2$  is bound to the  $\text{O}_2$ -reduction site when both metal sites are in the reduced state ( $\text{Fe}_{a_3}^{2+}$  and  $\text{Cu}_b^{1+}$ ). The fully reduced state is designated as the R-intermediate. The R-intermediate receives  $\text{O}_2$  to form  $\text{Fe}_{a_3}^{3+}-\text{O}_2^-$  (the A-intermediate), which is spontaneously converted to the P-intermediate without any electron transfer from the low-potential metal sites ( $\text{Fe}_a$  and  $\text{Cu}_A$ ). By the time P has formed, the bound  $\text{O}_2$  has accepted four electron equivalents (two

equivalents from  $\text{Fe}_{a3}$ , one from  $\text{Cu}_B$ , and the fourth from a nearby tyrosine OH). In the resulting P-intermediate, an oxide ( $\text{O}^{2-}$ ) and a hydroxide ( $\text{OH}^-$ ) are bound to  $\text{Fe}_{a3}$  and  $\text{Cu}_B$ , respectively. Next, the P-intermediate receives four electron equivalents from cytochrome *c* via the low-potential metal sites,  $\text{Cu}_A$  and  $\text{Fe}_a$  (heme *a*). These equivalents are added one at a time, forming the F-, O-, and E-intermediates and ultimately reproducing the R-intermediate [Yamashita and Voth, 2012; Yoshikawa *et al.*, 2012; Yoshikawa and Shimada, 2015].

The assembly pathway of CIV has been extensively studied in human [Nijtmans *et al.*, 1998; Williams *et al.*, 2004] and yeast [Barrientos *et al.*, 2004; Horan *et al.*, 2005], showing that it is very conserved between these organisms, still highlighting the important role of yeast as a model for human proteins [Fontanesi *et al.*, 2006]. Cox2 is translated as a precursor (pCox2) with a N-terminal 15 amino acids extension. It is transported across the membrane and kept in an assembly-competent state by Cox20. Next, Cox1 assembles with the first nuclear-encoded subunits, Cox6 and Cox5. Cox2 is further processed with copper insertion, a necessary prerequisite for the association with the Cox1–Cox5–Cox6 complex. The next step is the association of Cox2 or Cox3 with the Cox1–Cox5–Cox6 complex, it is unknown whether Cox2 is the first subunit associated or it is Cox3. Cox7, Cox8 and Cox9 form a complex prior to their incorporation, mediated by Pet100. The incorporation of Cox12 and Cox13 closes the complex biogenesis (Figure 1.15). See Table 1.3 for the nomenclature in mammals [Mick *et al.*, 2011; Soto *et al.*, 2012].

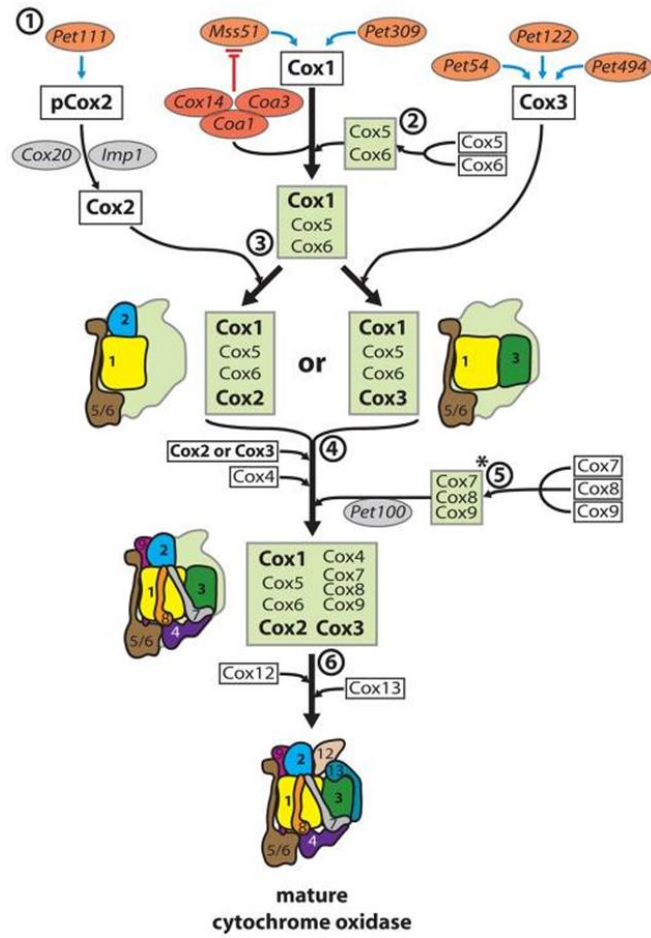


Figure 1.15 Schematic representation of the CIV assembly pathway [from Mick *et al.*, 2011].

| Table 1.3 Nomenclature of CIV subunits |                |
|--|----------------|
| <i>Yeast</i>                           | <i>Mammals</i> |
| <b>mtDNA encoded subunits</b>          |                |
| Cox1                                   | COX1 or MTCO1  |
| Cox2                                   | COX2 or MTCO2  |
| Cox3                                   | COX3 or MTCO3  |
| <b>nDNA encoded subunits</b>           |                |
| Cox4                                   | COX5b          |
| Cox5a and b                            | COX4-1 and -2  |
| Cox6                                   | COX5a          |
| Cox7                                   | COX7a          |
| Cox8                                   | COX7c          |
| Cox9                                   | COX6c          |
| Cox12                                  | COX6b          |
| Cox13                                  | COX6a          |
| -                                      | COX7b          |
| -                                      | COX8           |

Table 1.3 Nomenclature of yeast and mammals CIV subunits.

## 1.4 Reactive oxygen species production by respiratory complexes

The free radical is defined as a chemical specie, an atom or molecule, that has one or more unpaired electrons in valance shell and is capable of existing independently. It can react quickly with other compound, trying to capture the needed electron to gain stability. Generally, free radical attacks the nearest stable molecule, “stealing” its electron [Vishal-Tandon *et al.*, 2005].

The most important free radicals in biological systems are those deriving from partial oxygen reduction. Reactive oxygen species (ROS) are a collective term including oxygen derivatives, either radical or non-radical, that are oxidizing agents and/or are easily converted into radicals. If a single electron is supplied to  $O_2$ , the superoxide radical anion  $O_2^{\cdot-}$  is formed. Addition of another electron to  $O_2^{\cdot-}$  gives the peroxide ion, which is a weak acid that can be protonated to hydrogen peroxide  $H_2O_2$ . Addition of two more electrons splits the molecule producing water  $H_2O$ . If one single electron is added to  $H_2O_2$  by a reduced metal ion (e.g.,  $Fe^{2+}$ ), the hydroxyl radical  $OH\cdot$  is produced by the Fenton reaction. The hydroxyl radical is extremely reactive with a half-life of less than 1ns, thus it reacts close to its site of formation [Genova and Lenaz, 2015].

ROS can increase in cells from exogenous and endogenous sources. Exogenous sources of ROS include UV and visible light, ionizing radiation, drugs, and environmental toxins. Among endogenous sources are many enzymes including the mitochondrial respiratory complexes [Genova and Lenaz, 2015]. In fact the electron transport chain has been recognized as one of the major cellular generators of ROS. In particular, the respiratory CI, CII, and CIII are known to generate ROS through the leak of electrons to molecular oxygen (Figure 1.16) [Hamanaka and Chandel, 2010]. CI has been considered one of the main sites of production of ROS, as also confirmed by recent studies showing that electron leak at CI can release single electrons to oxygen and give rise to the superoxide anion in several types of mitochondria [Lenaz and Genova, 2010]. It is well known that superoxide production by CI is higher during the reverse electron transport from succinate to  $NAD^+$ , whereas during the forward electron transport, it is much lower [Jezek and Hlavatá, 2005]. Rotenone enhances ROS formation during forward electron transfer and inhibits it during reverse electron transfer [Ohnishi *et al.*, 2005]. Several prosthetic groups in the complex have been suggested to be responsible of direct oxygen reduction, such as FMN [Esterházy *et al.*, 2008], the Fe-S cluster N2 [Fato *et al.*, 2009] and the quinone-binding site [Ohnishi *et al.*, 2005]. Also CII is a significant source of ROS

---

either directly, presumably by electron leak from FAD [Moreno-Sánchez *et al.*, 2013] or indirectly through reverse electron transfer from succinate to quinone and back to CI. ROS release by reverse electron transfer primarily occurs at sites upstream of the rotenone inhibition site, as indicated by the prevention of this formation by rotenone. Furthermore, reverse electron transfer is strongly stimulated by high  $\Delta\Psi$ , which thermodynamically allows electron donation from CII to CI [Hirst *et al.*, 2008; Quinlan *et al.*, 2012]. The formation of superoxide in CIII depends on this peculiar mechanism of electron transfer. Since the electron transfer from cytochrome  $b_L$  to  $b_H$  occurs against the electrical gradient, it is strongly retarded when the electrochemical potential is high. This delay prolongs the lifetime of  $Q_O$ , allowing reaction of the semiquinone with  $O_2$ , with superoxide formation. Antimycin A, by blocking quinone reduction by cytochrome  $b_H$  at  $Q_I$  [Jezek and Hlavatá, 2005] also enhances the superoxide production. More recent evidence, however, suggests that the source of the electron to reduce oxygen is the semiquinone formed in the so-called semi-reverse reaction in which cytochrome  $b_L$  reduces the fully oxidized quinone. In fact, superoxide formation is stimulated by the presence of oxidized quinone [Dröse and Brandt, 2008] and by mutations preventing the proximity of the Fe-S cluster of the Rieske protein to the ubiquinone site. This latter condition does not allow an interaction of semiquinone with the Rieske cluster and thus favors its reaction with oxygen [Lanciano *et al.*, 2013; Sarewicz *et al.*, 2010].

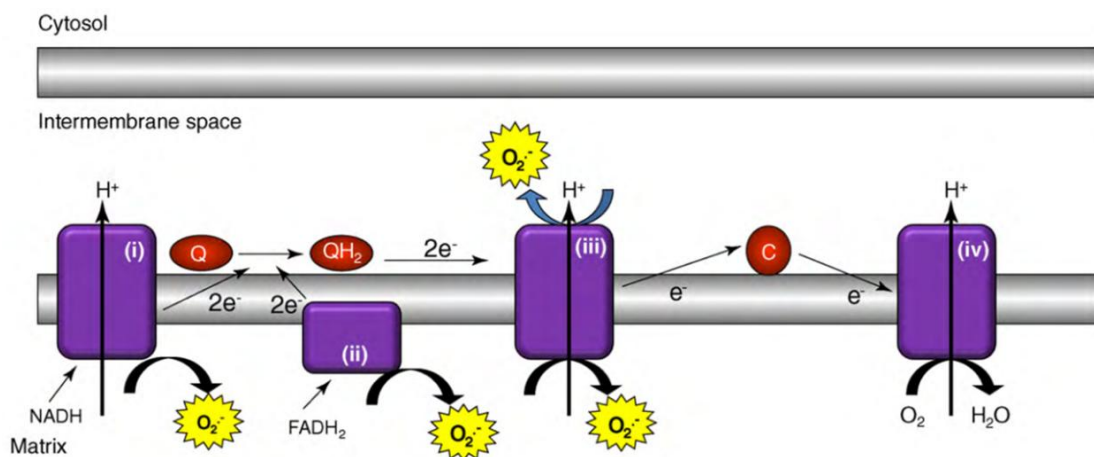


**Figure 1.16** Scheme of superoxide production by CI, CII and CIII [from Hamanaka and Chandel, 2010].

ROS are recognized either as important physiological intracellular signals, affecting the redox state of signaling proteins, and as the major determinants of toxicity in cells and organisms [Genova and Lenaz, 2015]. Indeed, at moderate concentrations ROS act as second messengers by interfering with the expression of a number of signal transduction pathways and genes. Many of the ROS-mediated responses actually protect the cell against oxidative stress and re-establish redox homeostasis. Because ROS are oxidants, they directly influence the redox state of signaling proteins and are suitable for signal transduction. ROS are associated with positive (cell proliferation) or negative responses (cell death). At high concentrations, their accumulation causes oxidative damage within cells. As oxidative damage we intend several modifications which are accumulating with aging, such as protein carbonylation and methionine oxidation, advanced glycation end-products (AGE), lipid peroxidation, and nucleotide modifications. The damage caused by ROS strictly depends on their reactivity. Free radicals can meet each other forming non-radical products or products even more dangerous. A radical can meet a non-radical species generating a new radical and initiating a chain reaction [Lenaz, 2012].

The deleterious effects resulting from ROS overproduction at mitochondrion are prevented by various enzymes and non-enzymatic antioxidant systems. Among the antioxidant enzymes, the superoxide dismutase (SOD) scavenger enzymes convert superoxide radicals into  $H_2O_2$  and molecular oxygen. There are three SOD enzymes expressed in mammalian cells. MnSOD is the mitochondrial antioxidant that exists in homotetramers and localizes in the mitochondrial matrix [Candas and Li, 2014]. The resultant  $H_2O_2$  is largely removed by catalase, glutathione peroxidases and peroxiredoxins (Prx). Catalase converts  $H_2O_2$  into  $O_2$  and  $H_2O$ . It is localized in peroxisomes but it has been detected also in mitochondria of heart and liver of rat. Glutathione peroxidase is the mitochondrial enzyme that utilizes glutathione (GSH) for the reduction of  $H_2O_2$  to  $H_2O$ . Two main forms of glutathione peroxidase exist. The selenoenzyme can be detected in various cellular compartments including the mitochondrial matrix and inter-membrane space. Mitochondrial GSH is important for the maintenance of the appropriate mitochondrial redox environment to avoid or repair oxidative modifications. GSH must be regenerated by glutathione reductase (GR) using NADPH as the reductant [Lenaz, 2012]. Peroxiredoxins (Prx<sub>s</sub>) are a family of enzymes that catalyze the reduction of hydrogen peroxide to water. There are six isoforms of Prx<sub>s</sub>, categorized by their subcellular localization. Prx3 is the isoform found in the mitochondrial matrix together with the Prx5

[Song *et al.*, 2011]. Among the non-enzymatic antioxidant system, there are different molecules such as vitamin C, vitamin E, coenzyme Q, GSH, as introduced above, lipoic acid, uric acid, carotenoids and flavonoids [Lenaz, 2012].

## 1.5 The respiratory supercomplexes

How respiratory complexes are organized in the inner membrane has been an object of intense studies. Chance and Williams were the first to represent the respiratory chain as a solid-state assembly of coenzymes and cytochromes in a protein matrix, with electron transfer occurring between enzymes in very close proximity [Chance and Williams, 1955] and, in 1962, Hatefi observed that CI and CIII preferentially associated during purification of mitochondrial membrane [Hatefi *et al.*, 1962]. Much later, Hackenbrock proposed the fluid or random collision model for the organization of the respiratory chain [Hackenbrock *et al.*, 1986]. In this model, the respiratory complexes are viewed as independent entities embedded in the inner membrane, with CoQ and cytochrome *c* acting as mobile carriers that freely diffuse in the lipid membrane. The random collision model became a widely accepted model for the respiratory chain organization until seminal studies performed in 2000 in mammals and yeast introduced the use of blue native gel electrophoresis (BN-PAGE) to analyze the migration of native protein complexes in digitonin-solubilized mitochondrial membranes [Schägger and Pfeiffer, 2000] and their co-purification by sucrose-gradient centrifugation [Eubel *et al.*, 2004]. These observations led to a reformulation of the solid model, proposing that respiratory complexes are indeed organized in large structures named respiratory supercomplexes (SCs) [Acín-Pérez *et al.*, 2004; Schägger and Pfeiffer, 2000].

Very recently, this model has been implemented in the “plasticity model”, showing that the individual complexes and SCs can coexist within the inner membrane, depending on the different organisms and on the particular metabolic requirements of the cells [Lapiente-Brun *et al.*, 2013]. By monitoring the oxygen consumption in mitochondria in the presence of pyruvate plus malate and succinate together or separately, an additive effect on the respiratory activity was observed when both substrates are present. This effect was not detected when CIII<sub>2</sub>+IV were not assembled [Lapiente-Brun *et al.*, 2013]. Furthermore, it was proposed that the quite huge amount of CoQ present in the inner membrane exists at least as two distinct pools: one dedicated to NADH- and the other one to FAD-dependent enzymes. Conversely, cytochrome *c* is common to both NADH and

FADH enzymes, but it can be found associated with the SCs and also as a pool providing electrons to the free CIV [Enriquez and Lenaz, 2014]. However, the existence of these Q pools has been questioned by the Hirst's group, suggesting the presence of a single Q pool, since they failed to observe any additive effect by fuelling the respiratory activity with different substrates. These authors indeed reported a competition between CI and CII for a common Q pool [Blaza *et al.*, 2014].

### 1.5.1 Structural organization of SCs

During the last years BN-PAGE has been widely used to evaluate the organization of the respiratory complexes, revealing the existence of respiratory SCs in many different systems such as bacteria, fungi, higher plants mitochondria and mammals mitochondria, and suggesting that their organization in supra-molecular assemblies is a common and advantageous feature for OXPHOS systems [Ghelli *et al.*, 2015]. CI, CIII and CIV can associate in three types of SCs (see Figure 1.17). CI can associate with a CIII dimer to form the I+III<sub>2</sub> supercomplex, which is mainly found in plant mitochondria [Bultema *et al.*, 2009; Dudkina *et al.*, 2005a; Peters *et al.*, 2008]. Electron microscopy analysis revealed that the CIII<sub>2</sub> is laterally attached to the membrane arm of CI in its concave portion. In plants and yeast, CIII<sub>2</sub> was found to associate with one or two copies of CIV. The detailed EM analysis revealed that the CIII<sub>2</sub> is flanked from both sides by monomeric CIV [Bultema *et al.*, 2009; Dudkina *et al.*, 2006; Heinemeyer, *et al.*, 2006; Heinemeyer *et al.*, 2007; Krause *et al.*, 2004]. The largest respiratory chain supercomplex is formed by CI, CIII<sub>2</sub> and up to 4 copies of CIV. This is called the *respirasome* because it represents the minimal unit able to perform complete respiration from NADH to oxygen [Schägger and Pfeiffer, 2000]. Studies on bovine respirasome demonstrated that CIII<sub>2</sub> sits in the arc of the membrane arm of CI while CIV is attached to the tip of NADH dehydrogenase [Althoff *et al.*, 2011; Chaban *et al.*, 2014; Dudkina *et al.*, 2011]. Furthermore, there are suggestions that even higher levels of organization may exist (megacomplexes or respiratory strings) which seem to be important for the morphology of the inner mitochondrial membrane [Bultema *et al.*, 2009; Genova and Lenaz, 2014; Wittig and Schägger, 2008]. CII and CV were never found associated with other respiratory complexes [Genova and Lenaz, 2014], with the exception of mitochondria from mouse tissues [Acín-Pérez *et al.*, 2008]. Furthermore, Acín-Pérez and colleagues were able to directly measure the NADH oxidase activity of

bands excised from BN-PAGE by using a Clark electrode, demonstrating that the respirasomes, enriched in CoQ and cytochrome *c*, exhibit respiratory activity and therefore must provide some advantage in electron transfer [Acín-Pérez *et al.*, 2008].

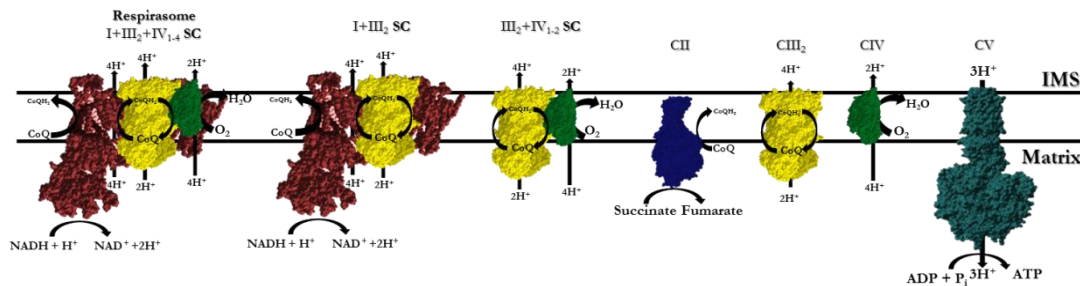


**Figure 1.17** SCs I-III-IV, I-III, III-IV and free complexes in the inner mitochondrial membrane.

### 1.5.2 Advantages of SCs organization

The organization in macromolecular assemblies is predicted to provide functional advantages to the mitochondrial respiratory function [Ghelli *et al.*, 2015].

It was speculated that the specific interaction between complexes to form SCs enhances either electron flow between the enzymes by direct channeling of ubiquinone and cytochrome *c* and catalysis of the enzymes. Evidence for this hypothesis derives from the 3D structure of the I+III<sub>2</sub>+IV<sub>1</sub> SC of bovine mitochondria obtained by electron cryo-microscopy, showing that the quinon-binding sites in CI and in CIII face each other [Althoff *et al.*, 2011]. On the other hand, demonstration of cytochrome *c* channeling is more controversial because of the experimental difficulties to test its functional role in CIII<sub>2</sub>+IV SC, although a portion of CIV has been recently reported to allow the channeling of cytochrome *c* [Lapueute-Brun *et al.*, 2013].

It has been proposed that SCs can limit the extent of superoxide generation by CI and CIII during the electron transfer, reducing the amount of electron leakage, as well as the sequestering of vulnerable sites which protects the complexes from oxidative damage. Indeed, a tighter organization of isolated complexes in SCs may protect auto-oxidizable prosthetic groups, preventing their reaction with oxygen. In accord with this view, it has been recently demonstrated that after impairing the SCs formation, ROS production by CI was strongly increased, suggesting that CI and CIII association prevents superoxide generation [Maranzana *et al.*, 2013]. This is in agreement with the recent finding that

MnSOD directly interacts with the I+III<sub>2</sub>+IV SC, protecting it from oxidative damage [Suthammarak *et al.*, 2013].

Finally, the supercomplex organization seems to be relevant for preserving the stability of CI. It was proposed that CI is bound to CIII under physiologic conditions to preserve its structural integrity and activity [Schägger *et al.*, 2004]. This hypothesis is supported by studies performed by using *in vitro* and *in vivo* models with mutations on the respiratory complexes. Indeed, CI was shown to be very unstable in absence of CIII in mice-derived cells [Acín-Pérez *et al.*, 2004] and to be stabilized by CIII in NDUFS4 subunit knock-out mice [Calvaruso *et al.*, 2012]. Furthermore, the assembly of CI was defective in cells lacking CIII or CIV [D'Aurelio *et al.*, 2006; Diaz *et al.*, 2006; Diaz *et al.*, 2012; Li *et al.*, 2007]. Moreover, it has been reported that dysfunction in CI can destabilize CIII [Budde *et al.*, 2000], but this view is still controversial [Acín-Pérez *et al.*, 2004; Li *et al.*, 2007].

### 1.5.3 SCs assembly and their assembly factors

In the last years, understanding the mechanism of SCs assembly has been the central point of research. So far, two models of SCs assembly have been proposed (Figure 1.18) [Porras and Bai, 2015; Vartak *et al.*, 2013]. The first one hypothesized that SCs assembly follows the assembly of individual respiratory complexes. Indeed, labeling of mitochondrial translational products indicated that there is sequential incorporation of mtDNA-encoded subunits into respective complexes followed by SC assembly [Acín-Pérez *et al.*, 2008]. In contrast, studies in *Neurospora Crassa* showed that CIII<sub>2</sub>+IV can assemble separately from CI, after that, CIII and CIV interact with the membrane arm of CI, this interaction being important for full assembly of CI [Marques *et al.*, 2007]. Recently, Moreno-Lastres and colleagues provided support to this mechanism by depleting the OXPHOS complexes after cell treatment with doxycycline and then monitoring the assembly of complexes by BN-PAGE. It was shown that CI can assemble independently of the 830 kDa, a CI subassembly lacking the NADH dehydrogenase module and additional subunits. At this point CIII and then CIV subunits start binding to the membrane arm of CI, being required for incorporation of the remaining CI catalytic subunits NDUFS4 and NDUFV1. These observations suggested that the SCs assembly precedes the assembly of individual respiratory complexes [Moreno-Lastres *et al.*, 2012].

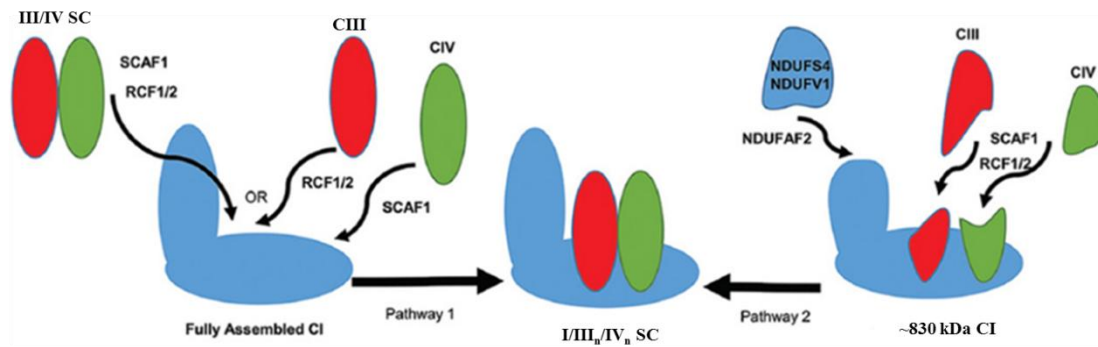


**Figure 1.18** Schematic representation of two possible pathways of SCs assembly and the assembly factors involved [from Porras and Bai, 2015].

Recently, many research groups focused their interest on SCs assembly factors. Several assembly factors for individual CI, CIII and CIV have been identified. Concerning the SCs, two hypotheses have been proposed: i) the presence of exclusive assembly factors that help SCs assembly after individual complexes have been completely assembled or ii) the assembly factors of the different respiratory enzymes are shared [Porras and Bai, 2015; Vartak *et al.*, 2013]. Certainly, it has been demonstrated that cardiolipin, a phospholipid which is almost exclusively found in the inner mitochondrial membranes, is necessary for electron transfer between CI and CIII and essential for the formation of the CIII<sub>2</sub>+IV SC [Bazán *et al.*, 2013]. True chaperones of SC assembly are two proteins named Rcf-1 and Rcf-2. In yeast these proteins were shown to directly interact with CIV and indirectly with CIII. In addition, this latter interaction is necessary for the formation of the CIII<sub>2</sub>+IV SC. The mammalian orthologs of these proteins are the hypoxia-induced genes HIG1A and HIG2A. Knockdown of HIG1A has no effect on the level of SCs, whereas loss of HIG2A reduced the levels of all SCs containing CIV without reduction in the amount of free CIV [Chen *et al.*, 2012; Vukotic *et al.*, 2012]. Another protein considered a SC assembly factor is Cox7a2l (SCAF1; SC assembly factor 1) which was shown to be present in I+III+IV and III+IV SCs, but not in free complexes. Mutations on SCAF1 does not allow the assembly of CIV in SCs [Lapuente-Brun *et al.*, 2013]. Finally, the co-chaperone MCJ/DnaJC15 was demonstrated to act as a negative regulator of SC assembly. This protein, localized in the inner membrane, binds CI and inhibits the formation of SCs [Hatle *et al.*, 2013].

## 1.6 Mitochondrial diseases

The mtDNA is localized in proximity to the inner membrane, near the respiratory complexes where the ROS are routinely produced. As discussed in paragraph 1.1.3, differently of nuclear DNA, mtDNA is not associated to histones whose role is also to protect DNA, thus mtDNA is much more exposed to oxidative damage and more vulnerable to insults. Although many antioxidant systems and DNA repair enzymes exist in mitochondria, it is believed that they are not sufficient to prevent DNA mutation caused by oxidative damage [Cha *et al.*, 2015]. In addition to oxidative damage exposure, the inefficiency of DNA maintenance and replication systems can generate errors, thus inducing mutations [Keogh and Chinnery, 2015]. Owing to this, the mitochondrial genome has a very high mutation rate, 10- to 17-fold higher than that of the nuclear DNA [Tuppen *et al.*, 2010]. The mtDNA alterations can be neutral or pathogenic. Usually, the neutral mutations are polymorphisms which do not alter proteins and are termed haplogroups. The pathogenic mutations (either point mutations or DNA arrangements, such as deletion, duplications or inversions) are associated with disorders termed mitochondrial diseases [Keogh and Chinnery, 2015].

Mitochondrial diseases are a clinically heterogeneous group of disorders that arise as a result of dysfunctions of the respiratory chain [Cha *et al.*, 2015]. The first genetic defect in the human mitochondrial genome were described in 1988 [Holt *et al.*, 1988; Wallace *et al.*, 1988]. Mitochondrial disorders can be caused by mutation in both nuclear DNA genes encoding mitochondrial proteins and in mtDNA genes, encoding protein subunits of OXPHOS complexes and the structural RNAs for their expression. Thus, these pathologies mainly affect tissues with high energy demands. Mitochondrial disorders can affect either a single organ or involve multiple organ systems, with prominent neurologic and myopathic features. Mitochondrial diseases can arise throughout each decade of life [Lightowlers *et al.*, 2015].

Many individuals with mutations of mtDNA often display a cluster of clinical features that fall into a discrete clinical syndrome. However, considerable clinical variability exists and many individuals do not fit neatly into one particular category. As introduced in 1.1.3, the presence of multiple DNA copies causes the homoplasmy and heteroplasmy conditions. These features are important to explain the several phenotypes of mitochondrial disorders. Indeed, the most severe pathogenic mutations associated with mitochondrial disorders are in heteroplasmic condition. The ratio of wild-type to mutant

mtDNA determines the onset of clinical symptoms. A minimum critical proportion of mutated mtDNA is necessary before biochemical defects and tissue dysfunction become apparent (threshold effect). The threshold level varies for each mutation and differs amongst tissues. Typically, the threshold value is in the range of 60%–90% mutant to wild-type mtDNA [D'Aurelio *et al.*, 2006; Keogh and Chinnery, 2015; Tuppen *et al.*, 2010].

Establishing the exact prevalence of mitochondrial diseases is difficult because of the clinical and genetic heterogeneity, a suggested value in children is 6.2/100,000 [Skladal *et al.*, 2003] [Skladal *et al.*, 2003]. Adult mitochondrial diseases, including pathogenic mutations of both genomes, is estimated to be approximately 1 in 4300 [Gorman *et al.*, 2015]. Treating patients with established mitochondrial disease remains a major challenge, at present therapy is limited to either preventing or treating the complications of the diseases [Lightowers *et al.*, 2015].

#### 1.6.1 Mitochondrial diseases associated with CIII

The deficiencies associated with mutations of CIII are the least frequently diagnosed because of the lack of the specific hallmarks. As for all mitochondrial disease, also the CIII deficiencies show different phenotypes. The majority of patients present exercise intolerance, lactic acidosis and involvement of skeletal muscles [Fernández-Vizarra and Zeviani, 2015]. The best known CIII-linked deficiencies are associated with three genes: *MT-CYB* encoding cytochrome *b* [Andreu *et al.*, 1999], the nuclear genes *BCS1L* [de Lonlay *et al.*, 2001], involved in the assembly of CIII, and *UQCRB* [Haut *et al.*, 2003], a subunit of CIII involved in electron transport. In the last years, mutations in seven more CIII-disease nuclear genes have been identified. *UQCRQ* [Barel *et al.*, 2008], *UQCRC2* [Miyake *et al.*, 2013] and *CYC1* [Gaignard *et al.*, 2013], encoding structural subunits of CIII, and *TTC19* [Ghezzi *et al.*, 2011], *LYRM7* [Invernizzi *et al.*, 2013], *UQCC2* [Tucker *et al.*, 2013] and *UQCC3* [Wanschers *et al.*, 2014] which are assembly factor. All mutations in nuclear genes follow an autosomal recessive pattern of inheritance [Fernández-Vizarra and Zeviani, 2015].

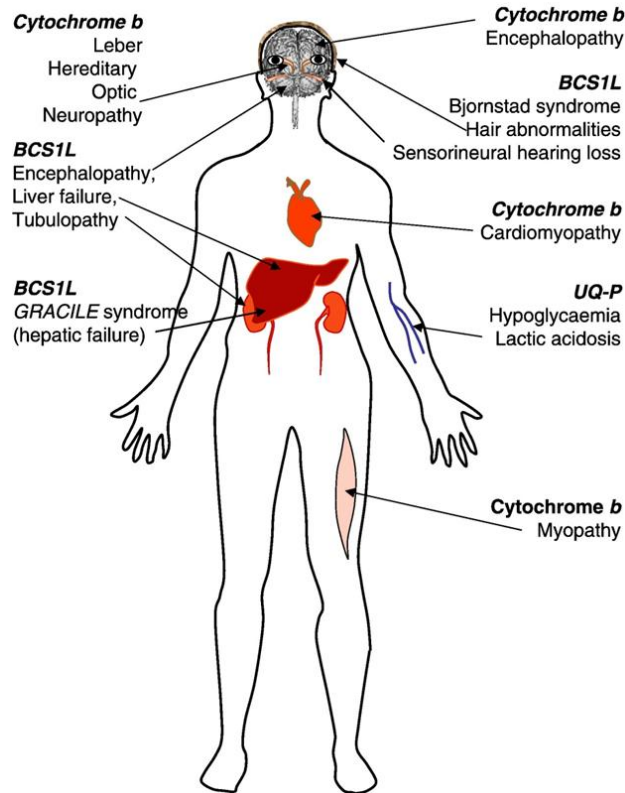


**Figure 1.19** Complex III deficiency in humans [from Bénit *et al.*, 2009].

#### 1.6.1.1 Pathogenic mutations in cytochrome *b*

The *MTCYB* gene exhibits a high level of variance. Although most variations are silent, those affecting critical regions involved in catalytic activity can prove very deleterious [Bénit *et al.*, 2009]. Usually the *MTCYB* mutations are associated with mitochondrial diseases causing myopathy and exercise intolerance; however, some mutations have been described also in patients with specific cancers [Dasgupta *et al.*, 2008; Polyak *et al.*, 1998].

Since 1970, many clinical cases of patients affected by muscle weakness, progressive ataxia, dementia, lactic acidosis and nervous system disorder, have been described, where biochemical studies performed on muscle biopsies revealed a defect on CIII and a lower content in cytochrome *b* [Birch-Machin *et al.*, 1989; Darley-USmar *et al.*, 1983; Hayes *et al.*, 1984; Morgan-Hughes *et al.*, 1982; Spiro *et al.*, 1970]. Given that complete sequencing of mtDNA was not routinely evaluated, most clinical cases were not analyzed at molecular level until 1990s. Since then, many mutations in *MT-CYB* causing CIII-linked disorders have been reported, including frame-shift and termination mutations, deletions, and missense mutations affecting amino acids in the trans-membrane portion of the protein [Meunier *et al.*, 2013]. The most recurrent *MTCYB* mutations are missense

mutations caused by A→G transition as a consequence of oxidative damage. Most of them are heteroplasmic, only one was reported as homoplasmic [Fragaki *et al.*, 2009]. Usually, they are sporadic and often detected in skeletal muscle tissues [Fernández-Vizarra and Zeviani, 2015].

The *MTCYB* missense mutation m.15579A>G, which substitutes Tyr at position 278 with Cys (p.278Y>C) was identified in a patient suffering severe exercise intolerance and multisystem manifestations (deafness, retinitis pigmentosa, cataract, cognitive impairment, growth retardation and epilepsy) [Wibrand *et al.*, 2001]. This mutation caused a dramatic decrease of CIII enzymatic activity and was present in heteroplasmy (88%) in the patient's muscle. Tyr<sup>278</sup> is a highly conserved amino acid, indicating an essential role in the enzymatic function and explaining the severe symptoms of the patient. Several previous studies in bacterial models (*Rhodobacter spheroides* and *Rhodobacter capsulatus*) where the molecular mechanisms involved in CIII electron transfer and catalytic activity have been deeply investigated, have highlighted that specific amino acids at the Q<sub>O</sub> site provided protective mechanisms against CIII oxidative damage [Crofts *et al.*, 2000; Mather *et al.*, 2005]. In particular, the conserved Tyr residue at position 302 of *R. Capsulatus* cytochrome *b*, corresponding to human Tyr<sup>278</sup>, was important, as demonstrated by its substitution with other amino acids. In particular Y302C substitution led to chemical cross-linking of cytochrome *b* to the Fe/S subunit, rendering the bacterial enzyme inactive and sensitive to oxidative disintegration of its catalytic [2Fe/2S] cluster [Lee *et al.*, 2011].

Another *MTCYB* mutation has been recently identified in a female patient suffering a multisystem disease characterized by sensorineural deafness, cataracts, retinal pigmentary dystrophy, dysphagia, postural and gait instability and myopathy with prominent exercise intolerance. The patient was treated at the IRCC Istituto delle Scienze Neurologiche, and DiBINEM, University of Bologna, by Prof. Valerio Carelli. Sequencing of entire mtDNA revealed a microdeletion of 18 bps at position 15649-15666, causing the loss of six amino acids (Ile-Leu-Ala-Met-Ile-Pro) in the protein, but leaving the remaining of the *MTCYB* sequence in frame. The percentage of mutant mDNA was very different in the proband's tissues: close to 50% in muscle and fibroblasts, at a much lower level in urinary epithelium, and not detectable in blood [Carossa *et al.*, 2014].

The detailed analysis of the biochemical alterations associated with *MTCYB* m.15579A>G missense mutation and 18 bps long microdeletion m.15649-15666 are the subjects of this thesis.

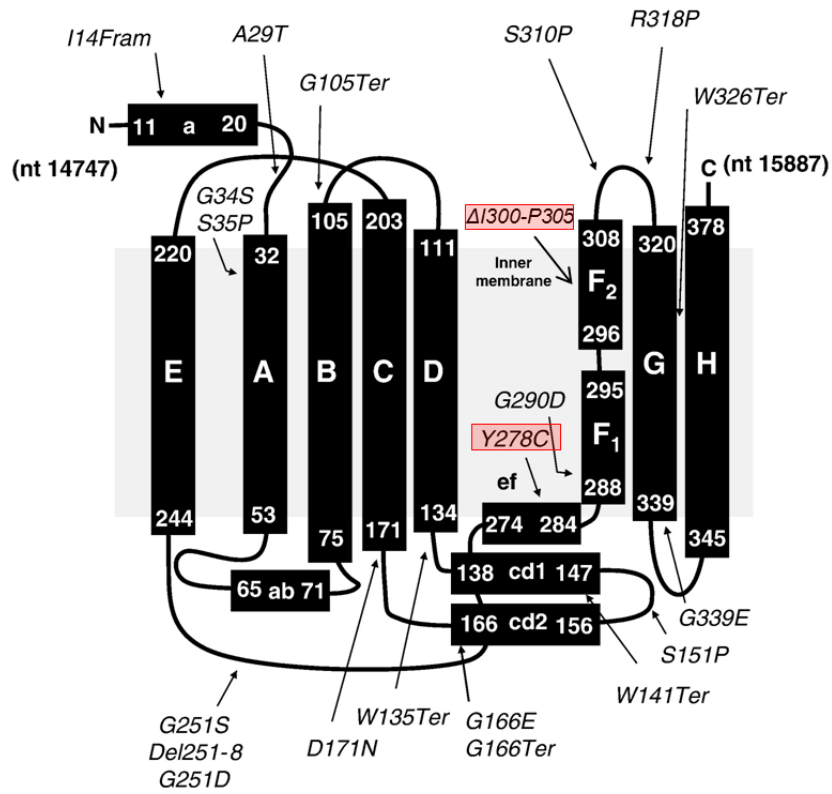


**Figure 1.20** Schematic representation of cytochrome *b* structure, where mutations associated with human diseases are indicated. Most of the trans-membrane domains (A–H) are free from mutations. The red squares highlight the two pathogenic mutations whose effect have been analyzed in this study [modified from Bénit *et al.*, 2009].

Complex III is the central component of the respiratory chain. In eukaryotes only one of the 11 subunits, cytochrome *b*, is encoded by the mtDNA. Cytochrome *b*, together with the Fe/S cluster and cytochrome *c*<sub>1</sub>, constitutes the central catalytic core of CIII, which is conserved from bacteria to mammals. Despite the cytochrome *b* is highly conserved during evolution, many polymorphic variants are found in the *MTCYB* gene sequence. Although most of the variants are silent, those affecting regions crucial for the catalytic activity have proved pathogenic. These mutations, rather rare in comparison with others hitting the mtDNA, are most probably all somatic events detected in skeletal muscle in heteroplasmy, expressing clinically mainly as exercise intolerance and fatigue. The most recurrent mutations are missense mutations caused by A→G transition as a consequence of oxidative damage. *MTCYB* mutations can cause different effects on CIII, impairing the enzymatic activity alone or also compromising its assembly. Moreover, given the strict interdependence of CI and CIII, these mutations can indirectly perturb also the activity and assembly of CI.

The main goal of the present study has been to get detailed information on the kinetics and structural characteristics of CIII and of the CIII containing supercomplexes in cells bearing two different *MTCYB* pathogenic mutations. The first one is a missense mutation causing the substitution of a highly conserved tyrosine with a cysteine at position 278 (m.15579A>G; p.278Y>C). Tyr<sup>278</sup> is close the Q<sub>O</sub> site, where QH<sub>2</sub> oxidation occurs, and it is part of the interaction domain of cytochrome *b* with the Fe/S protein. The p.278Y>C mutation was identified in a female patient with severe exercise intolerance and multisystem manifestations. The second mutation is a novel microdeletion 18 bps long causing the loss of six aminoacids (Ile-Leu-Ala-Met-Ile-Pro) from position 300 to 305 in the sixth transmembrane helix of the protein, but leaving the remaining of the *MTCYB* coding region in frame (Δ15649-15666; ΔI300-P305). ΔI300-P305 was identified in a female patient suffering a severe multisystem disease.

Given that *MTCYB* mutations are rare, it has been a great opportunity to acquire fibroblasts derived from these patients. The biochemical analysis has been carried out taking advantage of a cell model specifically developed to

investigate the mtDNA mutations, the cybrid cell model, that can be generated by fusion of the enucleated patient's fibroblasts with osteosarcoma cells devoid of their own mtDNA (Rho0 cells).

By using a combination of different spectrophotometric assays, the energetic efficiency of cells bearing the two *MTCYB* mutations has been evaluated, determining their viability after a metabolic stress, the redox activity of complexes and supercomplexes, along with their rate of mitochondrial ATP synthesis. Moreover, the pattern of respiratory complexes and supercomplexes has been investigated following their separation by gel electrophoresis under native conditions in the presence of different mild detergents.

Our final aim was to shed light on the mechanisms through which complexes stability and supercomplexes organization can be modified by the presence of defective cytochrome *b*. This issue is important because alterations of the supramolecular organization of respiratory complexes have been suggested to have profound effects on the efficiency of electron transport and, even more relevant, on superoxide generation and consequent oxidative damage. Furthermore, elucidation of these mechanisms might be a first step toward development of more focused therapeutic strategies for treatment of these patients.

# Experimental Procedures

---

## 3.1 Cell Lines and Culture Conditions

To study the effect of the two *MTCYB* mutations, trans-mitochondrial cytoplasmic hybrids (cybrids) were established from patient fibroblasts obtained, after informed consent, from skin biopsies as previously reported [King and Attardi, 1996]. Patient fibroblasts, bearing the mutation of interest, were enucleated by treatment with cytochalasin B followed by centrifugation, to obtain cytoplasts, which are cells lacking nuclei but containing mitochondria, and used to repopulate rho-0 cells, which are osteosarcoma (143B.TK<sup>-</sup>)-derived cells depleted of their own mtDNA. To obtain rho-0 cells, cells deficient in thymidine kinase activity (TK<sup>-</sup>), were exposed to ethidium bromide (EtBr), which is an inhibitor of mtDNA replication. The rho0 cells, which are auxotrophic for uridine and pyruvate (U<sup>-</sup>, P<sup>-</sup>), are repopulated by forming hybrids with cytoplasts from a patient cell line. After fusion, cells are plated in media containing bromodeoxyuridine (+BrdU) and lacking either pyruvate or uridine (-U or -P), which permits only the growth of  $\rho^0$  cells that have fused with cytoplasts containing functional mitochondria (TK<sup>+</sup> donor cells cannot grow in the presence of BrdU). If heteroplasmic cells are used as donors, it is possible to isolate cybrid clones that harbour varying proportions of mutated mtDNAs, ranging from 0% mutant (that is, 100% wild type) to 100% mutant (that is, 0% wild type). Both the parental rho-0 line and homoplasmic cybrid lines harbouring nonsense- or frameshift-mutated mtDNAs must be grown in media supplemented with uridine (+U; ~200  $\mu$ M) and pyruvate (+P; ~1 mM) (Figure 3.1) [King and Attardi, 1996; Schon *et al.*, 2012].

The p.278Y>C patient fibroblasts were heteroplasmic (88%) for the mutation, as well as the  $\Delta$ I300-P305 patient fibroblasts (50%). From the cybridization procedure, several syngeneic clones were obtained; homoplasmic wild-type clones (100% wild-type mtDNA) and homopasmic mutated clones (100% of mutated mtDNA) were selected. For the p.278Y>C mutation several heteroplasmic clones were obtained (58, 78, 96% of mutation load). For the  $\Delta$ I300-P305 microdeletion, only one clone 80% heteroplasmic was obtained.

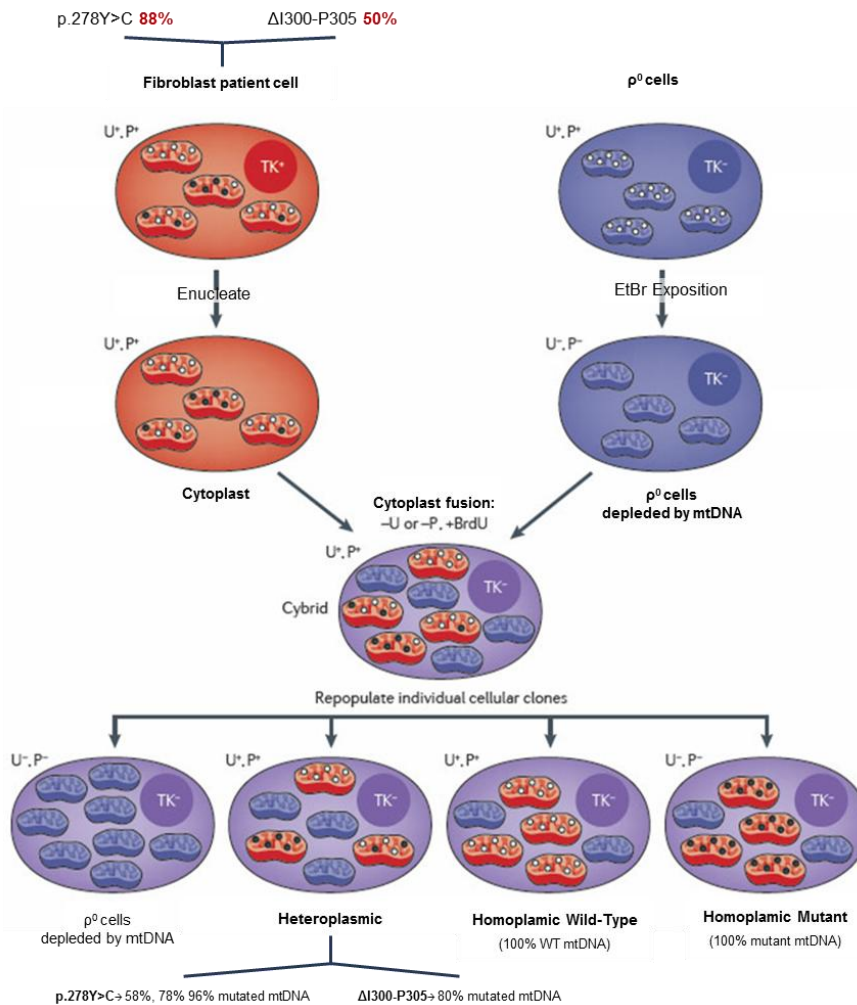


**Figure 3.1** Schematic representation of cybrids construction. The heteroplasmy of p.278Y>C and ΔI300-P305 patient fibroblasts are indicated [modified from Schon *et al.*, 2012].

Patient fibroblasts and wild-type clones were grown in DMEM with 25 mM Glucose (DMEM-HighGlucose) supplemented with 10% FBS, 2 mM L-Glutamine, 100 units/mL Penicillin and 100 μg/mL Streptomycin (all of components were from GIBCO). Mutant cybrids were grown in the same medium supplemented with 50 μg/mL Uridine. Uridine is used in cybrids carrying severe impairment of respiratory chain and in particular for severe mutations in *MTCYB* in order to provide an alternative pathway for pyrimidine synthesis, since the activity of enzyme dihydroorotate dehydrogenase is dependent on quinol oxidation [Evans and Guy, 2004; King and Attardi, 1996]. Cells were grown in an incubator with a humidified atmosphere of 5% CO<sub>2</sub> at 37°C.

In some experiments, cells were incubated with a glucose-free DMEM (DMEM-Galactose) supplemented with 10% FBS, 5 mM Galactose, 5 mM Sodium Pyruvate, 2 mM L-Glutamine, 100 units/mL Penicillin and 100 µg/mL Streptomycin (all components were from GIBCO).

### 3.2 Heteroplasmy Evaluation

Genomic DNA was extracted from wild-type, homoplasmic and heteroplasmic cybrid clones using NucleoSpin®Tissue Kit. To amplify the *MT-CYTB*, polymerase chain reaction (PCR) was performed using 5 ng of the template DNA, 1U of Taq Gold DNA Polymerase (Applied Biosystems), Reaction Buffer, 2.5 mM MgCl<sub>2</sub>, 200 µM Nucleotide Mix 10 nM (Roche), 400 pM of primers forward and reverse (see Table 3.1) in a final volume of 30 µl. Thermocycler was set as shown in Table 3.2. PCR products were first controlled on 2% agarose gel and then eluted in a denaturing high performance liquid chromatography (dHPLC) using a column for ion exchange in reverse phase chromatography that specifically allows separation of nucleic acids. The ion exchange is provided by trimethyl-ammonium acetate (TEAA) which binds both DNA, thanks to its positive charges, and the column with its hydrophobic portion. Analysis was performed at the non-denaturing temperature of 58.7°C for p.278Y>C and 50°C for ΔI300-P305. Difference in the length results in different elution times of PCR products, that finally results in different elution peak. We used a protocol already tested in characterization of heteroplasmy level of another mtDNA mutant [Kurelac *et al.*, 2012].

### 3.3 Mitochondria isolation from cybrid cells

Crude mitochondria were obtained by 15x10<sup>6</sup> cybrids. Cells were suspended in cold isolation buffer containing 200 mM D-Mannitol, 70 mM Sucrose, 1 mM EGTA, 10 mM HEPES, pH 7.6, with protease inhibitor cocktail (Roche) and mechanically homogenized with 50 strokes using a glass-teflon potter in melting ice. Unbroken cells and nuclei were centrifuged at 3000 rpm for 10' at 4°C, and the supernatant, containing mitochondria, was centrifuged at 13000 rpm for 20' at 4°C. The mitochondrial pellet was suspended with cold isolation buffer and stored at -80°C. Protein content was quantified according to Bradford [Bradford, 1976].

Membrane fractions enriched of mitochondrial proteins (mitoplasts) were isolated from cell pellets ( $10 \times 10^6$  cells) using digitonin (final concentration  $50 \mu\text{g}/\text{mL}$ ). Digitonin binds to membrane cholesterol, destabilizing and solubilizing the cellular membranes. The inner membrane, unlike the outer membrane, is almost devoid of cholesterol, therefore digitonin solubilizes cellular membranes, except the inner membrane, which remaining intact can be isolated. Briefly, cells were centrifuged and pellet suspended at a concentration of  $10 \times 10^6$  cells/mL with cold PBS ( $154 \text{ mM NaCl}$ ,  $1 \text{ mM KH}_2\text{PO}_4$ ,  $3 \text{ mM Na}_2\text{HPO}_4$ ), and after addition of digitonin, incubated on ice for 1'. Cold PBS was then added to 2.5- fold dilute the suspension volume, thus interrupting cell permeabilization. The digitonin treatment was repeated until at least 90% of the cells were permeabilized, as detected at the microscope by Trypan blue cell permeabilization. Cells were then centrifuged at 13000 rpm for 15' at  $4^\circ\text{C}$  and the pellet was stored at  $-80^\circ\text{C}$ . Protein content was quantified according to Bradford [Bradford, 1976].

### 3.4 Cellular lysates

$1 \times 10^6$  cells were seeded into 10 cm dish in DMEM-high glucose and after 48h, pelleted and washed in PBS. The pellet was suspended in 150-200  $\mu\text{l}$  lysis buffer (1% Triton X-100, 0.5 mM EDTA, 0.6 mM PMSF, pH 7.4) and protease inhibitor cocktail (Roche). The lysate was incubated on ice for 15', frozen and thawed twice, sonicated in a water-bath for 1' and centrifuged at 13000 rpm for 15' at  $4^\circ\text{C}$ . The supernatant was then collected and protein content was assessed according to Bradford [Bradford, 1976].

### 3.5 Solubilization of mitochondrial membranes

Mitoplasts or crude mitochondria were isolated from cultured cybrids as previously described. Mitochondrial proteins were solubilized by adding 2% n-Dodecyl  $\beta$ -D-maltoside (DDM), left on ice for 10' and centrifuged at 13000 rpm for 15' at  $4^\circ\text{C}$ . Supernatant was kept and protein content was determined.

### 3.6 Cell viability assay

Cell viability was determined by using the colorimetric Sulforhodamine B (SRB) assay. The assay is based on the ability of the SRB dye to bind electrostatically to protein

basic amino acid residues, in a pH dependent manner [Skehan *et al.*, 1990]. Cells (30.000/well) were seeded into 4- or 24-well plates. After 24h, cells were washed twice with PBS and incubated with different media for the times indicated in legends of figures. At the end of incubation, the medium was removed, fresh medium was added together with 10% trichloro-acetic acid, and cells were kept for 1h at 4°C, then washed five times with H<sub>2</sub>O and dried for 1h at room temperature. Cells were stained with 0.4% SRB in 1% acetic acid. Unbound dye was removed with four washes in 1% acetic acid. Bound dye was solubilized by addition of 10 mM Tris pH 10, after mild shaking for 10'. Absorbance was measured at 564 nm by using a micro-plate reader [VICTOR<sup>3</sup> Multilabel Plate Counter (PerkinElmer Life and Analytical Sciences, Zaventem Belgium)].

### 3.7 Mitochondrial ATP synthesis

Mitochondrial ATP synthesis was determined in digitonin-permeabilized cybrids, using a luciferin/luciferase assay (Sigma-Aldrich) and a Bio Orbit 1250 Luminometer, as previously described [Manfredi *et al.*, 2002], with minor modifications [Giorgio *et al.*, 2012].

Briefly, after trypsinization, cells were suspended ( $10 \times 10^6$ /mL) in Buffer A (150 mM KCl, 25 mM Tris-HCl, 2 mM EDTA, 10 mM KH<sub>2</sub>PO<sub>4</sub>, 0.1 mM MgCl<sub>2</sub>, pH 7.4) and one aliquot was taken to measure protein content. Then, cells were permeabilized with 50 µg/mL digitonin for 1' at room temperature in slight agitation. The action of digitonin was blocked by 2.5 fold dilution with Buffer B (Buffer A plus 0.1% BSA). After permeabilization, cells were centrifuged to eliminate digitonin and suspended again in Buffer B at the initial concentration and used to measure ATP synthesis and citrate synthase (CS, see below).

Aliquots of digitonin-permeabilized cells were incubated with the luciferin/luciferase buffer in the presence of substrates of different complexes: 1 mM Pyruvate and 1 mM Malate for CI, and 5 mM Succinate and 5 µM Rotenone for CII. The reaction was started by addition of 100 µM ADP. At the end, 5 µM Oligomycin and 10 µM ATP were added, to inhibit the ATP synthase activity and as an internal standard, respectively. The rate of ATP synthesis was normalized to protein content, and expressed as a ratio of CS activity and as percentage of the activity of untreated cells.

### 3.8 Citrate synthase activity

The activity of CS was evaluated in mitochondria suspended in a buffer containing 125 mM Tris-HCl, 0.1% Triton X-100, 100  $\mu$ M DTNB ( $\epsilon = 13.6 \text{ mM}^{-1}$ ), 300  $\mu$ M Acetyl-CoA, pH 8. The reaction was started by addition of 500  $\mu$ M Oxaloacetate [Trounce *et al.*, 1996] and measured at 412 nm at 30°C with UV-Vis spectrophotometer (V550 Jasco).

### 3.9 Respiratory complexes activities

Crude mitochondria, isolated as described in paragraph 3.3, were used to measure redox activities with a UV-Vis spectrophotometer (V550 Jasco).

For CI and CII activity, spectrophotometric assay was performed at 600nm wavelength, at 37°C and under continuous stirring, by following the 2,6-Dichlorophenolindophenol (DCIP) reduction. Kinetic was calculated using the DCIP molar extinction coefficient ( $19.1 \text{ mM}^{-1}\text{cm}^{-1}$ ). The CIII and CIV activities and combined CI+III and CII+III activities were analyzed with a dual-wavelength spectrophotometer (540 nm-550 nm), at 37 °C and under stirring, following the reduction or oxidation of cytochrome *c* (molar extinction coefficient  $19.1 \text{ mM}^{-1}\text{cm}^{-1}$ ).

25  $\mu$ g of crude mitochondria were used in each assay. The specific activity was measured after subtraction of non-specific activity conducted in a separate assay, adding the specific complex inhibitors at the beginning of the reaction (CI: 1  $\mu$ M Rotenone; CII: 5 mM Malonate; CIII: 1  $\mu$ M Antimycin A; CIV: 300  $\mu$ M KCN; CI+III: 1  $\mu$ M Rotenone and 1  $\mu$ M Antimycin A; CII+III: 5 mM Malonate and 1  $\mu$ M Antimycin A) [Carossa *et al.*, 2014; Ghelli *et al.*, 2013]. For details about reaction components see Table 3.3.

### 3.10 Determination of GSH/GSSG content

GSH and GSSG concentrations of cybrids incubated in DMEM and DMEM-Galactose were measured enzymatically, as described in [Anderson, 1985; Floreani *et al.*, 1997]. Briefly, the assay is based on the determination of a chromophoric product, 2-nitro-5-thiobenzoic acid, resulting from the reaction of 5,5'-dithiobis-(2-nitrobenzoic acid) with GSH. In this reaction, GSH is oxidized to GSSG, which is then reconverted into GSH in

the presence of glutathione reductase and NADPH. The rate of 2-nitro-5-thiobenzoic acid formation is measured spectrophotometrically at 412 nm.

Cells ( $\sim 10 \times 10^6$ ) were washed once with PBS. After collecting an aliquot for protein content determination, cells were treated with 6% metaphosphoric acid. After 10', the acid extract was collected, centrifuged for 5' at 16000 *g* at 4°C, and processed. For total GSH determination, the acid extract was diluted (1:6) in 6% metaphosphoric acid; an aliquot was added to 0.75 mL of  $KP_i$ /EDTA buffer (0.1 M  $KP_i$ , 5 mM EDTA, pH 7.4), 0.7 mM 5,5'-dithiobis-(2-nitrobenzoic acid) and 0.5 mM NADPH. After 3' incubation at 25°C, the reaction was started by addition of 2U glutathione reductase (type III; Sigma; from yeast). Product formation was continuously recorded at 412 nm by using a micro-plate reader [VICTOR<sup>3</sup> Multilabel Plate Counter (PerkinElmer Life and Analytical Sciences, Zaventem Belgium)]. The total amount of GSH in the samples was determined from a calibration line obtained by plotting known amounts of GSH against the rate of absorbance change at  $\lambda_{412}$ . GSH standards were prepared daily in 6% metaphosphoric acid and diluted in  $KP_i$ /EDTA buffer. For GSSG measurement, immediately after preparation, the supernatant of acid extract was treated for derivatization with 2-vinylpyridine at room temperature for 60'. In a typical experiment, 0.15 mL supernatant was treated with 3  $\mu$ L undiluted 2-vinylpyridine. Then 9  $\mu$ L triethanolamine was added. The mixture was vigorously mixed, and the pH was checked; it was generally between 6 and 7. After 60', 0.1 mL aliquots of the samples were assayed by the procedure described above for total GSH measurement. The amount of GSSG was quantified from a standard curve obtained by plotting known amounts of GSSG against the rate of absorbance change. GSH present in the samples was calculated as the difference between total glutathione and GSSG concentrations.

### 3.11 Hydrogen peroxide production analysis

$H_2O_2$  production was determined using 2',7'-dichlorodihydrofluorescein diacetate ( $H_2DCFDA$ ) as previously described [Porcelli *et al.*, 2010].  $H_2DCFDA$  is a cell-permeable non-fluorescent probe converted to highly fluorescent 2',7'-dichlorofluorescein (DCF) after oxidation by hydrogen peroxide.

Briefly, 40.000 cells/well were seeded into 24-well plates. After 24h, cells were incubated for 30' in DMEM without red phenol to avoid interference with  $H_2DCFDA$

fluorescence (DMEM-RedPhe: 25 mM Glucose, 25 mM HEPES pH 7.4, 5 mM Sodium Pyruvate and 2 mM/L L-Glutamine) and then 2 $\mu$ M H<sub>2</sub>DCFDA was added. After 30', the probe was removed, adding fresh medium, and fluorescence was determined ( $\lambda_{ex}$  = 492–495nm;  $\lambda_{em}$  = 517–527nm) using a multilabel plate reader [VICTOR<sup>3</sup> and Analytical Sciences, Zaventem Belgium]. At the end of the experiment, the number of cells present in each well was measured by using the SRB assay (see 3.6 paragraph).

### 3.12 SDS-PAGE

50  $\mu$ g of cellular lysates or 100  $\mu$ g of mitochondrial proteins were diluted in SDS Loading Buffer (60 mM Tris-HCl pH 6.8, 2% SDS, 2.5%  $\beta$ -mercaptoethanol, 0.025% Bromophenol Blue, 5% Glycerol) incubated for 5' at 100°C and loaded on 10% polyacrylamide gels (see Table 3.4). Electrophoresis was performed in SDS-Running Buffer (25 mM Tris, 192 mM Glycine, 3.5 mM SDS, pH ~8.3). Initial voltage was 30V and after ~1h was shifted to 100V.

### 3.13 Respiratory complexes analysis by Blue Native- and Clear Native-PAGE

Fully assembled respiratory complexes were separated through Blue Native-PAGE (BN-PAGE) or Clear Native-PAGE (CN-PAGE) [Wittig *et al.*, 2007]. Mitoplasts were suspended in mitochondrial buffer (750 mM 6-Aminocaproic Acid, 50 mM BisTris, pH 7.0), quantified and solubilized by adding DDM (2.5 mg/mg protein). Afterwards, samples were incubated on ice for 10' and then centrifuged at 13000 rpm for 15' at 4°C. The supernatant containing the mitochondrial proteins was then collected and protein content quantified again.

BN-Sample Buffer (0.5% Serva G Blue in 75 mM 6-Aminocaproic Acid, 5 mM BisTris, 0.05 mM EDTA, pH 7), or CN-Sample Buffer (0.01% Red Ponceaux in 5% Glycerol) was added to 100  $\mu$ g of solubilized mitoplasts and loaded onto a native gel constituted by a gradient of polyacrylamide from 4% to 12%, casted with a gradient mixer and a peristaltic pump (Delta-Pump) (see Table 3.5). For BN-Page it was used Anode Buffer (25 mM Imidazole, pH 7) and Cathode Buffer A (50 mM Tricine, 7.5 mM Imidazole, 0.02% Serva G Blue, pH 7), which was halfway replaced with Cathode Buffer B (50 mM Tricine, 7.5 mM Imidazole, pH 7). For CN-Page it was used Anode Buffer and

CN-Cathode Buffer (50 mM Tricine, 7.5 mM Imidazole, 0.02% DDM, 0.05% NaDOC, pH 7). The electrophoresis was run at 80V.

### **3.14 Supercomplexes analysis by BN-PAGE**

Mitoplasts were suspended in cold PBS and protein content quantified. Mitochondrial suspension was centrifuged at 13000 for 10' at 4°C, suspended (5 mg protein/ml) in supercomplex buffer [150 mM K-Acetate, 30 mM HEPES pH 7.4, 10% (w/v) Glycerol, 1% (w/v) Digitonin and 1 mM PMSF] and incubated for 30' on ice. Suspension was centrifuged at 3000 rpm for 2' at 4°C, then the supernatant collected and Sample Buffer added (0.25% Serva Blue G in 37.5 mM 6-Aminocaproic Acid). Native gel was prepared as described (see paragraph 3.13 and Table 3.5), with a gradient of polyacrylamide from 3% to 12%. Electrophoresis was run at 80V and performed with Anode Buffer and Cathode Buffer A, which was halfway replaced by the Cathode Buffer B.

### **3.15 Complex I In-Gel activity**

After electrophoresis, gels were submerged for 15' at room temperature, in the dark, in a solution containing 2 mM Tris-HCl, 0.5% 3-(4,5-dimethylthiazol-2-yl)-2,5-diphenyltetrazolium bromide (MTT) and 0.02% NADH [Wittig *et al.*, 2007]. Complexes and Supercomplexes containing CI appeared as black bands due to reduction of MTT to tetrazolium salts by NADH oxidation through CI.

### **3.16 Two dimensional blue native/SDS-PAGE**

Lanes, previously separated by BN-PAGE gel, were cut out from the first dimension gel and incubated 90' with a dissociating solution (1% SDS and 0.1%  $\beta$ -mercaptoethanol). Electrophoresis was then performed onto 10% polyacrylamide gel (see Table 3.6) by using Cathode (100 mM Tris-HCl, 100 mM Tricine, 0.1% SDS, pH 8.2) and Anode (200 mM Tris-HCl pH 8.9). Initial voltage was 30V, after ~1h was shifted to 100V.

### **3.17 Super-supercomplex band SDS-PAGE**

Supercomplexes were separated as described in the 3.14. paragraph. At the end of the electrophoresis, the gel was stained overnight in Colloidal Coomassie Blue (10% Ammonium Sulfate, 0.1% Coomassie G-250, 3% Ortho-Phosphoric Acid, 20% Ethanol,

H<sub>2</sub>O up to the final volume) and then de-stained with H<sub>2</sub>O until the bands were clearly visible. The bands at high molecular weights corresponding to the SSC were excised from the gel and separated on a 12% polyacrylamide gel (see Table 3.7). Electrophoresis was performed in Cathode (100 mM Tris-HCl, 100 mM Tricine, 0.1% SDS, pH 8.2) and Anode (200 mM Tris-HCl pH 8.9). Initial voltage was 30V, after ~1h was shifted to 100V.

### 3.18 Western Blotting

Proteins separated on acrylamide gels were transferred on nitrocellulose filters for further analysis with antibodies. Gel was incubated for 5' in Western Transfer Buffer (25 mM Tris, 192 mM Glycine, 0.02% SDS, 20% Methanol, pH ~8.3) together with the Whatman papers and nitrocellulose filters (thickness 0.2 mm, 0.22 mm porosity, BioRad). Sandwiches were composed with two sponges, two Whatman papers, gel and nitrocellulose filter. Full wet transfer was performed at 100V for 1h at 4°C in Western Transfer Buffer.

After transfer, unspecific sites of nitrocellulose were saturated with 5% fat-free milk in Tris-buffered saline (137 mM NaCl, 20 mM Tris-HCl, pH 7.6) with 0.05% Tween (TBS-T) for 1h at room temperature using a rotatory shaking. Nitrocellulose incubation with specific primary antibodies diluted in 5% fat-free milk in TBS-T was carried out overnight at 4°C, or alternatively for 2h at room temperature. The following antibodies were used: Complex I anti-NDUFA9 (Invitrogen, diluted 1:1000) and anti-NDUFS3 (Abcam, diluted 1:2000) antibodies; Complex II anti-SDHA antibody (Invitrogen, diluted 1:10000); Complex III anti-Core2 antibody (Invitrogen, diluted 1:1000); Complex IV anti-CoxIV and Cox5A antibodies (Abcam; diluted 1:1000); anti-Actin antibody (Santa Cruz, diluted 1:500); anti-Catalase antibody (Sigma Aldrich, diluted 1:2000); anti-MnSOD antibody (Upstate, diluted 1:2000); anti-P-Tyr antibody (Sigma Aldrich, diluted 1:2000); anti-Peroxiredoxin3 antibody (ABFrontiers, diluted 1:2000); anti-VDAC antibody (Abcam, diluted 1:1000).

After incubation, nitrocellulose membrane was washed 3 times for 10' with TBS-T and subsequently incubated for 1h with the proper peroxidase-conjugated secondary antibody (anti-mouse or anti-rabbit, Jackson Laboratories, diluted 1:2000 in 5% fat-free milk in TBS-T). After 3 washes in TBS-T, nitrocellulose was soaked for 1' in ECL Western Blot Solution (0.015% H<sub>2</sub>O<sub>2</sub>, 68 µM Coumaric Acid and 1.25 mM Luminol). The emitted light was detected by using the Gel Logic 1500 Imaging System (Kodak).

### 3.19 *In Vitro* mitochondrial translation assay

*In vitro* mitochondrial translation assay was performed in collaboration of Dott. Marina Roberti – Università di Bari. Cells (80% confluent) were washed twice and incubated with methionine/cysteine-free DMEM for 15' at 37°C at 5% CO<sub>2</sub>. Incubation medium was removed and replaced with mL of methionine-free DMEM supplemented with 5% dialyzed serum, 1 mM sodium pyruvate, 2 mM L-glutamine, 96 µg/mL cysteine and 100 µg/mL emetine dihydrochloride. Cells were incubated for 20' at 37°C at 5% CO<sub>2</sub> before addition of 166 µCi/mL [<sup>35</sup>S]-methionine to the culture medium. Labelling was performed for 60' at 37°C at 5% CO<sub>2</sub>, then cells were washed with ice-cold phosphate buffered saline (PBS) and harvested. Cell pellet was suspended in PBS containing 0.1% DDM and 2 U/µL benzonase and incubated on ice for 30'. Then 1% SDS was added and protein quantification was performed using the DC protein assay (Biorad). Protein samples (30 µg) were separated on 10–20% pre-casted SDS-PAGE gels (Invitrogen). Gels were stained with Coomassie Brilliant Blue for 10', destained for 1 hour and scanned. Gels were dried before exposure to a Phosphorimager screen. Radiolabelled proteins were analysed by using a Typhoon™ Phosphorimager system and an ImageQuant software (Molecular Dynamics, GE Healthcare).

### 3.20 *In silico* dynamic simulation for ΔI300-P305 mutation

This analysis was performed in collaboration with the Prof. Alejandro Hockoeppler – Università di Bologna.

PDB file of bovine mitochondrial CIII derived from the crystal structure obtained in 1998 was used to perform *in silico* analysis [Iwata *et al.*, 1998]. Swiss PBD viewer software has been utilized to isolate subunits 6Å closer to the deleted residues (I300-P305) of cytochrome *b* subunit in a single monomer of the entire CIII. Cytochrome *c1*, Sub6, Sub7 and Rieske were the subunits resulting from the operation described above. Residues I300-P305 of cyt *b* were deleted simulating the effect of the patient's microdeletion. Visual Molecular Dynamic software was used to run in vacuum for 10 ps the effect of the microdeletion on the selected subunits.

### 3.21 Statistics

All experiments were repeated at least three times, and the results are presented as the mean  $\pm$  SD, unless otherwise indicated. Statistical analysis was performed using the Student's t-test, with \*P  $\leq$  0.05 or \*\*P  $\leq$  0.01 as the level of significance.

| Table 3.1 Primers                            |  |         |                     |
|--|--|---------|---------------------|
| Mutation                                     | Sequence                               |         | PCR Product         |
| A15579G<br>p.278Y>C                          | 5'-CCGAATGATATTTCCTATTCGTC-3'          | Forward | 114 bp              |
|  | 5'-GGAGGATGGGGATTATTGCT-3'             | Reverse |                     |
| $\Delta$ 15.649-15.666<br>$\Delta$ I300-P305 | 5'-CAAACCTAGGAGGCGTCCTTGCCCTATTACGA-3' | Forward | 170 bp WT gene      |
|  | 5'-ACTGGTTGTCTCCGATTCAGG-3'            | Reverse | 152 bp Mutated gene |

**Table 3.1** The primer sequences and the length PCR products for both of mutations are indicated.

| Table 3.2 Thermocycler settings              |                            |             |      |        |
|--|----------------------------|-------------|------|--------|
| Mutation                                     | Phase                      | Temperature | Time | Cycles |
| A15579G<br>p.278Y>C                          | Initial Denaturation Phase | 94°C        | 5'   | 1      |
|  | Denaturation               | 94°C        | 30"  |        |
|  | Annealing                  | 56°C        | 30"  | 25     |
|  |                            | 60°C        | 30"  |        |
|  | Extention                  | 72°C        | 30"  |        |
| Final Phase Lasting                          | 72°C                       | 7'          | 1    |        |
| $\Delta$ 15.649-15.666<br>$\Delta$ I300-P305 | Initial Denaturation Phase | 95°C        | 5'   | 1      |
|  | Denaturation               | 95°C        | 30"  |        |
|  | Annealing                  | 55°C        | 30"  | 30     |
|  | Extention                  | 72°C        | 30"  |        |
|  | Final Phase Lasting        | 72°C        | 7'   | 1      |

**Table 3.2** The thermocycler settings for both of mutations.

| Table 3.3 Reaction components for Redox Activities measurement   |   |
|--|---|
| <p><b>Complex I</b></p> <p>50 mM KPi pH 7.8<br/>           3.5 mg/mL BSA<br/>           25 µg crude mitochondria<br/>           70 µM DUB<br/>           60 µM DCIP (in 5 mM KPi pH 7.8)<br/>           1 µM Antimycin A</p> <p><b>Starter:</b> 200 µM NADH</p>  | <p><b>Complex IV</b></p> <p>50 mM KPi pH 7.8<br/>           3.5 mg/mL BSA<br/>           1 mM EDTA<br/>           20 µM Cytochrome <i>c</i> Reduced<br/>           1 µM Antimycin A</p> <p><b>Starter:</b> 25 µg crude mitochondria</p>   |
| <p><b>Complex II</b></p> <p>100 mM KPi pH 7.8<br/>           1 mg/mL BSA<br/>           2 mM EDTA<br/>           25 µg crude mitochondria<br/>           200 µM ATP<br/>           50 µM DUB<br/>           80 µM DCIP<br/>           1 µM Antimycin A<br/>           1 µM Rotenone<br/>           300 µM KCN</p> <p><b>Starter:</b> 10 mM Succinate</p> | <p><b>Complex I+III</b></p> <p>50 mM KPi pH 7.8<br/>           3.5 mg/mL BSA<br/>           300 µM KCN<br/>           25 µg crude mitochondria<br/>           20 µM Cytochrome <i>c</i> Oxidized</p> <p><b>Starter:</b> 150 µM NADH</p>   |
| <p><b>Complex III</b></p> <p>50 mM KPi pH 7.8<br/>           3.5 mg/mL BSA<br/>           300 µM KCN<br/>           20 µM Cytochrome <i>c</i> Oxidized<br/>           25 µg crude mitochondria<br/>           1 µM Rotenone<br/>           5 mM Malonate</p> <p><b>Starter:</b> 50 µM DBH<sub>2</sub></p>  | <p><b>Complex II+III</b></p> <p>50 mM KPi pH 7.8<br/>           3.5 mg/mL BSA<br/>           300 µM KCN<br/>           2 mM EDTA<br/>           20 µM Cytochrome <i>c</i> Oxidized<br/>           25 µg crude mitochondria<br/>           1 µM Rotenone</p> <p><b>Starter:</b> 5 mM Succinate</p> |

**Table 3.3** Reaction components for redox activity measurement of complexes and supercomplexes.

## Experimental Procedures

| Table 3.4 SDS-PAGE gel components          |    |                 |                 |
|--|----|-----------------|-----------------|
|  |    | Stacking Gel 5% | Running Gel 10% |
| <b>BAM 30%*</b>                            | mL | 0.4             | 3.33            |
| <b>UGB**</b>                               | mL | 0.61            | -               |
| <b>LGB***</b>                              | mL | -               | 2.67            |
| <b>MilliQ</b>                              | mL | 1.5             | 4               |
| <b>APS 10%</b>                             | μL | 25              | 50              |
| <b>TEMED</b>                               | μL | 10              | 20              |
| *BAM 30%: acrylamide/bis-acrylamide 37:1   |    |                 |                 |
| **UGB: 500 mM Tris-HCl, 14 mM SDS, pH 6.8  |    |                 |                 |
| ***LGB: 1.5 M Tris-HCl, 14 mM SDS, pH= 8.8 |    |                 |                 |

**Table 3.4** Composition of polyacrylamide gel for SDS-Page

| Table 3.5 BN/CN-PAGE gel components                         |    |                 |                 |                |                |                 |
|---|----|-----------------|-----------------|----------------|----------------|-----------------|
|   |    | Stacking Gel 3% | Stacking Gel 4% | Running Gel 3% | Running Gel 4% | Running Gel 12% |
| <b>BAM 40%*</b>   | mL | 0.3             | 0.4             | 0.375          | 0.5            | 1.5             |
| <b>BN-GB3X**</b>  | mL | 1.33            | 1.33            | 1.67           | 1.67           | 1.67            |
| <b>Glycerol</b>   | mL | -               | -               | -              | -              | 0.5             |
| <b>MilliQ</b>   | mL | 2.37            | 2.27            | 3.29           | 2.83           | 1.33            |
| <b>APS 10%</b>  | μL | 80              | 80              | 25             | 25             | 15              |
| <b>Temed</b>  | μL | 8               | 8               | 2.5            | 2.5            | 1.5             |
| *BAM 40%: acrylamide/bis-acrylamide 19:1                    |    |                 |                 |                |                |                 |
| **BN-GB3X: 75 mM Imidazole, 1.5 M 6-Aminocaproic Acid, pH 7 |    |                 |                 |                |                |                 |

**Table 3.5** Composition of polyacrylamide gel for BN/CN-Page.

| Table 3.6 2D BN/SDS-PAGE gel components     |    |                 |                 |
|---|----|-----------------|-----------------|
|   |    | Stacking Gel 4% | Running Gel 10% |
| <b>BAM 30%*</b>                             | mL | 0.533           | 3.33            |
| <b>SDS-GB3X**</b>                           | mL | 1.33            | 3.33            |
| <b>Glycerol 50%</b>                         | mL | -               | 2.1             |
| <b>MilliQ</b>                               | mL | 2.14            | 1.24            |
| <b>APS 10%</b>                              | μL | 100             | 80              |
| <b>Temed</b>                                | μL | 10              | 8               |
| *BAM 30%: acrylamide/bis-acrylamide 37:1    |    |                 |                 |
| **SDS-GB3X: 3 M Tris-HCl, 0.3% SDS, pH 8.45 |    |                 |                 |

**Table 3.6** Composition of polyacrylamide gel for 2D/SDS-Page.

| Table 3.7 SSC-SDS-PAGE gel components |         |                 |                 |
|---------------------------------------|---------|-----------------|-----------------|
|                                       |         | Stacking Gel 4% | Running Gel 12% |
| <b>BAM 30%*</b>                       | mL      | 0.533           | 4               |
| <b>SDS-GB3X**</b>                     | mL      | 1.33            | 3.33            |
| <b>Glycerol 80%</b>                   | mL      | -               | 1.3             |
| <b>MilliQ</b>                         | mL      | 2.14            | 1.4             |
| <b>APS 10%</b>                        | $\mu$ L | 100             | 80              |
| <b>Temed</b>                          | $\mu$ L | 10              | 8               |

\*BAM 30%: acrylamide/bis-acrylamide 37:1  
\*\*SDS-GB3X: 3 M Tris-HCl, 0.3% SDS, pH 8.45

**Table 3.7** Composition of polyacrylamide gel for SSC-SDS-PAGE.

# Results

---

In the present study, the biochemical profile of cells bearing the pathogenic *MTCYB* mutations p.278Y>C and  $\Delta$ I300-P305 was investigated. The p.278Y>C mutation (m.15579A>G) was identified in a female patient with severe exercise intolerance and multisystem manifestations (deafness, retinitis pigmentosa, cataract, cognitive impairment, growth retardation and epilepsy), and it was present in patient's skeletal muscle in heteroplasmy (88%). The mutation causes the substitution of a highly conserved tyrosine with a cysteine at position 278 (Figure 4.1B) [Wibrand *et al.*, 2001]. The tyrosine is close the  $Q_O$  site, where  $QH_2$  oxidation occurs (Figure 4.1A). This residue is part of the docking niche of the iron-sulfur protein subunit of the enzyme and is H-bonded to the backbone of a cysteine residue of this subunit to correctly position its [2Fe-2S] cofactor at the  $Q_O$  site [Lee *et al.*, 2011]. The role of this residue has been deeply studied in bacteria. In particular, it has been shown that the substitution of this conserved residue (Tyr<sup>302</sup> in *R. capsulatus*) with a cysteine led to formation of a chemical cross-linking between cytochrome *b* and the Fe/S subunits, rendering the bacterial enzyme inactive and sensitive to oxidative disintegration of its catalytic [2Fe/2S] cluster [Lee *et al.*, 2011].

The  $\Delta$ I300-P305 ( $\Delta$ 15649-15666) is a novel mutation identified in a female patient with a heteroplasmy close to 50% in muscle and fibroblasts. The patient suffered of a multisystem disease characterized by sensorineural deafness, cataracts, retinal pigmentary dystrophy, dysphagia, postural and gait instability and myopathy with prominent exercise intolerance. The mutation causes a deletion of 18 bps and consequently the loss of six aminoacids (Ile-Leu-Ala-Met-Ile-Pro) from the position 300 to 305 in the sixth trans membrane helix of the protein (Figure 4.1A and B), but leaving the remaining of the cytochrome *b* sequence in frame [Carossa *et al.*, 2014].

To evaluate in detail the biochemical alterations associated with the two *MTCYB* mutations, we took advantage of the cybrid clones generated from the patient's fibroblasts [King and Attardi, 1996]. For more details see paragraph 3.1 of Experimental Procedures. Cybrid clones were obtained by the fusion of enucleated patient fibroblasts bearing the mutation of interest with 143B.TK<sup>-</sup> osteosarcoma cells depleted by their own mtDNA (Rho0 cells). Cybrids are a useful tool in studying mtDNA mutations,

since they allow assaying the donor mitochondrial function in a “standard” nuclear background, thus excluding nuclear influences and variables. In general, from the cybridization process of each mutation, several syngeneic clones were obtained harboring various percentage of mutated mtDNA, so that the mutant cell line can be compared with a control cell line bearing the 100% of its own wild-type mtDNA.

Homoplasmic wild-type clones (100% wild-type mtDNA) and homoplasmic mutated clones (100% of mutated mtDNA) were selected for the present studies. For the p.278Y>C mutation several heteroplasmic clones were obtained from the cybridation procedure (58, 78, 96% of mutation load). For the  $\Delta$ I300-P305 microdeletion, only one clone 80% heteroplasmic was obtained. The level of heteroplasmy was evaluated by PCR, amplifying *MT-CYB* gene and then using denaturing high-performance liquid chromatography (DHPLC) [Kurelac *et al.*, 2012], as described in Experimental Procedures.

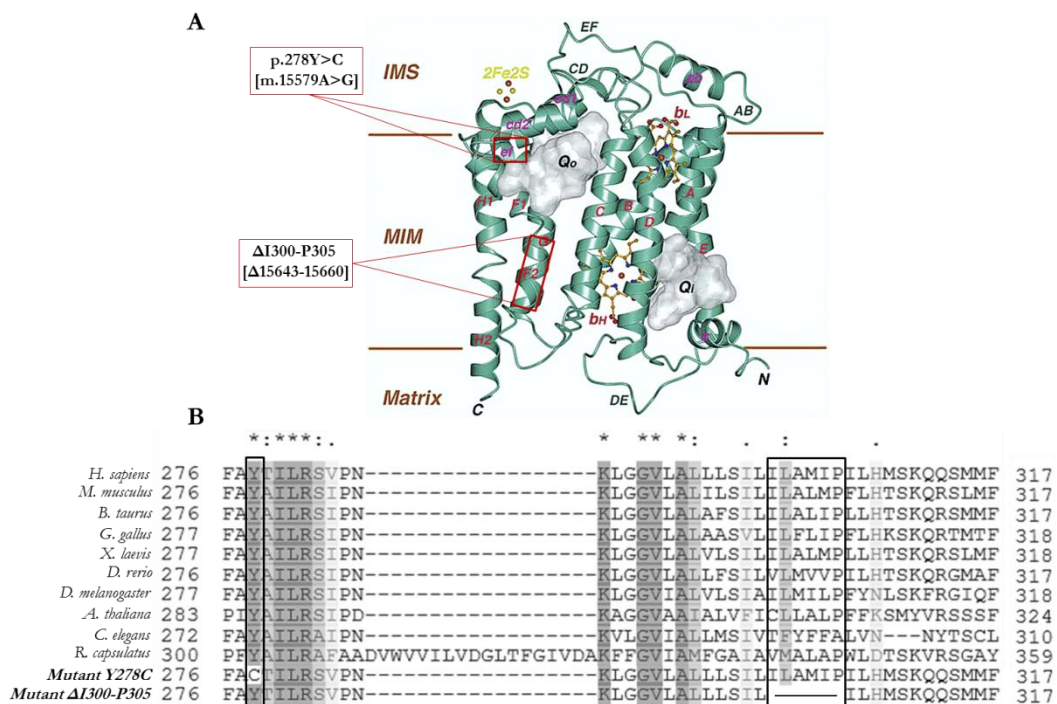


**Figure 4.1** (A) Representation of cytochrome *b* protein structure. The position of p.278Y>C and  $\Delta$ I300-P305 mutations are indicated [modified from Gao *et al.*, 2003]. (B) Cytochrome *b* protein sequence alignment of p.278Y>C and  $\Delta$ I300-P305 mutations in different organisms.

#### 4.1 Viability of cybrids bearing the *MTCYB* mutations after metabolic stress

The effect of the p.278Y>C and  $\Delta$ I300-P305 mutations on the mitochondrial energetic function was first investigated by measuring the viability of cybrid clones during incubation in a glucose-free medium containing galactose and pyruvate [DMEM-galactose]. Under these conditions, the rate of glycolysis is markedly reduced, and cells are forced to rely solely on OXPHOS for ATP production [Robinson, 1996]. Figure 4.2, panel A, illustrates the data obtained in cells bearing the p.278Y>C mutation. The viability of the homoplasmic mutated clone was dramatically decreased compared with control cybrids after 16–24 hours of incubation in DMEM-galactose. Conversely, all the heteroplasmic clones were not significantly different from wild-type cybrids. On the basis of these results, our subsequent studies were performed in the homoplasmic 100% mutant clone only.

In Figure 4.2, panel B, the results of analysis carried out in cybrids with the  $\Delta$ I300-P305 microdeletion are reported. Already after 6 hours of incubation in DMEM-galactose, less than 20% of the homoplasmic mutant cybrids were still viable. Conversely, approximately 70% of the heteroplasmic cybrids were still viable after 24 hours of incubation in DMEM-galactose, being significantly different from control cybrids. These findings clearly indicate that the  $\Delta$ I300-P305 deletion is very detrimental when homoplasmic and that the presence of 80% mutated gene can affect OXPHOS efficiency. From these results we decided, in the case of the  $\Delta$ I300-P305 deletion, to carry out further experiments in the homoplasmic and 80% heteroplasmic clones.

It is apparent in Figure 4.2 that the viability in DMEM-galactose is different in the two control cybrids (panel A *versus* panel B). As described above, the control cybrids were obtained through the cybridation of fibroblasts derived from the two patients, each with its own mtDNA, characterized by a specific variability mainly due to the polymorphisms present in the mtDNA sequence. The mtDNA haplogroup of patient bearing the p.278Y>C mutation was X2c, whereas that of patient with the  $\Delta$ I300-P305 microdeletion was T2c1. This difference can explain the different viability shown by the two control cell lines.

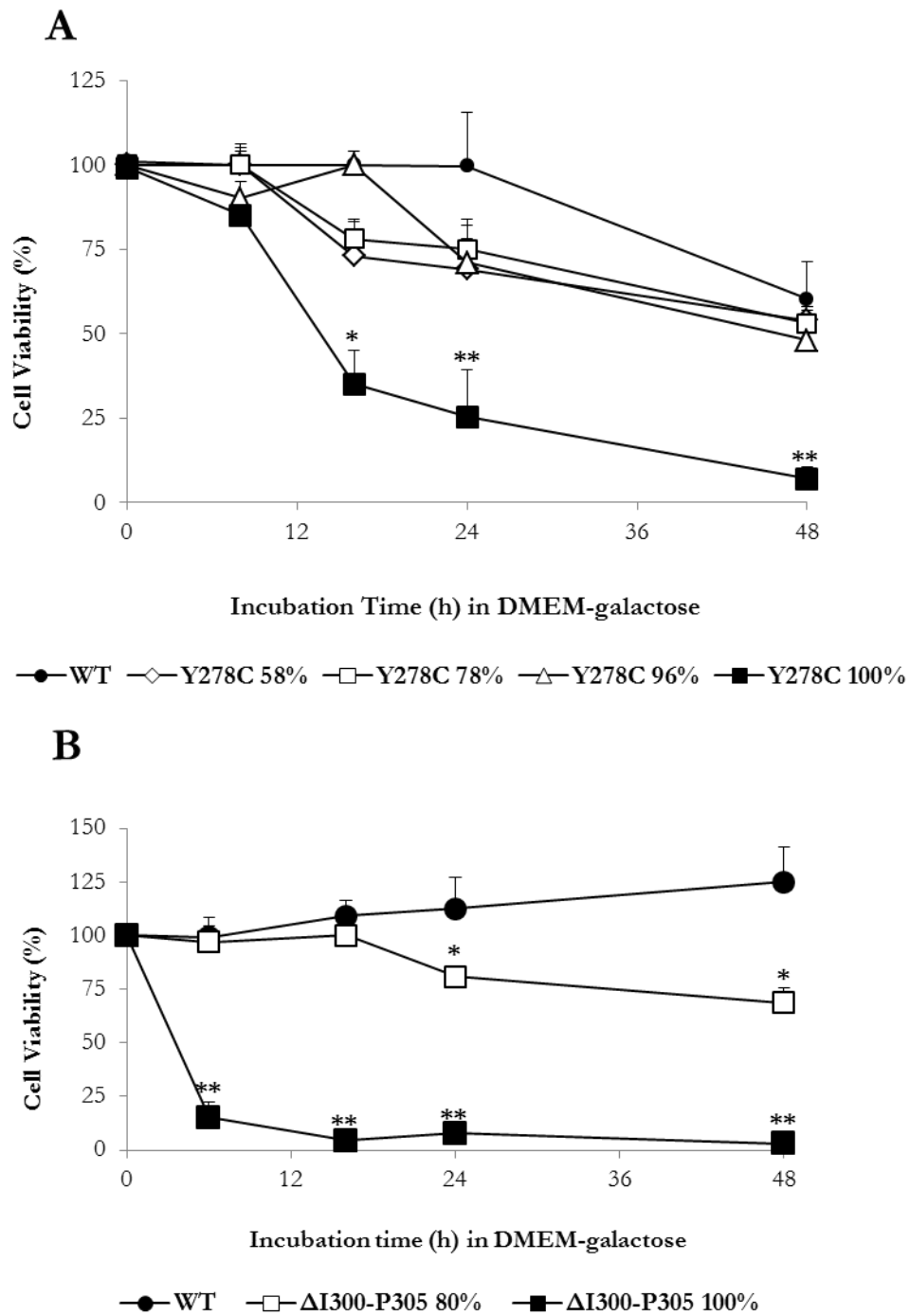


**Figure 4.2** Time course of cell viability in DMEM-galactose. (A) p.278Y>C and (B) ΔI300-P305; the mutation load of each clone is indicated in the legend. The SRB absorbance value at time zero corresponds to 100% viable cells. Each data point represents mean  $\pm$  SEM of at least three experiments ( $P^* \leq 0.05$ ;  $P^{**} \leq 0.01$ ).

## 4.2 Expression level of respiratory complex subunits

We then inquired whether the p.278Y>C and  $\Delta$ I300-P305 mutations alter the steady-state expression level of respiratory complex subunits. Crude mitochondria were isolated from cybrid clones and separated on SDS-PAGE using a 12% acrylamide gel, as described in Experimental Procedures. As reported in Figure 4.3, the levels of representative subunits of different complexes were similar in control cybrids and in cybrids bearing the p.278Y>C mutation, ruling out a reduction of respiratory complexes. Conversely, representative subunits of both CI and CIII were significantly reduced in the homoplasmic cybrids with  $\Delta$ I300-P305 deletion and also in the heteroplasmic cybrids the expression of CIII-Core2 subunit was decreased. It follows that the *MTCYB* microdeletion markedly affects the amount of CIII in the heteroplasmic clone and the content of both CI and CIII in the homoplasmic clone.

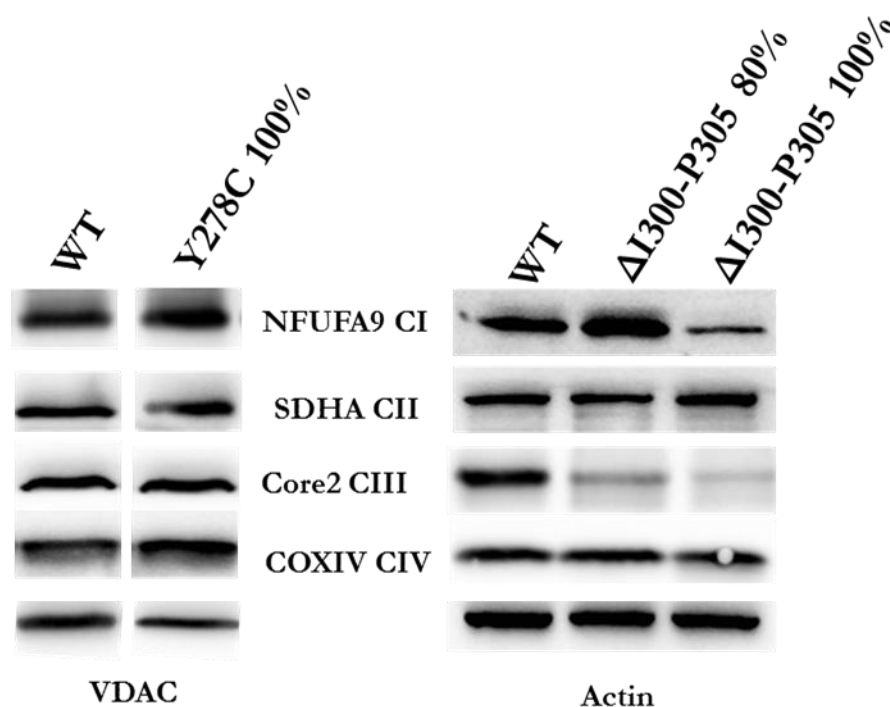


**Figure 4.3** Expression level of representative respiratory complexes subunits in mitochondria isolated from the indicated cybrids. Mitochondrial proteins were separated by SDS-PAGE and western blot analysis carried out using the antibodies against NDUFA9-CI, SDHA-CII, Core2-CIII and CoxIV-CIV. VDAC and actin were used for protein content normalization.

Given that the  $\Delta$ I300-P305 mutation causes the loss of six amino acids in the protein, but leaves the remaining sequence in frame, we questioned whether the mutated cytochrome *b* was translated or not. To address this question, cells were labeled with  $^{35}\text{S}$ -

methionine to identify mitochondrially synthesized proteins. Figure 4.4A shows that the homoplasmic mutant clone still expressed cytochrome *b* though at lower amount (about 50-60%, Figure 4.4B) compared with control, after normalization for total protein loaded (Coomassie staining, on the top of panel). A significant reduction was also apparent in the level of other mitochondrially encoded subunits of CI and CIV, whereas ATP6 and ATP8 subunits of CV were not changed (Figure 4.4A and B). Noticeably, in the heteroplasmic clone a general increase of mitochondrial protein level, and also of cytochrome *b*, was observed, in agreement with a possible compensatory effect. These results indicate that despite the loss of six amino acids, a certain amount of cytochrome *b* is still expressed.

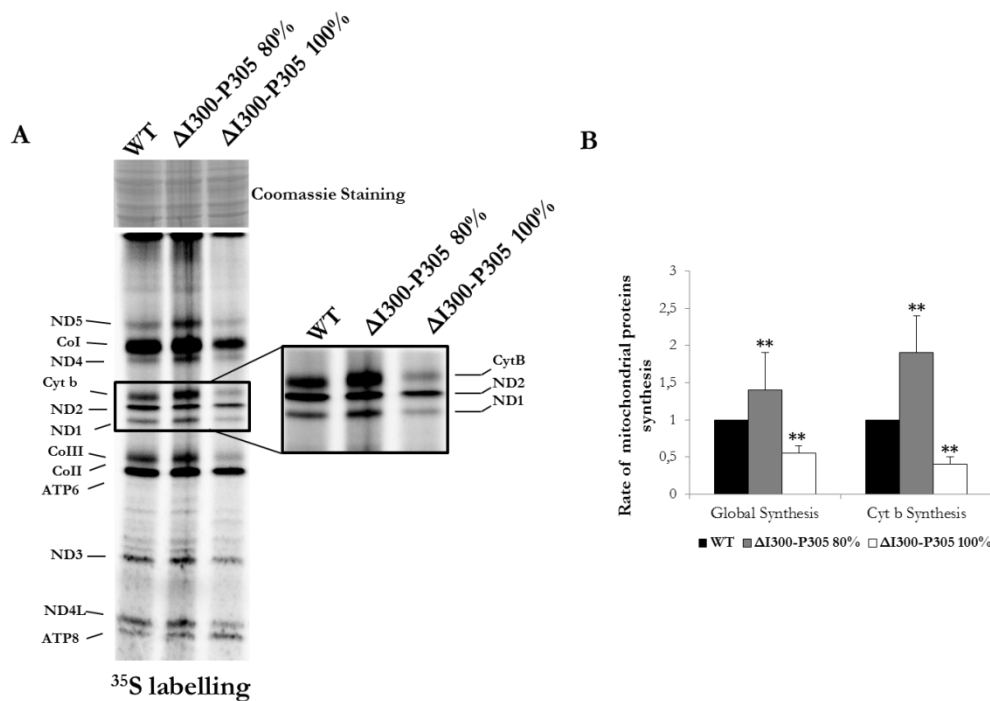


**Figure 4.4** Mitochondrial *in vitro* translation. (A) The autoradiogram displaying the radiolabeled mitochondrial translation products and the respective Coomassie stained gel, as a control for loading, are shown, with magnification of the area containing cytochrome *b*. (B) Rate of the global mitochondrial proteins and cytochrome *b* synthesis. Each data point represents mean  $\pm$  SD of two experiments ( $P^{**} \leq 0.01$ ).

### 4.3 Molecular dynamic simulation of $\Delta$ I300-P305 mutation

Given that cytochrome *b* plays a key role in the first assembly step of the mature CIII, we decided to define the predicted structure of the  $\Delta$ I300-P305 cytochrome *b* and its putative effect on the assembly of the entire CIII. To this purpose, we used a variety of

bioinformatics programs, as described in Experimental Procedures, to remove the deleted aminoacids from the PDB file based on the crystal structure of the entire CIII in *Bos taurus* obtained by Iwata and colleagues in 1998 [Iwata *et al.*, 1998], and isolated the  $\alpha$ -helices of the neighboring subunits.

The entire mutated cytochrome *b* along with cytochrome *c*, Rieske protein, subunits 6 and 7 were tested in a simulation run *in silico* for 10ps in vacuum to evaluate the reorganization of mutated protein in comparison with wild-type. The microdeletion causes the shortening of the sixth trans-membrane  $\alpha$ -helix; as a result the neighboring loop, including some hydrophilic aminoacids, becomes longer and gives more mobility to the structure, being the subunit less stable within the membrane. The four cytochrome *b*  $\alpha$ -helices that form the bundle coordinating the prosthetic groups heme  $b_H$  and heme  $b_L$  (in blue-green, Figure 4.5, right panel) seem not to be involved in the general re-arrangement of the protein, suggesting that it might be still functional. The most significant change regards the adjacent subunits, being their position quite different from the wild-type, likely influencing the structure of the entire CIII. This simulation only provides us a general view of structure, being run *in vacuum*, so we cannot rule out a protective effect of the membrane, in particular of cardiolipin, the mitochondrial phospholipid hallmark, which has been recently reported to be present with a stoichiometry of at least eight molecules per CIII [Bazán *et al.*, 2013]. In addition, CIII does not exist in the inner mitochondrial membrane only as a dimer, but it is also associated within SCs with CI and CIV; the interaction with other respiratory enzymes can stabilize the CIII at least in that forms.

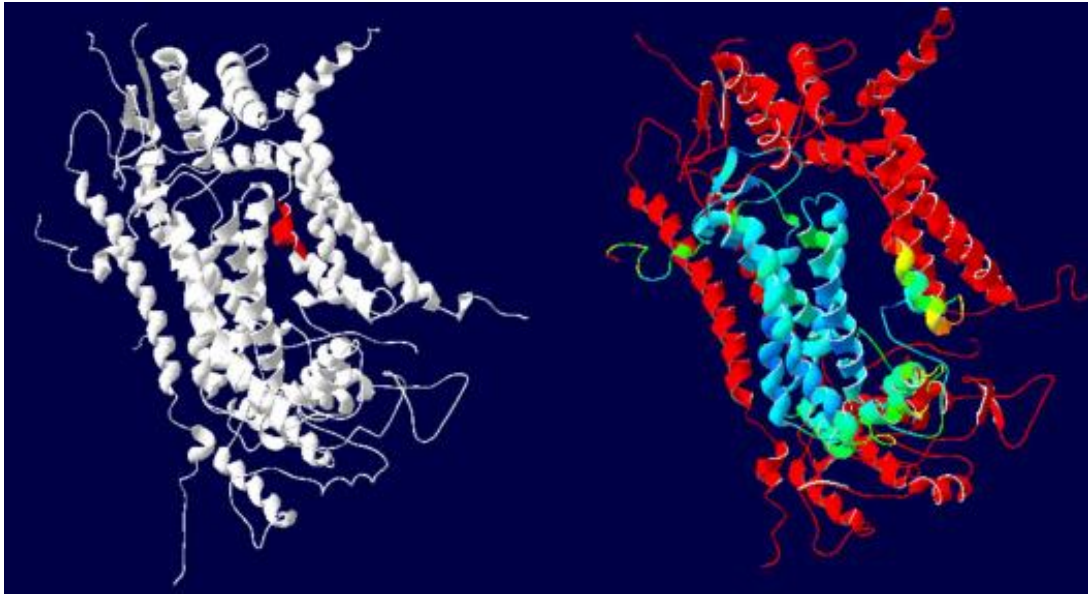


**Figure 4.5** *In silico* simulation of the mutated protein re-organization. **Left:** structure of wild-type subunits (Cyt *b*, Cyt *c*, Sub6, Sub7 and Rieske protein) within CIII<sub>2</sub>, the amino acids deleted in the mutant are evidenced in red. **Right:** simulation of the structure changes in mutated cytochrome *b*. Blue and green colors represent the unchanged residues compared to WT, red residues represent residues that have been rearranged after the simulation.

#### 4.4 Analysis of respiratory complexes assembly and activity

The assembly and activity of the respiratory chain complexes were then investigated. Figure 4.6 shows the assembly of respiratory complexes, analyzed by using BN-PAGE of mitoplasts treated with 2% dodecyl-maltoside (DDM), a detergent which completely dispersed the respiratory supercomplexes [Nijtmans *et al.*, 2002].

The p.278Y>C mutated clones did not show any significant difference compared with control cells, when normalized to the amount of CII, except for the absence of the CIII<sub>2</sub>+IV SC. Given the strong interactions between CIII<sub>2</sub> and CIV, the CIII<sub>2</sub>+IV SC was detected also in the presence of DDM, as apparent in the wild type clone. It seems therefore that the missense mutation did not affect CIII<sub>2</sub> assembly, but rather weakened the CIII<sub>2</sub> and IV interaction.

In the  $\Delta$ I300-P305 homoplasmic mutated clone, the level of a representative subunit of CI, as well as the CI-In Gel Activity, were almost not detectable, whereas no significant difference was observed in the heteroplasmic compared with control clone. Furthermore, no band corresponding to CIII<sub>2</sub> and the CIII<sub>2</sub>+IV SC was detected in the homoplasmic mutant clone, while in heteroplasmic cells only the band corresponding to CIII<sub>2</sub> was present. The amount of assembled CIV and CII was normal in the homoplasmic mutant

clones and even increased in heteroplasmic cells, in agreement with the results of the *in vitro* translation experiments (Figure 4.4A and B; Figure 4.6). These results suggest that when mutant cytochrome *b* only is present, the assembly of both CIII<sub>2</sub> and CI is affected, whereas, when both mutant and wild-type proteins are expressed, the formation of the CIII<sub>2</sub>+IV SC only is compromised.

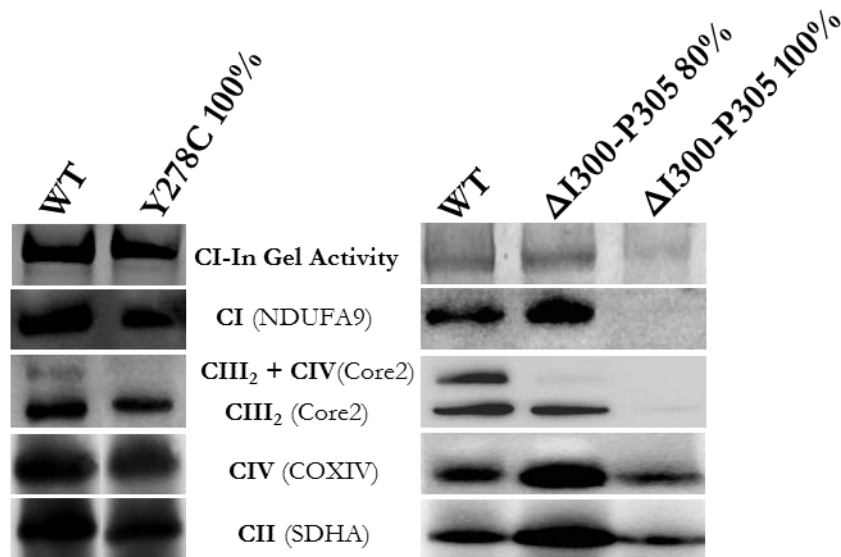


**Figure 4.6** Analysis of respiratory complexes assembly in crude mitochondria. BN-PAGE of p.278Y>C and ΔI300-P305 mitoplasts, in the presence of 2% DDM; for the western-blot analysis, antibodies against NDUFA9-CI, SHDA-CII, Core2-CIII and CoxIV-CIV were used.

Figures 4.7A and B report the p.278Y>C and ΔI300-P305 respiratory complexes redox activities, measured in crude mitochondria, as described in Experimental Procedures. In mitochondria with the p.278Y>C mutation, CIII specific redox activity was almost completely lost when compared with control, while the redox activity of CI, CII and CIV was not affected (Figure 4.7A).

As shown in the Figure 4.7B, the ΔI300-P305 heteroplasmic clone displayed a significant reduction of CIII and CIV redox activities, while the homoplasmic mutant clone exhibited a significant decrease in CI, III, and IV activities, suggesting a more general effect of this *MTCYB* mutation on the respiratory chain activity. Remarkably, a significantly increase in CII redox activity was detected in the homoplasmic clones.

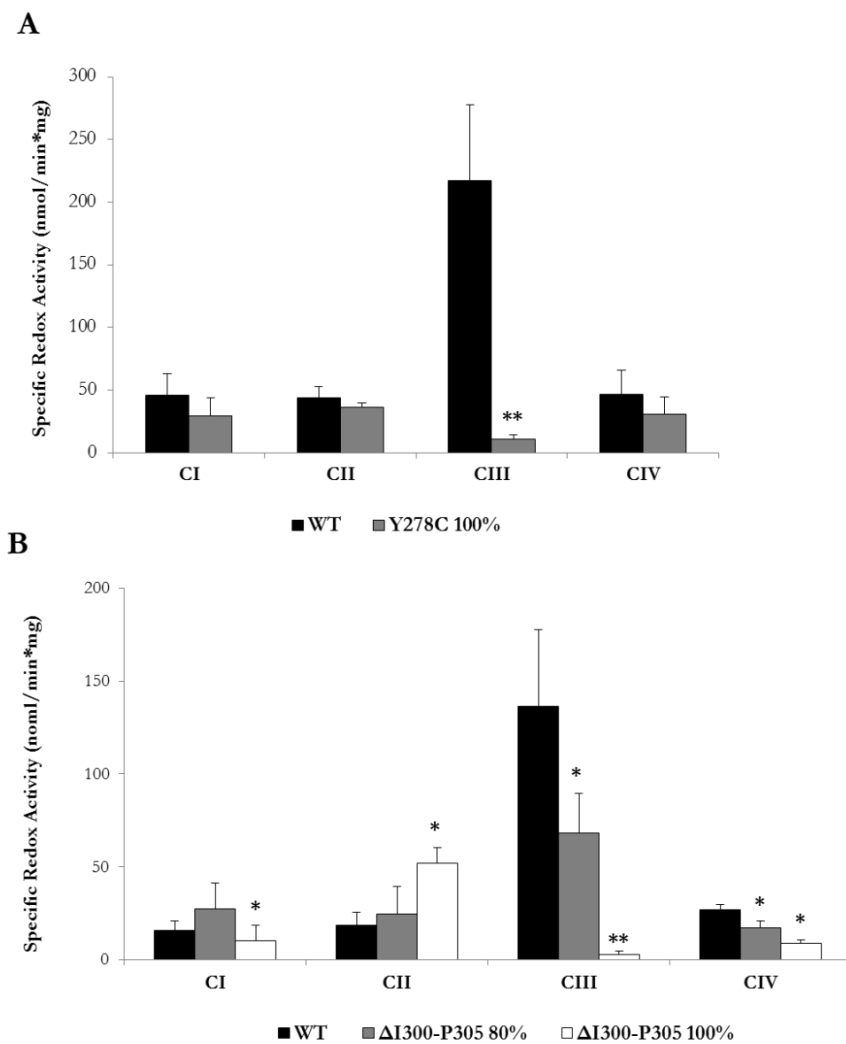


**Figure 4.7** Analysis of the respiratory complexes redox activity in crude mitochondria. Measurement of CI, CII, CIII and CIV redox activity in p.278Y>C (**A**) and in  $\Delta$ I300-P305 (**B**). Each data point represents the mean  $\pm$  SD of at least three experiments ( $P^* \leq 0.05$ ;  $P^{**} \leq 0.01$ ).

#### 4.5 Analysis of the respiratory complexes supramolecular organization

We also examined the supramolecular organization of the respiratory complexes in cybrids bearing the two *MTCYB* mutations. Figures 4.8 and 4.9 show the SCs assembly of p.278Y>C and  $\Delta$ I300-P305 mitoplasts solubilized with digitonin, a mild detergent which keeps intact loose interactions among complexes [Schägger and Pfeiffer, 2000], by measuring the CI-In Gel Activity after Blue Native-PAGE (BN-PAGE) and performing western blotting after two dimensional BN/SDS-PAGE (2D BN/SDS-PAGE).

In p.278Y>C mitoplasts, the CI-In Gel Activity was slightly increased in the band corresponding to the CI+III<sub>2</sub>+IV SC while the other CI-containing SCs were similar to

control (Figure 4.8A). The 2D BN/SDS-PAGE analysis showed a similar behavior, and in addition evidenced that the spots corresponding to the  $\text{CIII}_2$  and the  $\text{CIII}_2+\text{IV}$  SC were reduced when compared with control cells (Figure 4.8B). These findings suggest that the p.278Y>C *MTCYB* mutation only slightly affect the organization of respiratory complexes into SCs.

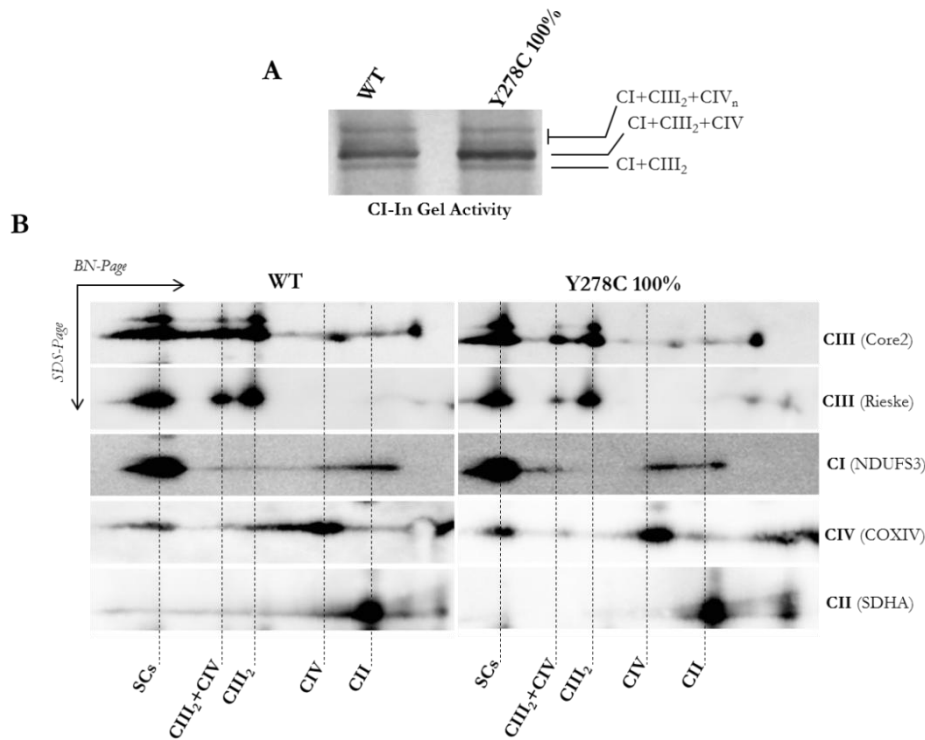


**Figure 4.8** BN-PAGE analysis of SCs in digitonin-treated mitoplasts from cybrids bearing the p.278Y>C mutation. **(A)** CI-In Gel Activity; **(B)** 2D BN/SDS-PAGE followed by western-blot; antibodies against NDUFS3-CI, SDHA-CII, Core2/Rieske-CIII and CoxIV-CIV were used.

In Figure 4.9A, a representative gel of CI-In Gel Activity of mitoplasts obtained from cybrids with the  $\Delta\text{I300-P-305}$  deletion is reported. It is apparent that the band corresponding to the  $\text{CI-CIII}_2$  SC is detected in all clones, indicating that its assembly is preserved also in homoplasmic mutant cells, despite the strong reduction of CI and CIII levels. Furthermore, it is clear that the other SCs containing various amounts of CI,  $\text{III}_2$  and IV were similar in control and heteroplasmic clones, but not present in the homoplasmic mutant clone. These results were also confirmed by performing 2D BN/SDS-PAGE as shown in the Figure 4.9B. Moreover, the spots corresponding to  $\text{CIII}_2$  and  $\text{CIII}_2+\text{IV}$  SC were reduced in the heteroplasmic clone and almost abolished in the homoplasmic clone, in agreement with the results obtained with the isolated complexes. In addition, the mutant clones showed a peculiar high molecular weight supercomplex (called

super-supercomplex, SSC), which was enzymatically active, as demonstrated by the CI-In Gel Activity (Figure 4.9A), and contained CIII and CI (Figure 4.9B). To better evaluate the composition of the SSC, we excised the bands corresponding to SSC from the gels of both mutated clones and from the apparently empty gel of the control clone. Then, we run the bands on SDS-PAGE and performed western blot for representative subunits of the three complexes. Figure 4.10 shows that in all clones the bands were positive to CIII and CIV, whereas CI was detected in mutant clones only. The presence of CIII and CIV also in the wild-type clone may be due to the presence of SC with different CIII/CIV stoichiometry, much more abundant than CI, as reported by others [D'Aurelio *et al.*, 2006; Schägger, 2002].

Altogether the results obtained in complexes/SCs analysis allow us to conclude that  $\Delta I300-P305$  microdeletion causes the almost complete disassembly of CIII and CI as well as re-organization of SCs, with formation of very high molecular weight aggregate. However, also in the homoplasmic mutant clone, the CI and CIII interaction is still preserved.

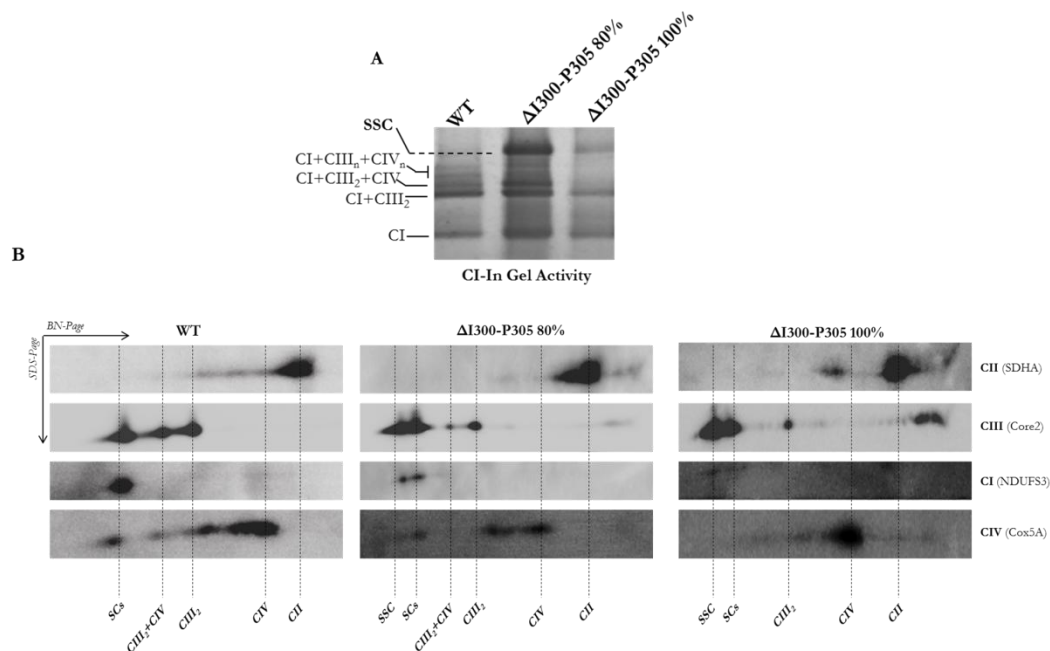


**Figure 4.9** BN-PAGE analysis of SCs in digitonin-treated mitoplasts from cybrids bearing the  $\Delta I300-P305$  deletion. **(A)** CI-In Gel Activity; **(B)** 2D BN/SDS-PAGE followed by western-blot with antibodies against NDUFS3-CI, SDHA-CII, Core2-CIII and Cox5A-CIV.

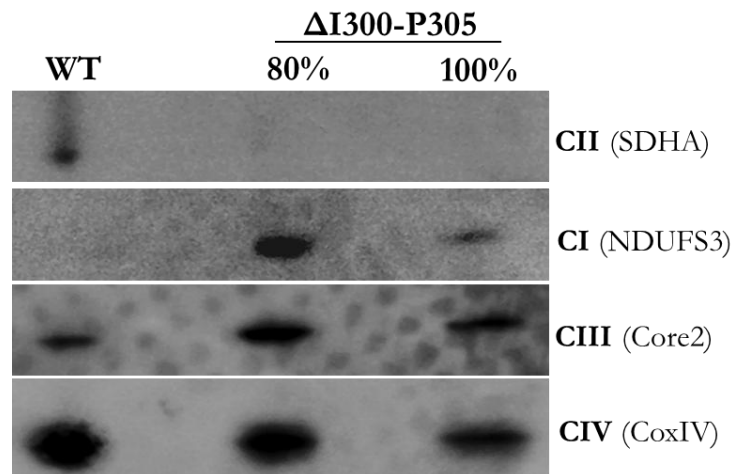


**Figure 4.10** SDS-PAGE followed by western-blot analysis of the bands corresponding to the SSC excised from the gels. Antibodies against NDUFS3-CI, SDHA-CII, Core2-CIII and CoxIV-CIV were used.

#### 4.6 Combined redox activities and ATP synthesis

The combined redox activities (CI+CIII and CII+CIII) were measured in crude mitochondria isolated from cybrids bearing the two *MTCYB* mutations.

In cells with the p.278Y>C mutation, the CI+CIII combined redox activity of homoplasmic mutant clone was markedly reduced compared with control, but less severely than CIII alone (Figure 4.7A), whereas the CII+CIII did not show significant difference (Figure 4.10A).

In cybrids harboring the  $\Delta I300-P305$  deletion, the CI+III and CII+III integrated activities of the heteroplasmic clone were not different from control. In the homoplasmic mutant clone the CI+CIII integrated activity was also similar to control, in accord with the results of BN-PAGE, while the CII+CIII activity was almost abolished (Figure 4.11B).

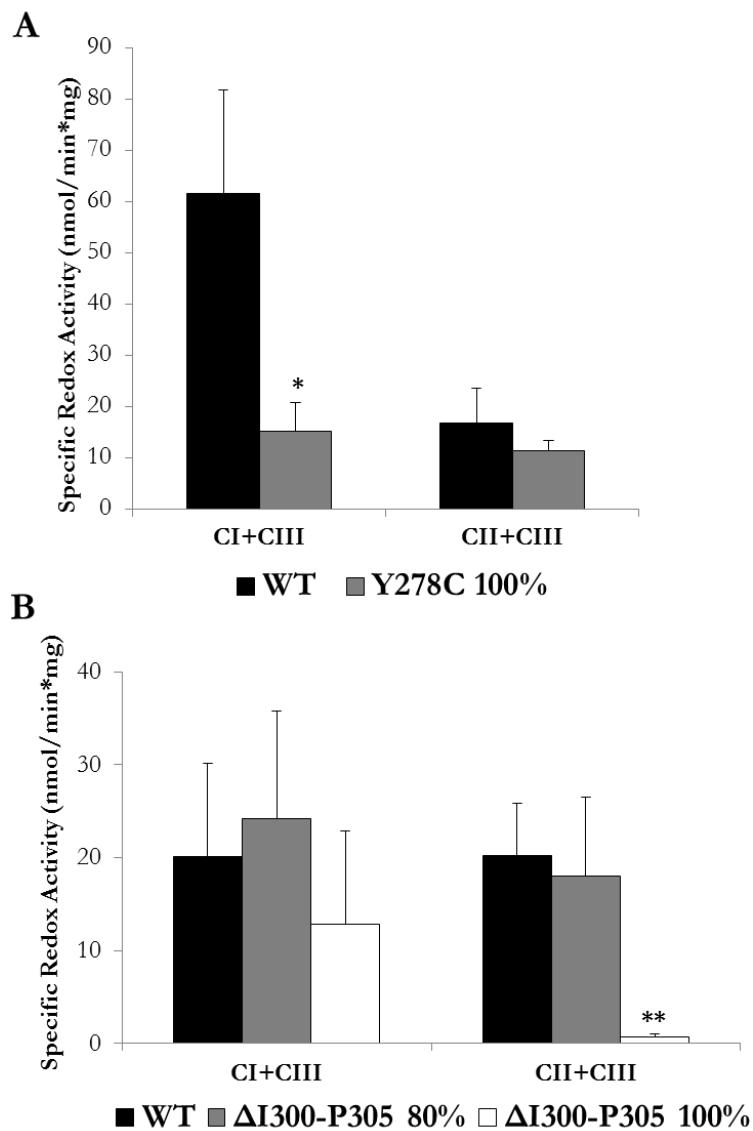


**Figure 4.11** Analysis of combined redox activities (CI+CIII and CII+CIII) measured in crude mitochondria and expressed in nmol/min\*mg. **(A)** p.278Y>C; **(B)** ΔI300-P305. Each data point represents mean  $\pm$  SD of three experiments ( $P^* \leq 0.05$ ;  $P^{**} \leq 0.01$ ).

Further analysis of the OXPHOS efficiency was performed by measuring the rate of mitochondrial ATP synthesis in digitonin-permeabilized cells, after normalization for the citrate synthase activity, which is an indicator of the mitochondrial mass [Trounce *et al.*, 1996].

The ATP synthesis rate of p.278Y>C cybrids was reduced ( $\sim 35\%$ ) in presence of the CI substrates malate plus pyruvate, but only slightly affected in presence of the CII substrate succinate (Figure 4.12A). These results are in accord with the findings obtained

by analysis of respiratory SCs (Figure 4.8 A and B), which were not significantly affected by the mutation.

In  $\Delta I300$ -P305 mutated cybrids, the rates of ATP synthesis driven by CI and CII substrates were all severely reduced or abolished in the homoplasmic mutant clone only. In heteroplasmic cybrids, the ATP synthesis was similar or only slightly reduced compared with controls, indicating that the presence of about 20% wild-type mtDNA is sufficient to sustain the mitochondrial function (Figure 4.12B). The residual ATP synthesis value in homoplasmic clone is in accord with the presence of the CI+III<sub>2</sub> SC and CI+CIII integrated activity, indicating that mutated CIII associated with CI within the SCs is able to perform some residual activity.

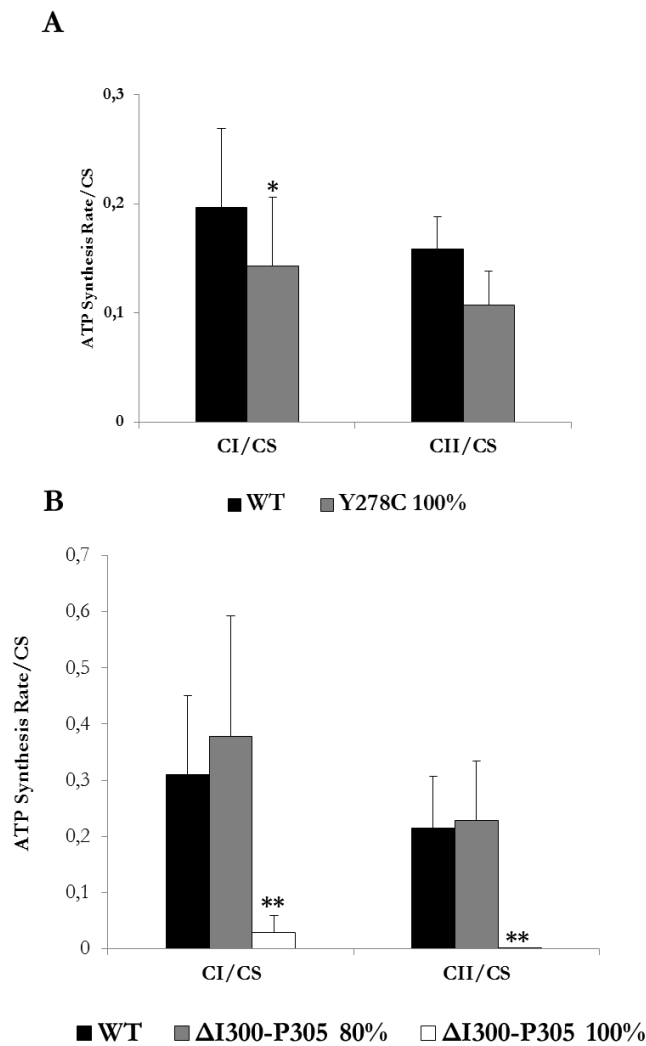


**Figure 4.12** Mitochondrial ATP synthesis rate driven by CI and CII substrates in (A) p.278Y>C and (B)  $\Delta I300$ -P305. Data are expressed as ATP synthesis/CS activity. Each data point represents mean  $\pm$  SD of three experiments ( $P^* \leq 0.05$ ;  $P^{**} \leq 0.01$ ).

#### 4.7 Oxidative damage associated with p.278Y>C mutation

Recently, it has been demonstrated that the *R. capsulatus* cytochrome *b* p.302Y>C substitution, which is homologous to human cytochrome *b* p.278Y>C, induced superoxide production by CIII. Remarkably, mass spectrometry analysis showed that this mutation caused chemical cross-linking of cytochrome *b* to the Fe/S subunit by a disulfide bond, rendering the bacterial enzyme inactive [Lee et al., 2011]. Enhanced superoxide production was also measured in mitochondria isolated from p.278Y>C mutant cybrids, compared to wild type cells [Lanciano *et al.*, 2013]. Therefore we decided to determine the amounts of reduced glutathione (GSH) and oxidized glutathione (GSSG) in cybrids grown in galactose-containing media, given that glutathione is involved in the detoxification of a number of oxidizing species and changed GSSG/GSH ratio provide strong evidence for occurrence of an oxidative stress [Hansen *et al.*, 2006]. Although the GSSG/GSH+GSSG ratio was only slightly increased in mutant cybrids grown in DMEM in comparison with wild-type cells (Figure 4.12A), a significant increase of this ratio was detected after 6 hours of incubation in DMEM-galactose (Figure 4.13A), a time point where most of the mutant cells were still viable (see Figure 4.2A). This finding indicates that an imbalance in the homeostasis of the major intracellular tripeptide antioxidant, likely as a consequence of the superoxide production by mutated CIII, becomes apparent when cells are forced to use oxidative metabolism.

This result prompted us to determine whether the addition of exogenous antioxidants might ameliorate the viability of mutated cells incubated in DMEM-galactose. As illustrated in Figure 4.13B, addition of the selective superoxide scavenger sodium 4,5-dihydroxybenzene-1,3-disulfonate (Tiron; 10 mM) [Taiwo, 2008] improved the viability of mutated cybrids after 24 hours of incubation in DMEM-galactose (48% increase). Furthermore, the presence of 10mM GSH or N-acetylcysteine (NAC) significantly increased the viability already after 16 hours of incubation (30 and 76% increase, respectively) and also after 24 hours of incubation (54 and 32% increase, respectively). All these compounds slightly reduced the viability of control cybrids. Taken together, these results indicate that the loss of viability of cybrids carrying the cytochrome *b* p.278Y>C mutation in DMEM-galactose is due, at least in part, to an imbalance of the GSSG/GSH ratio, as a consequence of increased superoxide production.

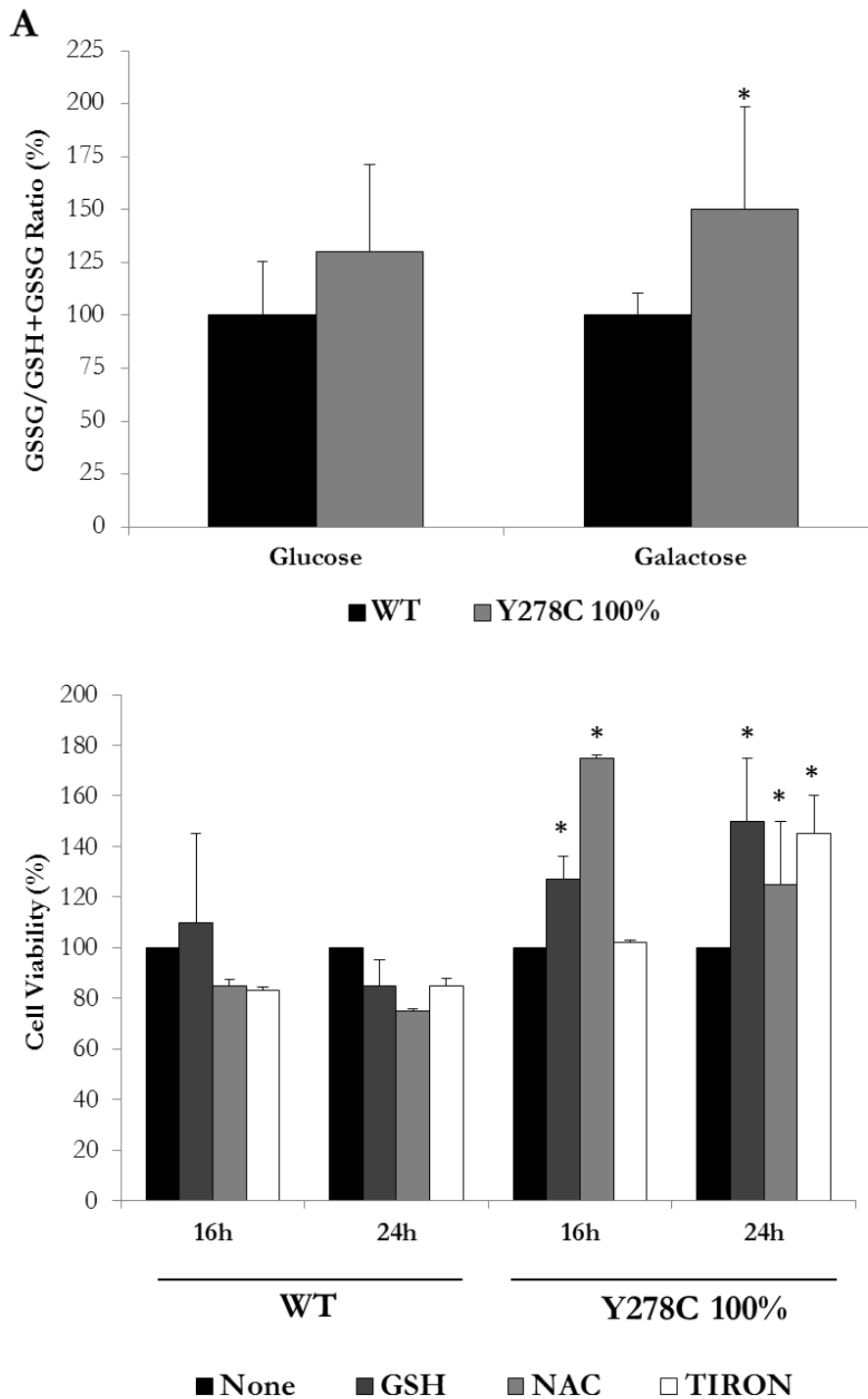


**Figure 4.13** Analysis of superoxide production in p.278Y>C. **(A)** The GSSG/GSH+GSSG ratio was measured in cells grown in DMEM or incubated in DMEM-galactose for 6 hours, as described in Experimental Procedures. Values are expressed as percent increase over respective control (none). Data are presented as the means  $\pm$  SD of three determinations ( $P^* \leq 0.05$ ). **(B)** Cybrids were incubated in DMEM-galactose in the absence or the presence of 10 mM GSH or 10 mM NAC or 10 mM Tiron. The 100% value corresponds to viability determined for each cell line after incubation for the indicated times in DMEM-galactose. Values are presented as the means  $\pm$  SD of three determinations ( $P^* \leq 0.05$ ).

Then we asked whether the addition of the strong reducing agent dithiothreitol (DTT) to the mitochondrial isolation buffer could improve the CI, CIII and CI+III activities of p.278Y>C crude mitochondria. In the presence of DTT, the CIII and CI+III activities significantly increased (Figure 4.14A), but not in control mitochondria (data not shown). These results suggested that the CIII activity is affected by enhanced oxidative stress, and that reducing conditions significantly preserving the CIII and CI+CIII activities, contribute to improve the viability in galactose medium.

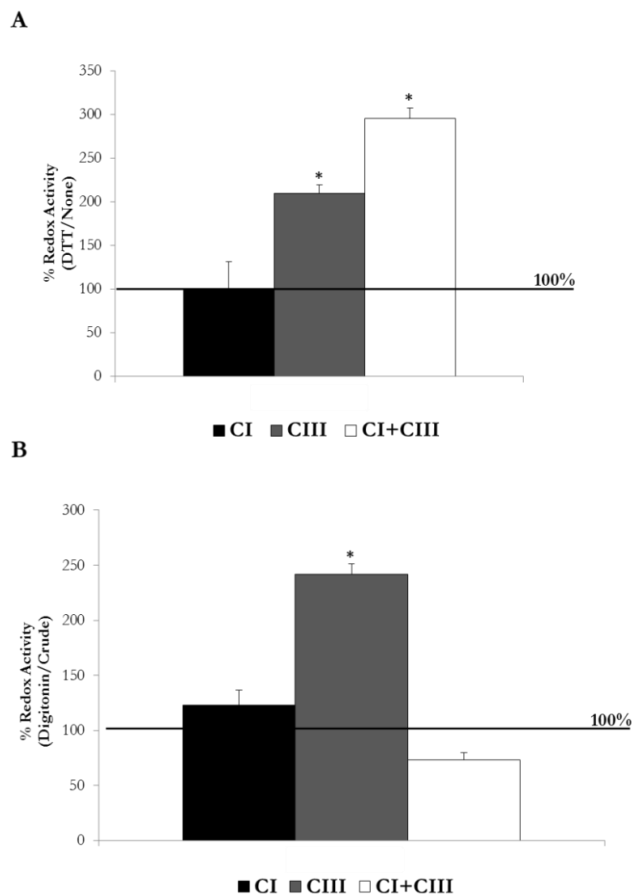


**Figure 4.14** (A) CI, CIII and CI+III redox activities were determined in crude mitochondria from Y278C mutant cybrids isolated in a buffer without or with 10mM DTT, as described in Experimental Procedures. Data are presented as % values  $\pm$  SD of five determinations ( $P^* \leq 0.05$ ). (B) CI, CIII and CI+III activities were determined in crude mitochondria and in mitoplasts solubilized with digitonin, as detailed in Experimental Procedures. Data are expressed as ratio of digitonin-treated mitoplasts to crude mitochondria enzymatic activity. Data are presented as mean  $\pm$  SD of five determinations ( $P^* \leq 0.05$ ).

Furthermore, we considered the possibility that isolation of mitoplasts by digitonin-treatment should better protect mitochondrial membranes from the damaging effects of oxygen, and therefore we decided to measure the CI, CIII and CI+CIII activities in digitonin-extracted mitoplasts. These activities have been compared with those obtained in

crude mitochondria, that we believed were likely more exposed to oxygen during the isolation procedure involving potter homogenization. Figure 4.14B shows that the CIII activity was significantly higher in digitonin-treated mitoplasts compared with crude mitochondria, whereas the CI and CI+III activity were similar. No difference was observed in a similar experiment carried out in control cybrids (data not shown). These findings support the hypothesis that, similarly to bacteria [Lee *et al.*, 2011] also in human mutant cells, oxygen plays a detrimental effect on the respiratory CIII.

#### **4.8 Hydrogen peroxide production and CII activation in cell bearing the $\Delta$ I300-P305 deletion**

It has been recently reported that CI dysfunction associated with marked increase in hydrogen peroxide production, causes stimulation of CII redox activity, through a mechanism mediated by Fgr tyrosine kinase phosphorylation. Interestingly CII activation was shown to be specific for CI-deficient cells, since it was not detected in cells with defective CIII or CIV. Accordingly, CII activation was proposed to act as a compensatory mechanism for counteracting impaired activity of CI [Acín-Pérez *et al.*, 2014].

As already reported in Figure 4.7B, the homoplasmic clone harbouring the  $\Delta$ I300-P305 microdeletion exhibited a marked increase of CII redox activity compared to wild-type cells, without any increase in CII protein content (Figure 4.6). In Figure 4.15 the CII redox activity of p.278Y>C and  $\Delta$ I300-P305 homoplasmic clones is shown. The CII redox activity of homoplasmic clone with the  $\Delta$ I300-P305 microdeletion was strongly increased (more than 2-fold) compared with control, whereas no stimulation was apparent in the p.278Y>C homoplasmic clone. Thus, we decided to investigate whether the increased CII activity of the homoplasmic  $\Delta$ I300-P305 clone was associated *in vivo* with an overproduction of H<sub>2</sub>O<sub>2</sub>. Cybrids bearing the p.278Y>C mutation were used as a negative control.

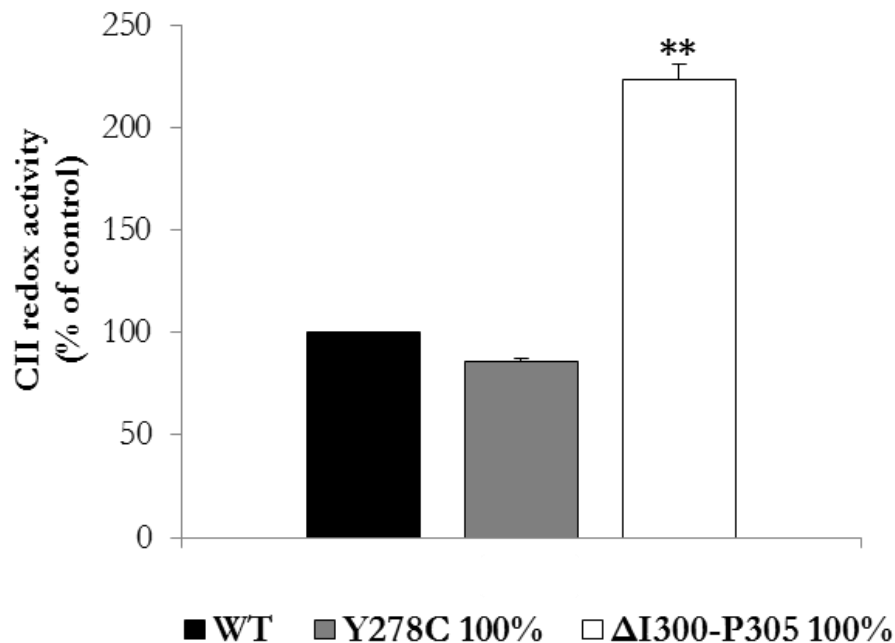


**Figure 4.15** Measurement of CII redox activity in mitochondria isolated from cybrids bearing the indicated mutation. Data are expressed as percentage of activity in mutated clone over respective control clone. Data are mean  $\pm$  SD of three determinations ( $P^{**} \leq 0.01$ ).

Figure 4.16A reports the production of  $H_2O_2$ , measured by using 2',7'-Dichlorofluorescein diacetate ( $H_2DCFDA$ ) as described in Experimental Procedures. A highly significant increase in  $H_2O_2$  production was apparent in the homoplasmic  $\Delta I300$ -P305 clone compared with control and the p.278Y>C mutant clone, suggesting that the increased CII activity is associated with an overproduction  $H_2O_2$  production, in agreement with [Acín-Pérez *et al.*, 2014].

Analysis of the antioxidant enzymes expression by western blotting revealed that only the level of peroxiredoxin3, a mitochondrial enzyme known to reduce hydrogen peroxide to water and oxygen, was markedly increased in  $\Delta I300$ -P305 compared to control and p.278Y>C clones. The levels of the other antioxidant enzymes catalase and Mn-SOD were not affected (Figure 4.16B).

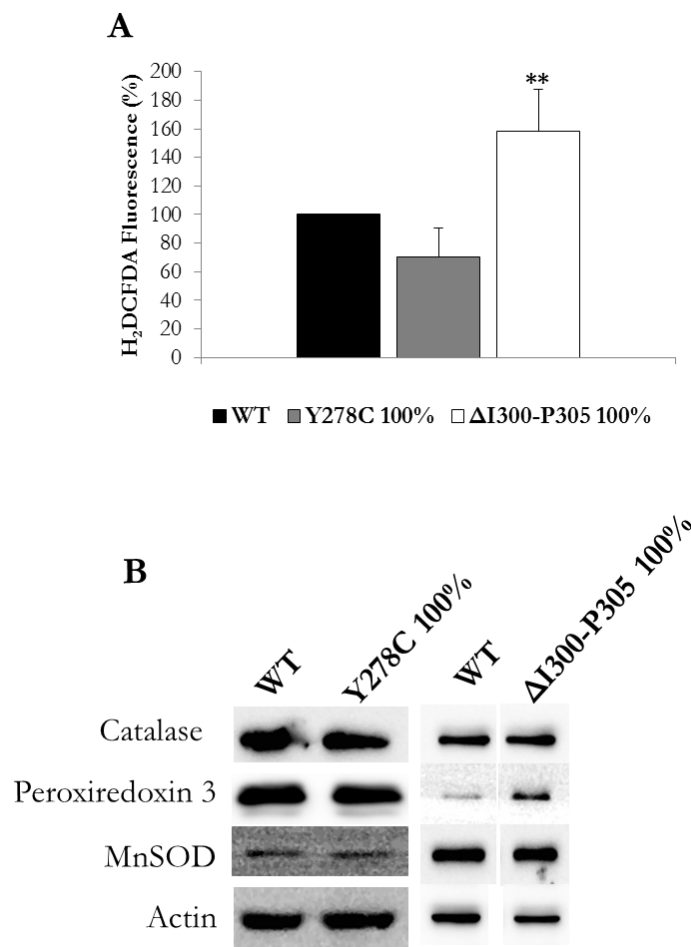


**Figure 4.16** (A) Hydrogen peroxide production in homoplasmic p.278Y>C and  $\Delta$ I300-P305 clones, measured by H<sub>2</sub>DCFDA fluorescence, expressed as percentage of fluorescence signal of mutated over wild-type clone. Data are presented as the means  $\pm$  SD of three determinations ( $P^{**} \leq 0.01$ ). (B) Western-blot analysis of antioxidant enzymes level using antibodies against catalase, peroxiredoxin 3 and MnSOD. Actin was used for protein normalization.

#### 4.9 Phosphorylation of the SDHA subunit of CII

Activation of CII activity in CI-defective cells was shown to be associated with phosphorylation at the tyrosine 604 residue of the SDHA subunit of CII, triggered by the tyrosine kinase Fgr [Acín-Pérez *et al.*, 2014]. To assess whether a similar mechanism is also active in CIII defective cells, tyrosine phosphorylation of SDHA subunit was determined by western blotting (Figure 4.17A).

By using a P-Tyr antibody, we were able to detect a band at the same molecular weight of SDHA in  $\Delta$ I300-P305, but not in control or p.278Y>C mitochondria, in agreement with stimulation of CII activity and hydrogen peroxide production. Further evidence for SDHA subunit tyrosine phosphorylation was obtained from 2D BN/SDS-PAGE experiments. Indeed, as reported in Figure 4.17B, the CII migration pattern was

different in wild-type and  $\Delta I300$ -P305 mutant cells, as apparent from both the SDHA and P-tyr positive spots, compatible with an increased protein phosphorylation.

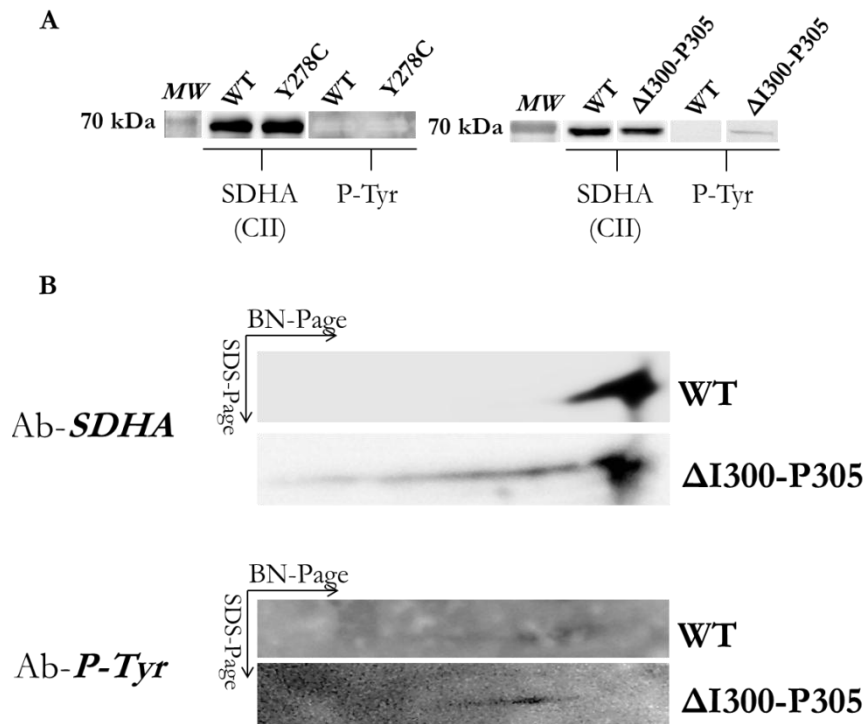


**Figure 4.17** Analysis of CII SDHA-subunit phosphorylation. **(A)** SDS-PAGE followed by immunoblot using antibodies against SDHA subunit and P-Tyr in p.278Y>C and  $\Delta I300$ -P305 mutated mitochondria. **(B)** 2D BN/SDS-PAGE using antibodies against SDHA and P-Tyr in  $\Delta I300$ -P305 mutant clones.

#### 4.10 Effect of treatment of $\Delta I300$ -P305 cybrids with NAC

N-Acetyl-Cysteine (NAC) is a well-known antioxidant involved in hydrogen peroxide detoxification, being a GSH precursor [Atkuri *et al.*, 2007]. Thus, to evaluate whether increased CII activity and phosphorylation of SDHA subunit were associated with hydrogen peroxide production, we incubated homoplasmic  $\Delta I300$ -P305 cybrids with 5mM NAC for a prolonged time (10 days). The CII activity was significantly reduced after treatment with NAC compared with untreated cells (Figure 4.18A). Likewise, the hydrogen peroxide production was also reduced (Figure 4.18B). Furthermore, the analysis of SDHA subunit showed that the band positive to P-Tyr antibody could not be detected in cybrids treated with NAC (Figure 4.19). These findings suggest that also in cell defective in CIII, a marked stimulation of CII activity occurs, provided that  $H_2O_2$  production is enhanced, leading to phosphorylation of a tyrosine in SDHA subunit. This activation seems strictly

dependent on H<sub>2</sub>O<sub>2</sub> overproduction, given that it is abolished after prolonged treatment with NAC.

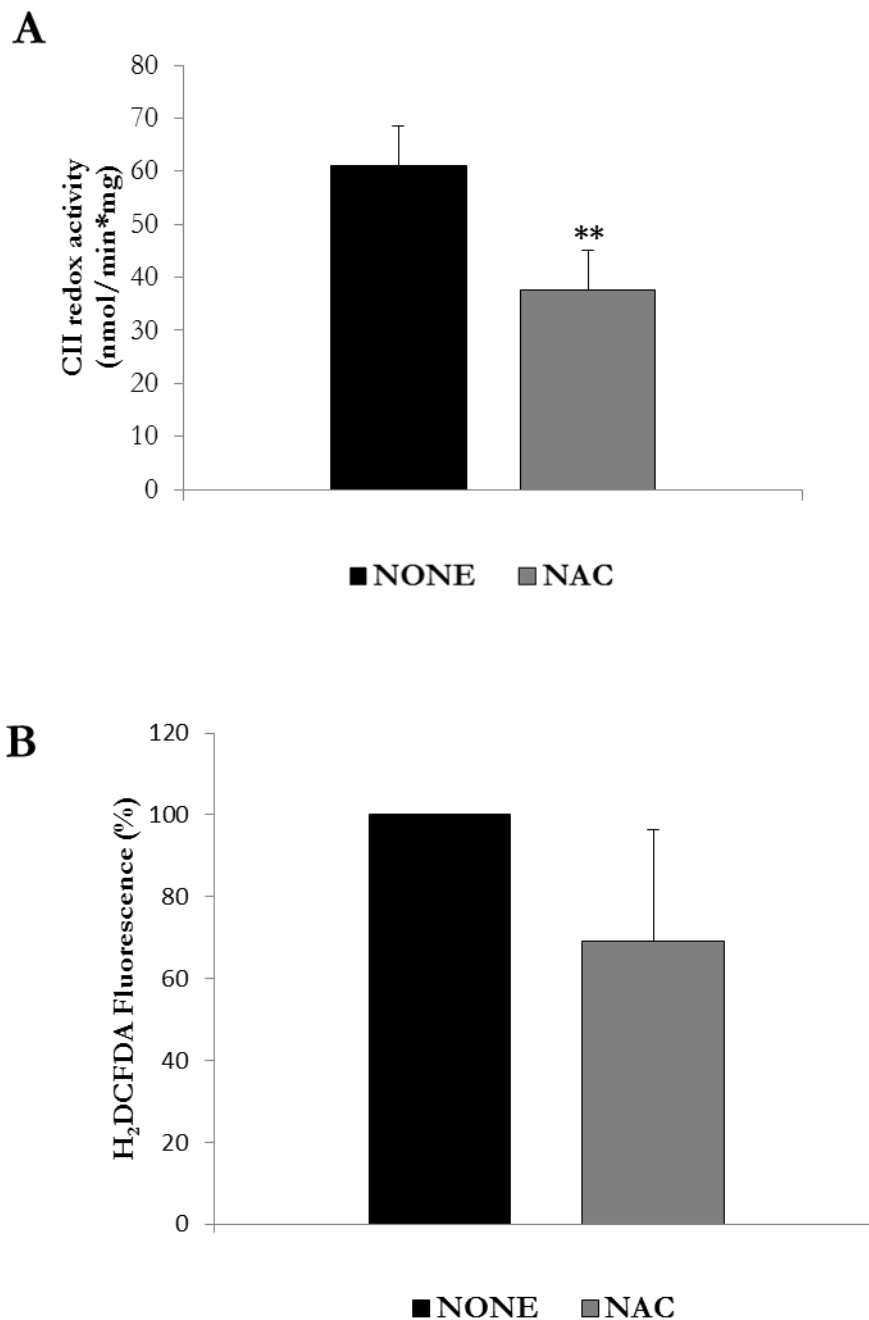


**Figure 4.18** (A) Measurement of CII redox activity in mitochondria from untreated  $\Delta$ I300-P305 cybrids and after 10 days treatment with 5mM NAC. Activity is expressed as percentage of treated over untreated cells. Data are presented as the means  $\pm$  SD of three determinations ( $P^{**} \leq 0.01$ ). (B) Measurement of hydrogen peroxide production by using H<sub>2</sub>DCFDA. Data are expressed as percentage of fluorescence of treated over untreated cells. Data are presented as means  $\pm$  SD of three determinations ( $P^{**} \leq 0.01$ ). (C) SDS-PAGE followed by immunoblot using antibodies against SDHA-CII and P-Tyr.

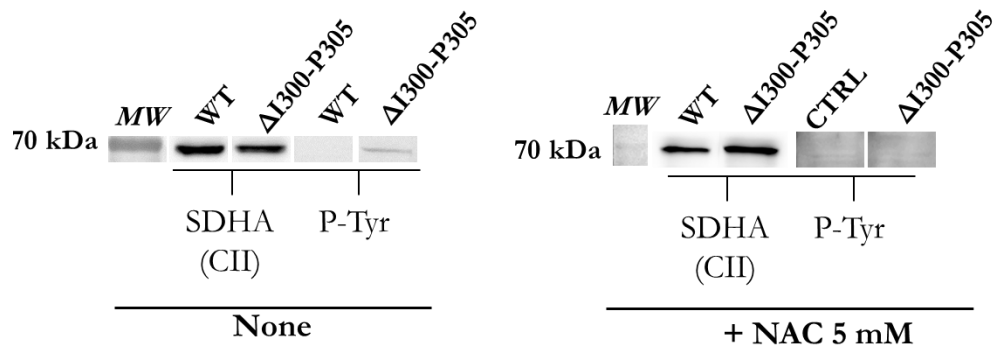


**Figure 4.19** Effect of treatment of  $\Delta I300-P305$  cybrids with NAC: Western blot analysis of SDHA subunit of CII and P-Tyr.

# Discussion and Conclusions

---

The biochemical analysis described in this study was focused on two mutations affecting *MTCYB* gene: the first is the p.278Y>C missense mutation causing the substitution of the highly conserved Tyr<sup>278</sup>, located close the Q<sub>O</sub> site, and leading to formation of a chemical cross-linking between cytochrome *b* and the Fe/S cluster protein. The second one, the ΔI300-P305 microdeletion, is located on the sixth transmembrane helix and severely reduces the expression level of the protein.

Although the two mutations differently affected the cytochrome *b*, similar repercussions on CIII activity were observed. In fact, both mutations severely impaired the activity of CIII through different mechanisms: the microdeletion caused CIII disassembly, conversely, the missense mutation was associated with oxidative injury of CIII, due to increased superoxide production. This was confirmed by the imbalance in the cellular GSSG/GSSG+GSH ratio detected when the p.278Y>C mutated cells were forced to use the OXPHOS and by the efficacy of treatment with the specific superoxide scavenger Tiron or with antioxidant compounds such as GSH and NAC. It is noteworthy that in *R. capsulatus* the homologous cytochrome *b* mutation (p.302Y>C) caused the formation of a chemical cross-link between cytochrome *b* and the Fe/S subunit, enhancing superoxide generation and inactivating the bacterial enzyme [Lee *et al.*, 2011]. Further, the same authors reported that CIII activity was lower when p.302Y>C cells were grown and membranes were isolated in the presence of oxygen. Conversely, the CIII activity was increased under anoxygenic photosynthetic growth conditions, and when *R. capsulatus* membranes were isolated in the absence of oxygen [Lee *et al.*, 2011]. In agreement with these results, the CIII activity of the p.278Y>C mutant cells significantly increased when measured in mitochondria isolated in the presence of the reducing agent DTT.

It is well established that mutations affecting CIII and causing its loss, indirectly impair the assembly of CI [Acín-Pérez *et al.*, 2004; D'Aurelio *et al.*, 2006; Diaz *et al.*, 2006; Diaz *et al.*, 2012a, 2012b; Li *et al.*, 2007]. Our results confirm the hypothesis that CI and CIII are strictly dependent, given that in ΔI300-P305 cells the impairment of CI correlated with the absence of CIII. On the other hand, the missense *MTCYB*

mutation, which did not perturb the assembly of CIII, failed to affect CI activity and assembly.

The analysis of SCs organization in cells with the two mutations revealed the absence of CIII<sub>2</sub>+IV SC together with the attempt to preserve the respirasome. Indeed, in p.278Y>C, we observed a slightly increase of CI+III<sub>2</sub>+IV SC. Furthermore, we observed that the residual CIII activity of mutated cells was higher when measured in digitonin-solubilized mitoplasts compared with crude mitochondria, suggesting that CIII activity is protected when included within the CI+III<sub>2</sub>+IV SC. Further support to this derives from the finding that the combined CI+CIII activity significantly increased when measured under reducing conditions. It is therefore likely that during the isolation procedure of crude mitochondria by using potter omogenization, cells are more exposed to the damaging effect of oxygen than when mitochondria are isolated by digitonin treatment. Under these milder conditions, CIII and SCs should be protected from detrimental effects of oxygen. In this regard, the importance of SCs association to safeguard the respiratory complexes from oxidative damage, not only allowing a better substrate channeling but also maintaining the redox centers of the complexes less exposed to oxygen has been recently underlined [Maranzana *et al.*, 2013].

In ΔI300-P305 homoplasmic cells, we observed the maintenance of a small amount of enzymatically active CI+CIII<sub>2</sub> SC, despite disassembly of CI and CIII and severe impairment of redox activities, allowing for a minimum rate of ATP synthesis. Moreover, in the heteroplasmic mutant cells, the amount of the CI+III<sub>2</sub>+IV SC was similar to controls. These results strongly confirm the proposal that CI has a very high affinity for CIII [Schägger *et al.*, 2004; Schägger and Pfeiffer, 2001] and this association is preferred when a partial loss of CIII occurs [Lapunte-Brun *et al.*, 2013], supporting further that the organization in SCs is necessary to preserve the structural stability of the complexes but also is necessary to maintain their functionality [Maranzana *et al.*, 2013].

Recently, it has been suggested that the quinone in the inner membrane exists at least as two distinct pools: one dedicated to NADH- and the other one to FADH<sub>2</sub>-dependent enzymes (CoQ<sub>NADH</sub> pool and CoQ<sub>FAD</sub> pool, respectively). In this scenario, one fraction of CIII could bind to CI forming SCs and oxidize the CoQ<sub>NADH</sub> pool, whereas the other fraction, mainly present as a dimer, could oxidize the CoQ<sub>FAD</sub> pool. Lapunte-Brun and colleagues also observed that the loss of CIII caused the preferential maintenance of CoQ<sub>NADH</sub> oxidation, promoting the association of CI to CIII, despite of the CoQ<sub>FAD</sub>

oxidation [Lapiente-Brun *et al.*, 2013]. Our results are in disagreement with this hypothesis, since both homoplasmic p.278Y>C and heteroplasmic  $\Delta I300$ -P305 clones did not significantly decrease the ATP synthesis driven by CII and of CII+III combined redox activity, suggesting that the SCs association is mostly important to stabilize structurally the respiratory complexes, rather than to compartmentalize CoQ into NADH- and the FAD-dedicated fractions.

A peculiar finding mostly associated with heteroplasmic  $\Delta I300$ -P305 is the presence of the SSC, a band at very high molecular weight. This unusual high molecular weight SC, which was not detected in controls, might derive from the presence of both wild-type and mutant cytochrome *b* in the same cells, a situation similar to that occurring in many patient's tissues. This SSC comprises CI, CIII and CIV, and seems to be enzymatically active, as indicated by CI-In Gel Activity. It is known that the SCs can organize themselves in megacomplexes (or respiratory strings), creating a higher level of organization. It has been shown that a supercomplex composed by two copies of CI and the CIII<sub>2</sub> is present in potato mitochondria (CI<sub>2</sub>+III<sub>2</sub> SC). In turn, this SC can assemble with two copies of CIV (CI<sub>2</sub>+III<sub>2</sub>+IV<sub>2</sub> SC) (Figure 5.1) [Bultema *et al.*, 2009]. It can be speculated that the  $\Delta I300$ -P305 deletion, by deeply altering the structure of CIII, might in some way favor its binding with two copies of CI, thus, forming a CI<sub>2</sub>+III<sub>2</sub>+IV<sub>2</sub> SC. The presence of two copies of CI in the SSC might help stabilizing the defective structure of CIII, allowing CIV binding. In other words, the lack of CIII<sub>2</sub>+IV and CI+CIII<sub>2</sub>+CIV SCs might be due to structural changes of mutated CIII which prevent the binding of CIV. Our simulation of the structural features of the mutated cytochrome *b* might support this hypothesis. In fact, the "core" structure of the cytochrome *b* coordinating the *b*<sub>L</sub> and *b*<sub>H</sub> hemes was not significantly changed, whereas the external portion of the protein underwent several conformational changes, resulting in increased mobility and possibly reduced stability within the membrane. Noticeably, the outer portion is involved in interaction with the other subunits of CIII, thus, we speculate that these changes might influence the entire structure of the complex and result in a low stability, in turn impairing its assembly, function and the capability to bind CIV. However, it has to be considered that this bio-informatic analysis was performed considering the protein structure *in vacuo*. Indeed, the respiratory enzymes are embedded within the inner membrane, in a highly hydrophobic environment. Therefore, these are only speculations to predict the effect of

altered cytochrome *b* structure, further studies using more sophisticated approaches are required to address this issue.

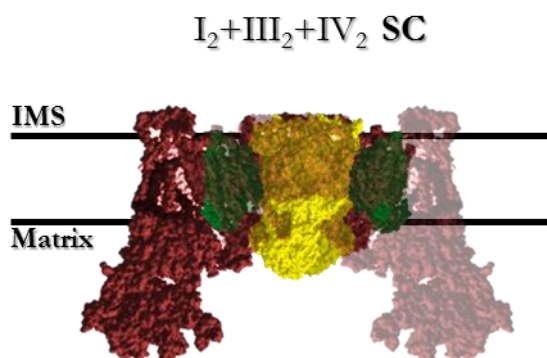


**Figure 5.1** Representation of  $CI_2 + CIII_2 + CIV_2$  SC. CI is indicated in red, CIII in yellow and CIV in green.

In conclusion, the analysis of the supramolecular organization of mitochondrial respiratory complexes in cells bearing the p.278Y>C and  $\Delta I300$ -P305 mutations allowed us to shed light on the subtle underlying molecular alterations, providing information that could be possibly useful for optimization of future treatment of patients. Furthermore, our studies favor the hypothesis that SCs are necessary not only for channeling electron transport between complexes but also, and likely more importantly, to preserve the structure and stability of respiratory complexes, attenuating the mitochondrial dysfunction due to mutations affecting the enzymes. In fact, our results reinforce the notion that CI and CIII have a strict structural dependence, which is a crucial element for their proper functioning (Figure 5.2).

The other original finding emerging from our biochemical studies on cells bearing the  $\Delta I300$ -P305 deletion is the strong increase of CII redox activity associated with the complete inhibition of CIII. This finding is in disagreement with previous reports [Acín-Pérez *et al.*, 2014] where over-stimulation of CII activity was not detected in CIII defective cells, but only in those bearing mutated ND6 subunit of CI. Accordingly, increased CII activity was proposed to be a compensatory mechanism to bypass the CI defect. In our case, hyper-activation of CII activity in the homoplasmic  $\Delta I300$ -P305 clone bearing a faulty CIII, makes it difficult to envisage the occurrence of any compensatory mechanism.

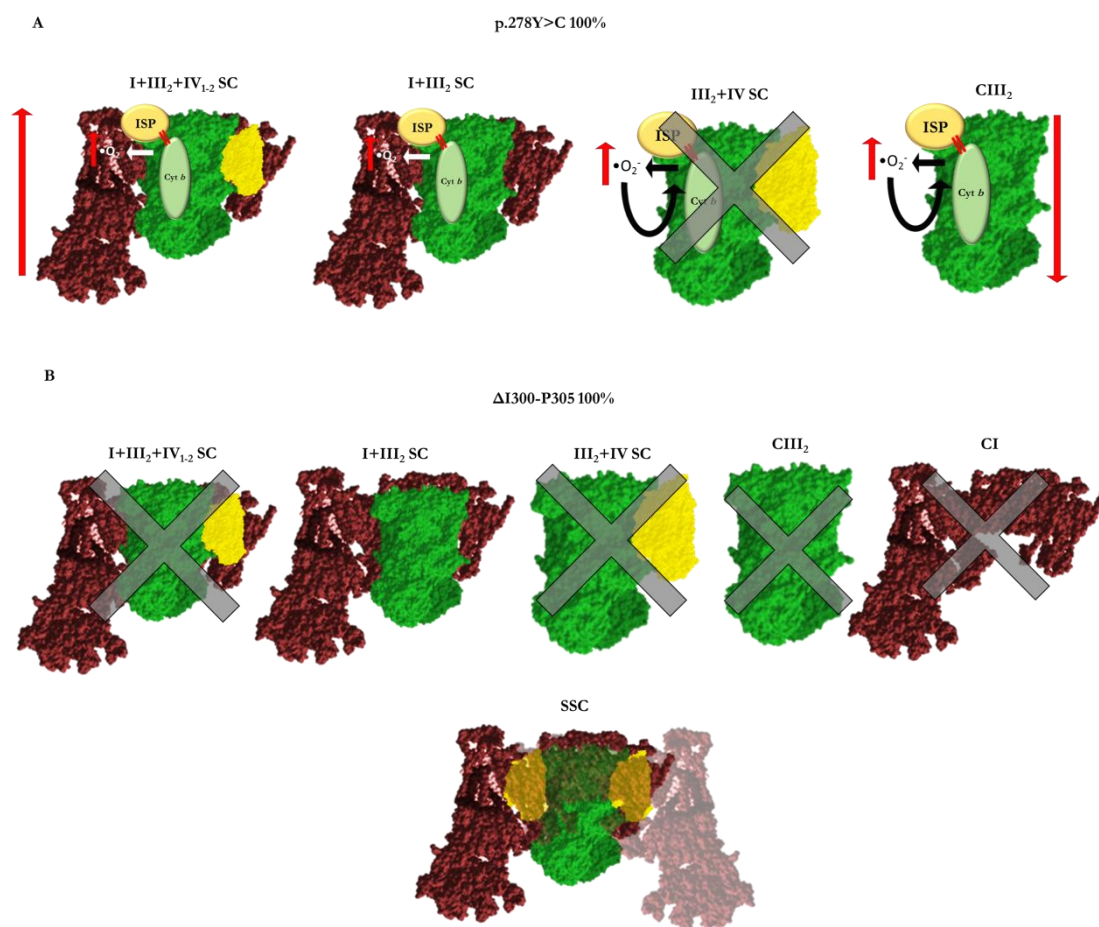


**Figure 5.2** Schematic representation of SCs and complexes organization in (A) p.278Y>C and (B) ΔI300-P305. CI is indicated in red, CIII in green and CIV in yellow.

Our efforts have been focused on investigation of the mechanism underlying the activation of CII redox activity. It is well known that CII is a substrate of the Fgr tyrosine kinase, resulting in phosphorylation of several tyrosine residues [Salvi *et al.*, 2005]. Furthermore, the association of the CII activation with phosphorylation of the SDHA-CII subunit on the Tyr<sup>604</sup> has been recently demonstrated [Acín-Pérez *et al.*, 2014]. In agreement, we also evidenced that stimulation of CII activity was associated with tyrosine phosphorylation of the SDHA subunit of CII. Furthermore, cells bearing the ΔI300-P305 deletion exhibited a marked increase of H<sub>2</sub>O<sub>2</sub> production associated with the hyperactivation of CII.

The source of H<sub>2</sub>O<sub>2</sub> in the homoplamic ΔI300-P305 cells remains to be identify. The small amount of CI+III still present might be involved, given that CI and CIII are considered the major ROS producers within the inner membrane. However, also CII can generate free radicals [Quinlan *et al.*, 2012]. Thus, it is possible that the high H<sub>2</sub>O<sub>2</sub>

production can originate from CII consequently to its hyper-activation. Moreover, we have shown that the over-production of  $H_2O_2$  is associated with a markedly increased level of Prx3, an antioxidant enzyme specifically involved in  $H_2O_2$  detoxification. It is well known that ROS can act as signaling molecules activating transcriptional factors involved in the expression of genes responsible for translation of antioxidant proteins, such as Keap1. This protein has been reported to be a sensor of oxidative stress, since it contains many cysteine residues through which Keap1 should sense the oxidative stress [Holland and Fishbein, 2010]. Under basal conditions, Keap1 sequesters Nrf2 in the cytosol facilitating its ubiquitination and proteasomal degradation. When a redox stress occurs, the reactive cysteine residue oxidation causes conformational changes in Keap1, resulting in the release of Nrf2 which is no longer ubiquitinated and degraded, allowing its translocation to nucleus. Here, Nrf2 binds to the antioxidant response element (ARE) activating the expression of genes involved in the oxidative stress detoxification [Bryan *et al.*, 2013]. Our preliminary experiments of western blotting indicate that in  $\Delta I300$ -P305 cells Nrf2 was stabilized and found associated with the nuclear fractions (data not shown). It is therefore likely that over-production of  $H_2O_2$  could trigger the activation of antioxidant enzymes such as Prx3 through Nrf2-Keap1 pathway. In Figure 5.3, a model of the pathways possibly activated in  $\Delta I300$ -P305 cells is summarized.

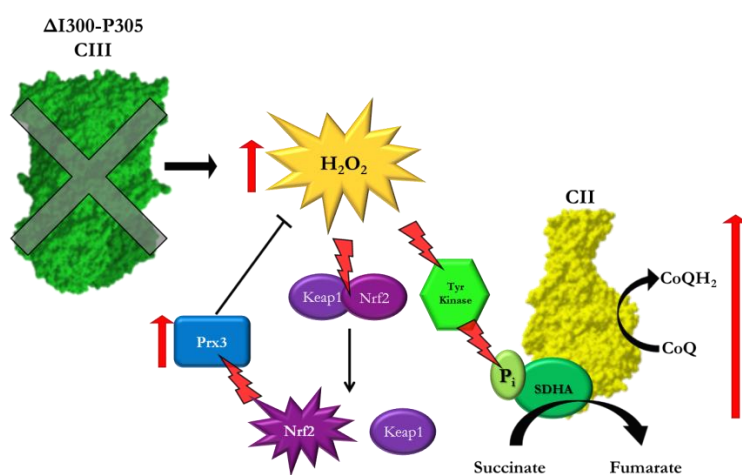


**Figure 5.3** Scheme of the pathways possibly activated in homoplasmic  $\Delta I300$ -P305 cells.

Finally, experimental conditions leading to reduction of oxidative stress, such as prolonged treatment of  $\Delta I300$ -P305 mutant cells with NAC, significantly decreased  $H_2O_2$  production. The diminished  $H_2O_2$  production and, consequently, decreased CII activity were associated with de-phosphorylation of SDHA-CII subunit, indicating that the

signaling mechanism involves a ROS-type molecule. Further experiments are required to confirm the occurrence of this pathway. Noticeably, cells with the p.278Y>C *MTCYB* mutation did not exhibit any H<sub>2</sub>O<sub>2</sub> overproduction, nor increased Prx3 expression level or phosphorylation of SDHA-CII subunit, in accord with the normal CII redox activity. This also suggests that defective CIII in the absence of H<sub>2</sub>O<sub>2</sub> overproduction is not sufficient to induce CII activation.

In conclusion, our data suggest that hyper activation of CII, associated with *MTCYB* microdeletion and dependent on CIII alteration and hydrogen peroxide overproduction, is a more general phenomenon than predicted. The consequences of CII stimulation is still poorly understood, and this is particularly relevant in the case of association with defective CIII, where a compensatory role has to be ruled out. It is possible that it is associated with production of specific signaling metabolites, that might trigger activation of particular cellular responses. Indeed significant changes in the metabolic intermediates of the tricarboxylic acid cycle have been recently described in cells exposed to OXPHOS complexes inhibitors or containing mitochondrial dysfunctions [Mullen *et al.*, 2014]. Therefore cells bearing the homoplasmic  $\Delta$ I300-P305 deletion represent a precious model to better understand CII activation and the related cellular events, and to shed light on metabolic adaptation/remodeling due to respiratory chain dysfunctions.

# References

---

- Abrahams JP, Leslie AG, Lutter R, Walker JE. *Structure at 2.8 Å resolution of F1-ATPase from bovine heart mitochondria*. Nature 1994; 370: 621–628.
- Acín-Pérez R, Bayona-Bafaluy MP, Fernández-Silva P, Moreno-Loshuertos R, Pérez-Martos A, Bruno C, et al. *Respiratory complex III is required to maintain complex I in mammalian mitochondria*. Mol. Cell 2004; 13: 805–815.
- Acín-Pérez R, Carrascoso I, Baixauli F, Roche-Molina M, Latorre-Pellicer A, Fernández-Silva P, et al. *ROS-triggered phosphorylation of complex II by Fgr kinase regulates cellular adaptation to fuel use*. Cell Metab. 2014; 19: 1020–1033.
- Acín-Pérez R, Fernández-Silva P, Peleato ML, Pérez-Martos A, Enriquez JA. *Respiratory active mitochondrial supercomplexes*. Mol. Cell 2008; 32: 529–539.
- Althoff T, Mills DJ, Popot J-L, Kühlbrandt W. *Arrangement of electron transport chain components in bovine mitochondrial supercomplex I1III2IV1*. EMBO J. 2011; 30: 4652–4664.
- Altmann R. *Die Elementarorganismen und ihre Beziehungen zu den Zellen*. Veit Leipzig. 1980
- Anderson ME. *Determination of glutathione and glutathione disulfide in biological samples*. Methods Enzymol. 1985; 113: 548–555.
- Anderson S, Bankier AT, Barrell BG, de Bruijn MH, Coulson AR, Drouin J, et al. *Sequence and organization of the human mitochondrial genome*. Nature 1981; 290: 457–465.
- Andreu AL, Hanna MG, Reichmann H, Bruno C, Penn AS, Tanji K, et al. *Exercise intolerance due to mutations in the cytochrome b gene of mitochondrial DNA*. N. Engl. J. Med. 1999; 341: 1037–1044.
- Andrews RM, Kubacka I, Chinnery PF, Lightowlers RN, Turnbull DM, Howell N. *Reanalysis and revision of the Cambridge reference sequence for human mitochondrial DNA*. Nat. Genet. 1999; 23: 147.
- Arnold I, Pfeiffer K, Neupert W, Stuart RA, Schägger H. *Yeast mitochondrial F1F0-ATP synthase exists as a dimer: identification of three dimer-specific subunits*. EMBO J. 1998; 17: 7170–7178.
- Atkinson A, Khalimonchuk O, Smith P, Sabic H, Eide D, Winge DR. *Mzm1 influences a labile pool of mitochondrial zinc important for respiratory function*. J. Biol. Chem. 2010; 285: 19450–19459.
- Atkuri KR, Mantovani JJ, Herzenberg LA, Herzenberg LA. *N-Acetylcysteine—a safe antidote for cysteine/glutathione deficiency*. Curr. Opin. Pharmacol. 2007; 7: 355–359.
- Baradaran R, Berrisford JM, Minhas GS, Sazanov LA. *Crystal structure of the entire respiratory complex I*. Nature 2013; 494: 443–448.
- Barel O, Shorer Z, Flusser H, Ofir R, Narkis G, Finer G, et al. *Mitochondrial complex III deficiency associated with a homozygous mutation in UQCRCQ*. Am. J. Hum. Genet. 2008; 82: 1211–1216.
- Barrientos A, Zambrano A, Tzagoloff A. *Mss51p and Cox14p jointly regulate mitochondrial Cox1p expression in Saccharomyces cerevisiae*. EMBO J. 2004; 23: 3472–3482.
- Bazán S, Mileykovskaya E, Mallampalli VKPS, Heacock P, Sparagna GC, Dowhan W. *Cardiolipin-dependent reconstitution of respiratory supercomplexes from purified Saccharomyces cerevisiae complexes III and IV*. J. Biol. Chem. 2013; 288: 401–411.

- Benda C. *Arch Anal Physiol* 1898; 393–398.
- Bénit P, Lebon S, Rustin P. *Respiratory-chain diseases related to complex III deficiency*. *Biochim. Biophys. Acta* 2009; 1793: 181–185.
- Bernardi P. *Mitochondrial transport of cations: channels, exchangers, and permeability transition*. *Physiol. Rev.* 1999; 79: 1127–1155.
- Bernardi P, Di Lisa F, Fogolari F, Lippe G. *From ATP to PTP and Back: A Dual Function for the Mitochondrial ATP Synthase*. *Circ. Res.* 2015; 116: 1850–1862.
- Berrisford JM, Sazanov LA. *Structural basis for the mechanism of respiratory complex I*. *J. Biol. Chem.* 2009; 284: 29773–29783.
- Birch-Machin MA, Shepherd IM, Watmough NJ, Sherratt HS, Bartlett K, Darley-Usmar VM, et al. *Fatal lactic acidosis in infancy with a defect of complex III of the respiratory chain*. *Pediatr. Res.* 1989; 25: 553–559.
- Blaza JN, Serreli R, Jones AJY, Mohammed K, Hirst J. *Kinetic evidence against partitioning of the ubiquinone pool and the catalytic relevance of respiratory-chain supercomplexes*. *Proc. Natl. Acad. Sci. U. S. A.* 2014; 111: 15735–15740.
- Bradford MM. *A rapid and sensitive method for the quantitation of microgram quantities of protein utilizing the principle of protein-dye binding*. *Anal. Biochem.* 1976; 72: 248–254.
- Bryan HK, Olayanju A, Goldring CE, Park BK. *The Nrf2 cell defence pathway: Keap1-dependent and -independent mechanisms of regulation*. *Biochem. Pharmacol.* 2013; 85: 705–717.
- Budde SM, van den Heuvel LP, Janssen AJ, Smeets RJ, Buskens CA, DeMeirleir L, et al. *Combined enzymatic complex I and III deficiency associated with mutations in the nuclear encoded NDUFS4 gene*. *Biochem. Biophys. Res. Commun.* 2000; 275: 63–68.
- Bultema JB, Braun H-P, Boekema EJ, Kouril R. *Megacomplex organization of the oxidative phosphorylation system by structural analysis of respiratory supercomplexes from potato*. *Biochim. Biophys. Acta* 2009; 1787: 60–67.
- Calvaruso MA, Willems P, van den Brand M, Valsecchi F, Kruse S, Palminter R, et al. *Mitochondrial complex III stabilizes complex I in the absence of NDUFS4 to provide partial activity*. *Hum. Mol. Genet.* 2012; 21: 115–120.
- Candas D, Li JJ. *MnSOD in oxidative stress response-potential regulation via mitochondrial protein influx*. *Antioxid. Redox Signal.* 2014; 20: 1599–1617.
- Carossa V, Ghelli A, Tropeano CV, Valentino ML, Iommarini L, Maresca A, et al. *A novel in-frame 18-bp microdeletion in MT-CYB causes a multisystem disorder with prominent exercise intolerance*. *Hum. Mutat.* 2014; 35: 954–958.
- Carroll J, Fearnley IM, Skehel JM, Shannon RJ, Hirst J, Walker JE. *Bovine complex I is a complex of 45 different subunits*. *J. Biol. Chem.* 2006; 281: 32724–32727.
- Chaban Y, Boekema EJ, Dudkina NV. *Structures of mitochondrial oxidative phosphorylation supercomplexes and mechanisms for their stabilisation*. *Biochim. Biophys. Acta* 2014; 1837: 418–426.
- Cha M-Y, Kim DK, Mook-Jung I. *The role of mitochondrial DNA mutation on neurodegenerative diseases*. *Exp. Mol. Med.* 2015; 47: e150.
- Chance B, Williams GR. *A method for the localization of sites for oxidative phosphorylation*. *Nature* 1955; 176: 250–254.
- Chen C, Ko Y, Delannoy M, Ludtke SJ, Chiu W, Pedersen PL. *Mitochondrial ATP synthasome: three-dimensional structure by electron microscopy of the ATP synthase in complex formation with carriers for Pi and ADP/ATP*. *J. Biol. Chem.* 2004; 279: 31761–31768.

- Chen C, Saxena AK, Simcoke WN, Garboczi DN, Pedersen PL, Ko YH. *Mitochondrial ATP synthase. Crystal structure of the catalytic F1 unit in a vanadate-induced transition-like state and implications for mechanism.* J. Biol. Chem. 2006; 281: 13777–13783.
- Chen Y-C, Taylor EB, Dephoure N, Heo J-M, Tonhato A, Papandreou I, et al. *Identification of a protein mediating respiratory supercomplex stability.* Cell Metab. 2012; 15: 348–360.
- Chinnery PF, Hudson G. *Mitochondrial genetics.* Br. Med. Bull. 2013; 106: 135–159.
- Cimen H, Han M-J, Yang Y, Tong Q, Koc H, Koc EC. *Regulation of succinate dehydrogenase activity by SIRT3 in mammalian mitochondria.* Biochemistry (Mosc.) 2010; 49: 304–311.
- Clayton DA. *Replication of animal mitochondrial DNA.* Cell 1982; 28: 693–705.
- Crofts AR, Guergova-Kuras M, Kuras R, Ugulava N, Li J, Hong S. *Proton-coupled electron transfer at the Q(o) site: what type of mechanism can account for the high activation barrier?* Biochim. Biophys. Acta 2000; 1459: 456–466.
- Cui T-Z, Smith PM, Fox JL, Khalimonchuk O, Winge DR. *Late-stage maturation of the Rieske Fe/S protein: Mxm1 stabilizes Rip1 but does not facilitate its translocation by the AAA ATPase Bcs1.* Mol. Cell. Biol. 2012; 32: 4400–4409.
- Dan Dunn J, Alvarez LA, Zhang X, Soldati T. *Reactive oxygen species and mitochondria: A nexus of cellular homeostasis.* Redox Biol. 2015; 6: 472–485.
- Darley-Usmar VM, Kennaway NG, Buist NR, Capaldi RA. *Deficiency in ubiquinone cytochrome c reductase in a patient with mitochondrial myopathy and lactic acidosis.* Proc. Natl. Acad. Sci. U. S. A. 1983; 80: 5103–5106.
- Dasgupta S, Hoque MO, Upadhyay S, Sidransky D. *Mitochondrial cytochrome B gene mutation promotes tumor growth in bladder cancer.* Cancer Res. 2008; 68: 700–706.
- D'Aurelio M, Gajewski CD, Lenaz G, Manfredi G. *Respiratory chain supercomplexes set the threshold for respiration defects in human mtDNA mutant cybrids.* Hum. Mol. Genet. 2006; 15: 2157–2169.
- Davies KM, Daum B, Gold VAM, Mühleip AW, Brandt T, Blum TB, et al. *Visualization of ATP synthase dimers in mitochondria by electron cryo-tomography.* J. Vis. Exp. JoVE 2014: 51228.
- Diaz F, Enriquez JA, Moraes CT. *Cells Lacking Rieske Iron-Sulfur Protein Have a Reactive Oxygen Species-Associated Decrease in Respiratory Complexes I and IV.* Mol. Cell. Biol. 2012; 32: 415–429.
- Diaz F, Fukui H, Garcia S, Moraes CT. *Cytochrome c oxidase is required for the assembly/stability of respiratory complex I in mouse fibroblasts.* Mol. Cell. Biol. 2006; 26: 4872–4881.
- Diaz F, Garcia S, Padgett KR, Moraes CT. *A defect in the mitochondrial complex III, but not complex IV, triggers early ROS-dependent damage in defined brain regions.* Hum. Mol. Genet. 2012; 21: 5066–5077.
- Dibrov E, Fu S, Lemire BD. *The Saccharomyces cerevisiae TCM62 gene encodes a chaperone necessary for the assembly of the mitochondrial succinate dehydrogenase (complex II).* J. Biol. Chem. 1998; 273: 32042–32048.
- Dröse S, Brandt U. *The mechanism of mitochondrial superoxide production by the cytochrome bc1 complex.* J. Biol. Chem. 2008; 283: 21649–21654.
- Dudkina NV, Eubel H, Keegstra W, Boekema EJ, Braun H-P. *Structure of a mitochondrial supercomplex formed by respiratory-chain complexes I and III.* Proc. Natl. Acad. Sci. U. S. A. 2005; 102: 3225–3229.

- Dudkina NV, Heinemeyer J, Keegstra W, Boekema EJ, Braun H-P. *Structure of dimeric ATP synthase from mitochondria: an angular association of monomers induces the strong curvature of the inner membrane*. FEBS Lett. 2005; 579: 5769–5772.
- Dudkina NV, Heinemeyer J, Sunderhaus S, Boekema EJ, Braun H-P. *Respiratory chain supercomplexes in the plant mitochondrial membrane*. Trends Plant Sci. 2006; 11: 232–240.
- Dudkina NV, Kudryashev M, Stahlberg H, Boekema EJ. *Interaction of complexes I, III, and IV within the bovine respirasome by single particle cryoelectron tomography*. Proc. Natl. Acad. Sci. U. S. A. 2011; 108: 15196–15200.
- Dudkina NV, Sunderhaus S, Braun H-P, Boekema EJ. *Characterization of dimeric ATP synthase and cristae membrane ultrastructure from Saccharomyces and Polytomella mitochondria*. FEBS Lett. 2006; 580: 3427–3432.
- Efremov RG, Baradaran R, Sazanov LA. *The architecture of respiratory complex I*. Nature 2010; 465: 441–445.
- Efremov RG, Sazanov LA. *Structure of the membrane domain of respiratory complex I*. Nature 2011; 476: 414–420.
- Efremov RG, Sazanov LA. *The coupling mechanism of respiratory complex I - a structural and evolutionary perspective*. Biochim. Biophys. Acta 2012; 1817: 1785–1795.
- Enriquez JA, Lenaz G. *Coenzyme q and the respiratory chain: coenzyme q pool and mitochondrial supercomplexes*. Mol. Syndromol. 2014; 5: 119–140.
- Esterházy D, King MS, Yakovlev G, Hirst J. *Production of reactive oxygen species by complex I (NADH:ubiquinone oxidoreductase) from Escherichia coli and comparison to the enzyme from mitochondria*. Biochemistry (Mosc.) 2008; 47: 3964–3971.
- Eubel H, Heinemeyer J, Braun H-P. *Identification and characterization of respirasomes in potato mitochondria*. Plant Physiol. 2004; 134: 1450–1459.
- Evans DR, Guy HI. *Mammalian pyrimidine biosynthesis: fresh insights into an ancient pathway*. J. Biol. Chem. 2004; 279: 33035–33038.
- Fato R, Bergamini C, Bortolus M, Maniero AL, Leoni S, Ohnishi T, et al. *Differential effects of mitochondrial Complex I inhibitors on production of reactive oxygen species*. Biochim. Biophys. Acta 2009; 1787: 384–392.
- Fernández-Vizarra E, Zeviani M. *Nuclear gene mutations as the cause of mitochondrial complex III deficiency*. Front. Genet. 2015; 6.
- Ferreira A, Serafim TL, Sardão VA, Cunha-Oliveira T. *Role of mtDNA-related mitoeigenetic phenomena in cancer*. Eur. J. Clin. Invest. 2015; 45 Suppl 1: 44–49.
- Finkel T, Menazza S, Holmström KM, Parks RJ, Liu J, Sun J, et al. *The ins and outs of mitochondrial calcium*. Circ. Res. 2015; 116: 1810–1819.
- Finley L, Haas W, Desquiret-Dumas V, Wallace DC, Procaccio V, Gygi S, et al. *Succinate dehydrogenase is a direct target of sirtuin 3 deacetylase activity*. PLoS One 2011; 6: e23295.
- Floreani M, Petrone M, Debetto P, Palatini P. *A comparison between different methods for the determination of reduced and oxidized glutathione in mammalian tissues*. Free Radic. Res. 1997; 26: 449–455.
- Fontanesi F, Soto IC, Horn D, Barrientos A. *Assembly of mitochondrial cytochrome c-oxidase, a complicated and highly regulated cellular process*. Am. J. Physiol. Cell Physiol. 2006; 291: C1129–1147.

- Fragaki K, Procaccio V, Bannwarth S, Serre V, O'Hearn S, Potluri P, et al. *A neonatal polyvisceral failure linked to a de novo homoplasmic mutation in the mitochondrially encoded cytochrome b gene*. *Mitochondrion* 2009; 9: 346–352.
- Futai M, Nakanishi-Matsui M, Okamoto H, Sekiya M, Nakamoto RK. *Rotational catalysis in proton pumping ATPases: from E. coli F-ATPase to mammalian V-ATPase*. *Biochim. Biophys. Acta* 2012; 1817: 1711–1721.
- Gaignard P, Menezes M, Schiff M, Bayot A, Rak M, Ogier de Baulny H, et al. *Mutations in CYC1, encoding cytochrome c1 subunit of respiratory chain complex III, cause insulin-responsive hyperglycemia*. *Am. J. Hum. Genet.* 2013; 93: 384–389.
- Gao X, Wen X, Esser L, Quinn B, Yu L, Yu C-A, et al. *Structural Basis for the Quinone Reduction in the bc1 Complex: A Comparative Analysis of Crystal Structures of Mitochondrial Cytochrome bc1 with Bound Substrate and Inhibitors at the Qi Site†,‡*. *Biochemistry (Mosc.)* 2003; 42: 9067–9080.
- Genova ML, Lenaz G. *Functional role of mitochondrial respiratory supercomplexes*. *Biochim. Biophys. Acta* 2014; 1837: 427–443.
- Genova ML, Lenaz G. *The Interplay Between Respiratory Supercomplexes and ROS in Aging*. *Antioxid. Redox Signal.* 2015; 23: 208–238.
- Ghelli A, Tropeano CV, Calvaruso MA, Marchesini A, Iommarini L, Porcelli AM, et al. *The cytochrome b p.278Y>C mutation causative of a multisystem disorder enhances superoxide production and alters supramolecular interactions of respiratory chain complexes*. *Hum. Mol. Genet.* 2013; 22: 2141–2151.
- Ghelli A, Tropeano CV, Rugolo M. *Mitochondrial Respiratory Supercomplexes in Physiology and Diseases in 'Redox Proteins in Supercomplexes and Signalosomes'*. R.O. Louro and I. Diaz-Moreno Eds, CRC Press, Taylor & Francis Group; 2015.
- Ghezzi D, Arzuffi P, Zordan M, Da Re C, Lamperti C, Benna C, et al. *Mutations in TTC19 cause mitochondrial complex III deficiency and neurological impairment in humans and flies*. *Nat. Genet.* 2011; 43: 259–263.
- Ghezzi D, Goffrini P, Uziel G, Horvath R, Klopstock T, Lochmüller H, et al. *SDHAF1, encoding a LYR complex-II specific assembly factor, is mutated in SDH-defective infantile leukoencephalopathy*. *Nat. Genet.* 2009; 41: 654–656.
- Gibbons C, Montgomery MG, Leslie AG, Walker JE. *The structure of the central stalk in bovine F(1)-ATPase at 2.4 Å resolution*. *Nat. Struct. Biol.* 2000; 7: 1055–1061.
- Giorgio V, Petronilli V, Ghelli A, Carelli V, Rugolo M, Lenaz G, et al. *The effects of idebenone on mitochondrial bioenergetics*. *Biochim. Biophys. Acta* 2012; 1817: 363–369.
- Giorgio V, von Stockum S, Antoniel M, Fabbro A, Fogolari F, Forte M, et al. *Dimers of mitochondrial ATP synthase form the permeability transition pore*. *Proc. Natl. Acad. Sci. U. S. A.* 2013; 110: 5887–5892.
- Gorman GS, Schaefer AM, Ng Y, Gomez N, Blakely EL, Alston CL, et al. *Prevalence of nuclear and mitochondrial DNA mutations related to adult mitochondrial disease*. *Ann. Neurol.* 2015; 77: 753–759.
- Gruschke S, Kehrein K, Römpler K, Gröne K, Israel L, Imhof A, et al. *Cbp3-Cbp6 interacts with the yeast mitochondrial ribosomal tunnel exit and promotes cytochrome b synthesis and assembly*. *J. Cell Biol.* 2011; 193: 1101–1114.
- Gruschke S, Römpler K, Hildenbeutel M, Kehrein K, Kühl I, Bonnefoy N, et al. *The Cbp3-Cbp6 complex coordinates cytochrome b synthesis with bc(1) complex assembly in yeast mitochondria*. *J. Cell Biol.* 2012; 199: 137–150.

- Hackenbrock CR, Chazotte B, Gupte SS. *The random collision model and a critical assessment of diffusion and collision in mitochondrial electron transport*. J. Bioenerg. Biomembr. 1986; 18: 331–368.
- Hamanaka RB, Chandel NS. *Mitochondrial reactive oxygen species regulate cellular signaling and dictate biological outcomes*. Trends Biochem. Sci. 2010; 35: 505–513.
- Hansen JM, Go Y-M, Jones DP. *Nuclear and mitochondrial compartmentation of oxidative stress and redox signaling*. Annu. Rev. Pharmacol. Toxicol. 2006; 46: 215–234.
- Hao H-X, Khalimonchuk O, Schraders M, Dephoure N, Bayley J-P, Kunst H, et al. *SDH5, a gene required for flavination of succinate dehydrogenase, is mutated in paraganglioma*. Science 2009; 325: 1139–1142.
- Harner M, Körner C, Walther D, Mokranjac D, Kaesmacher J, Welsch U, et al. *The mitochondrial contact site complex, a determinant of mitochondrial architecture*. EMBO J. 2011; 30: 4356–4370.
- Hatefi Y, Haavik AG, Griffiths DE. *Studies on the electron transfer system. XL. Preparation and properties of mitochondrial DPNH-coenzyme Q reductase*. J. Biol. Chem. 1962; 237: 1676–1680.
- Hatle KM, Gummadijala P, Navasa N, Bernardo E, Dodge J, Silverstrim B, et al. *MCJ/DnaJC15, an endogenous mitochondrial repressor of the respiratory chain that controls metabolic alterations*. Mol. Cell. Biol. 2013; 33: 2302–2314.
- Haut S, Brivet M, Touati G, Rustin P, Lebon S, Garcia-Cazorla A, et al. *A deletion in the human QP-C gene causes a complex III deficiency resulting in hypoglycaemia and lactic acidosis*. Hum. Genet. 2003; 113: 118–122.
- Hayes DJ, Lecky BR, Landon DN, Morgan-Hughes JA, Clark JB. *A new mitochondrial myopathy. Biochemical studies revealing a deficiency in the cytochrome b-c1 complex (complex III) of the respiratory chain*. Brain J. Neurol. 1984; 107 ( Pt 4): 1165–1177.
- Heinemeyer J, Braun H-P, Boekema EJ, Kouril R. *A structural model of the cytochrome C reductase/oxidase supercomplex from yeast mitochondria*. J. Biol. Chem. 2007; 282: 12240–12248.
- Her YF, Maher LJ. *Succinate Dehydrogenase Loss in Familial Paraganglioma: Biochemistry, Genetics, and Epigenetics*. Int. J. Endocrinol. 2015; 2015: 296167.
- Hildenbeutel M, Hegg EL, Stephan K, Gruschke S, Meunier B, Ott M. *Assembly factors monitor sequential hemylation of cytochrome b to regulate mitochondrial translation*. J. Cell Biol. 2014; 205: 511–524.
- Hirst J. *Mitochondrial complex I*. Annu. Rev. Biochem. 2013; 82: 551–575.
- Hirst J, King MS, Pryde KR. *The production of reactive oxygen species by complex I*. Biochem. Soc. Trans. 2008; 36: 976–980.
- Holland R, Fishbein JC. *Chemistry of the cysteine sensors in Kelch-like ECH-associated protein 1*. Antioxid. Redox Signal. 2010; 13: 1749–1761.
- Holt IJ, Harding AE, Morgan-Hughes JA. *Deletions of muscle mitochondrial DNA in patients with mitochondrial myopathies*. Nature 1988; 331: 717–719.
- Holt IJ, Lorimer HE, Jacobs HT. *Coupled leading- and lagging-strand synthesis of mammalian mitochondrial DNA*. Cell 2000; 100: 515–524.
- Horan S, Bourges I, Taanman J-W, Meunier B. *Analysis of COX2 mutants reveals cytochrome oxidase subassemblies in yeast*. Biochem. J. 2005; 390: 703–708.
- Invernizzi F, Tigano M, Dallabona C, Donnini C, Ferrero I, Cremonese M, et al. *A homozygous mutation in LYRM7/MZM1L associated with early onset encephalopathy, lactic*

- acidosis, and severe reduction of mitochondrial complex III activity.* Hum. Mutat. 2013; 34: 1619–1622.
- Iwata S, Lee JW, Okada K, Lee JK, Iwata M, Rasmussen B, et al. *Complete structure of the 11-subunit bovine mitochondrial cytochrome bc<sub>1</sub> complex.* Science 1998; 281: 64–71.
- Jezeq P, Hlavatá L. *Mitochondria in homeostasis of reactive oxygen species in cell, tissues, and organism.* Int. J. Biochem. Cell Biol. 2005; 37: 2478–2503.
- Kadenbach B, Hüttemann M. *The subunit composition and function of mammalian cytochrome c oxidase.* Mitochondrion 2015; 24: 64–76.
- Karrasch S, Walker JE. *Novel features in the structure of bovine ATP synthase.* J. Mol. Biol. 1999; 290: 379–384.
- Keogh MJ, Chinnery PF. *Mitochondrial DNA mutations in neurodegeneration.* Biochim. Biophys. Acta 2015; 1847: 1401–1411.
- King MP, Attardi G. *Isolation of human cell lines lacking mitochondrial DNA.* Methods Enzymol. 1996; 264: 304–313.
- Krause F, Reifschneider NH, Vocke D, Seelert H, Rexroth S, Dencher NA. *'Respirasome'-like supercomplexes in green leaf mitochondria of spinach.* J. Biol. Chem. 2004; 279: 48369–48375.
- Kühlbrandt W. *Structure and function of mitochondrial membrane protein complexes.* BMC Biol. 2015; 13: 89.
- Kukat C, Davies KM, Wurm CA, Spähr H, Bonekamp NA, Kühl I, et al. *Cross-strand binding of TFAM to a single mtDNA molecule forms the mitochondrial nucleoid.* Proc. Natl. Acad. Sci. U. S. A. 2015; 112: 11288–11293.
- Kurelac I, Lang M, Zuntini R, Calabrese C, Simone D, Vicario S, et al. *Searching for a needle in the haystack: comparing six methods to evaluate heteroplasmy in difficult sequence context.* Biotechnol. Adv. 2012; 30: 363–371.
- Lackner LL. *Shaping the dynamic mitochondrial network.* BMC Biol. 2014; 12: 35.
- Lanciano P, Khalfaoui-Hassani B, Selamoglu N, Ghelli A, Rugolo M, Daldal F. *Molecular mechanisms of superoxide production by complex III: a bacterial versus human mitochondrial comparative case study.* Biochim. Biophys. Acta 2013; 1827: 1332–1339.
- Lapunte-Brun E, Moreno-Loshuertos R, Acín-Pérez R, Latorre-Pellicer A, Colás C, Balsa E, et al. *Supercomplex assembly determines electron flux in the mitochondrial electron transport chain.* Science 2013; 340: 1567–1570.
- Lee D-W, Selamoglu N, Lanciano P, Cooley JW, Forquer I, Kramer DM, et al. *Loss of a conserved tyrosine residue of cytochrome b induces reactive oxygen species production by cytochrome bc<sub>1</sub>.* J. Biol. Chem. 2011; 286: 18139–18148.
- Lenaz G. *Mitochondria and reactive oxygen species. Which role in physiology and pathology?* Adv. Exp. Med. Biol. 2012; 942: 93–136.
- Lenaz G, Genova ML. *Structure and organization of mitochondrial respiratory complexes: a new understanding of an old subject.* Antioxid. Redox Signal. 2010; 12: 961–1008.
- Letts JA, Sazanov LA. *Gaining mass: the structure of respiratory complex I-from bacterial towards mitochondrial versions.* Curr. Opin. Struct. Biol. 2015; 33: 135–145.
- Lightowlers RN, Taylor RW, Turnbull DM. *Mutations causing mitochondrial disease: What is new and what challenges remain?* Science 2015; 349: 1494–1499.

- Li Y, D'Aurelio M, Deng J-H, Park J-S, Manfredi G, Hu P, et al. *An assembled complex IV maintains the stability and activity of complex I in mammalian mitochondria*. J. Biol. Chem. 2007; 282: 17557–17562.
- Long Q, Yang K, Yang Q. *Regulation of mitochondrial ATP synthase in cardiac pathophysiology*. Am. J. Cardiovasc. Dis. 2015; 5: 19–32.
- de Lonlay P, Valnot I, Barrientos A, Gorbatyuk M, Tzagoloff A, Taanman JW, et al. *A mutant mitochondrial respiratory chain assembly protein causes complex III deficiency in patients with tubulopathy, encephalopathy and liver failure*. Nat. Genet. 2001; 29: 57–60.
- Lopez J, Tait SWG. *Mitochondrial apoptosis: killing cancer using the enemy within*. Br. J. Cancer 2015; 112: 957–962.
- Manfredi G, Yang L, Gajewski CD, Mattiazzi M. *Measurements of ATP in mammalian cells*. Methods San Diego Calif 2002; 26: 317–326.
- Maranzana E, Barbero G, Falasca AI, Lenaz G, Genova ML. *Mitochondrial respiratory supercomplex association limits production of reactive oxygen species from complex I*. Antioxid. Redox Signal. 2013; 19: 1469–1480.
- Margulis L. *Origin of Eukaryotic Cells*. Yale Univ Press N. Hav. CT 1970
- Marques I, Dencher NA, Videira A, Krause F. *Supramolecular organization of the respiratory chain in Neurospora crassa mitochondria*. Eukaryot. Cell 2007; 6: 2391–2405.
- Mather MW, Darrouzet E, Valkova-Valchanova M, Cooley JW, McIntosh MT, Daldal F, et al. *Uncovering the molecular mode of action of the antimalarial drug atovaquone using a bacterial system*. J. Biol. Chem. 2005; 280: 27458–27465.
- Mckenzie M, Ryan MT. *Assembly factors of human mitochondrial complex I and their defects in disease*. IUBMB Life 2010; 62: 497–502.
- McKinney EA, Oliveira MT. *Replicating animal mitochondrial DNA*. Genet. Mol. Biol. 2013; 36: 308–315.
- Meunier B, Fisher N, Ransac S, Mazat J-P, Bresseur G. *Respiratory complex III dysfunction in humans and the use of yeast as a model organism to study mitochondrial myopathy and associated diseases*. Biochim. Biophys. Acta 2013; 1827: 1346–1361.
- Mick DU, Fox TD, Rehling P. *Inventory control: cytochrome c oxidase assembly regulates mitochondrial translation*. Nat. Rev. Mol. Cell Biol. 2011; 12: 14–20.
- Mimaki M, Wang X, McKenzie M, Thorburn DR, Ryan MT. *Understanding mitochondrial complex I assembly in health and disease*. Biochim. Biophys. Acta 2012; 1817: 851–862.
- Mishra P, Chan DC. *Mitochondrial dynamics and inheritance during cell division, development and disease*. Nat. Rev. Mol. Cell Biol. 2014; 15: 634–646.
- Mitchell P. *Coupling of phosphorylation to electron and hydrogen transfer by a chemi-osmotic type of mechanism*. Nature 1961; 191: 144–148.
- Mitchell P. *Possible molecular mechanisms of the protonmotive function of cytochrome systems*. J. Theor. Biol. 1976; 62: 327–367.
- Miyake N, Yano S, Sakai C, Hatakeyama H, Matsushima Y, Shiina M, et al. *Mitochondrial complex III deficiency caused by a homozygous UQCRC2 mutation presenting with neonatal-onset recurrent metabolic decompensation*. Hum. Mutat. 2013; 34: 446–452.
- Moreno-Lastres D, Fontanesi F, García-Consuegra I, Martín MA, Arenas J, Barrientos A, et al. *Mitochondrial complex I plays an essential role in human respirasome assembly*. Cell Metab. 2012; 15: 324–335.

- Moreno-Sánchez R, Hernández-Esquivel L, Rivero-Segura NA, Marín-Hernández A, Neuzil J, Ralph SJ, et al. *Reactive oxygen species are generated by the respiratory complex II--evidence for lack of contribution of the reverse electron flow in complex I*. FEBS J. 2013; 280: 927–938.
- Morgan-Hughes JA, Hayes DJ, Clark JB, Landon DN, Swash M, Stark RJ, et al. *Mitochondrial encephalomyopathies: biochemical studies in two cases revealing defects in the respiratory chain*. Brain J. Neurol. 1982; 105 (Pt 3): 553–582.
- Mullen AR, Hu Z, Shi X, Jiang L, Boroughs LK, Kovacs Z, et al. *Oxidation of Alpha-Ketoglutarate Is Required for Reductive Carboxylation in Cancer Cells with Mitochondrial Defects*. Cell Rep. 2014; 7: 1679–1690.
- Nath S, Villadsen J. *Oxidative phosphorylation revisited*. Biotechnol. Bioeng. 2015; 112: 429–437.
- Na U, Yu W, Cox J, Bricker DK, Brockmann K, Rutter J, et al. *The LYR factors SDHAF1 and SDHAF3 mediate maturation of the iron-sulfur subunit of succinate dehydrogenase*. Cell Metab. 2014; 20: 253–266.
- Nijtmans LGJ, Henderson NS, Holt IJ. *Blue Native electrophoresis to study mitochondrial and other protein complexes*. Methods San Diego Calif 2002; 26: 327–334.
- Nijtmans LG, Taanman JW, Muijsers AO, Speijer D, Van den Bogert C. *Assembly of cytochrome-c oxidase in cultured human cells*. Eur. J. Biochem. FEBS 1998; 254: 389–394.
- Noji H, Yasuda R, Yoshida M, Kinosita K. *Direct observation of the rotation of F1-ATPase*. Nature 1997; 386: 299–302.
- Ohnishi ST, Ohnishi T, Muranaka S, Fujita H, Kimura H, Uemura K, et al. *A possible site of superoxide generation in the complex I segment of rat heart mitochondria*. J. Bioenerg. Biomembr. 2005; 37: 1–15.
- Page CC, Moser CC, Chen X, Dutton PL. *Natural engineering principles of electron tunnelling in biological oxidation-reduction*. Nature 1999; 402: 47–52.
- Park CB, Larsson N-G. *Mitochondrial DNA mutations in disease and aging*. J. Cell Biol. 2011; 193: 809–818.
- Park J, Chen Y, Tishkoff DX, Peng C, Tan M, Dai L, et al. *SIRT5-mediated lysine desuccinylation impacts diverse metabolic pathways*. Mol. Cell 2013; 50: 919–930.
- Perales-Clemente E, Fernández-Vizarra E, Acín-Pérez R, Movilla N, Bayona-Bafaluy MP, Moreno-Loshuertos R, et al. *Five entry points of the mitochondrially encoded subunits in mammalian complex I assembly*. Mol. Cell. Biol. 2010; 30: 3038–3047.
- Peters K, Dudkina NV, Jänsch L, Braun H-P, Boekema EJ. *A structural investigation of complex I and I+III<sub>2</sub> supercomplex from Zea mays at 11-13 Å resolution: assignment of the carbonic anhydrase domain and evidence for structural heterogeneity within complex I*. Biochim. Biophys. Acta 2008; 1777: 84–93.
- Polyak K, Li Y, Zhu H, Lengauer C, Willson JK, Markowitz SD, et al. *Somatic mutations of the mitochondrial genome in human colorectal tumours*. Nat. Genet. 1998; 20: 291–293.
- Porcelli AM, Ghelli A, Ceccarelli C, Lang M, Cenacchi G, Capristo M, et al. *The genetic and metabolic signature of oncogenic transformation implicates HIF1alpha destabilization*. Hum. Mol. Genet. 2010; 19: 1019–1032.
- Porrás CA, Bai Y. *Respiratory supercomplexes: plasticity and implications*. Front. Biosci. Landmark Ed. 2015; 20: 621–634.

- Quinlan CL, Orr AL, Perevoshchikova IV, Treberg JR, Ackrell BA, Brand MD. *Mitochondrial complex II can generate reactive oxygen species at high rates in both the forward and reverse reactions*. J. Biol. Chem. 2012; 287: 27255–27264.
- van Raaij MJ, Abrahams JP, Leslie AG, Walker JE. *The structure of bovine F1-ATPase complexed with the antibiotic inhibitor aurovertin*. B. Proc. Natl. Acad. Sci. U. S. A. 1996; 93: 6913–6917.
- Rich PR, Maréchal A. *The mitochondrial respiratory chain*. Essays Biochem. 2010; 47: 1–23.
- Rizzuto R, De Stefani D, Raffaello A, Mammucari C. *Mitochondria as sensors and regulators of calcium signalling*. Nat. Rev. Mol. Cell Biol. 2012; 13: 566–578.
- Robinson AJ, Kunji ERS. *Mitochondrial carriers in the cytoplasmic state have a common substrate binding site*. Proc. Natl. Acad. Sci. U. S. A. 2006; 103: 2617–2622.
- Robinson BH. *Use of fibroblast and lymphoblast cultures for detection of respiratory chain defects*. Methods Enzymol. 1996; 264: 454–464.
- Rubinstein JL, Walker JE, Henderson R. *Structure of the mitochondrial ATP synthase by electron cryomicroscopy*. EMBO J. 2003; 22: 6182–6192.
- Salvi M, Brunati AM, Toninello A. *Tyrosine phosphorylation in mitochondria: A new frontier in mitochondrial signaling*. Free Radic. Biol. Med. 2005; 38: 1267–1277.
- Sarewicz M, Borek A, Cieluch E, Świerczek M, Osyczka A. *Discrimination between two possible reaction sequences that create potential risk of generation of deleterious radicals by cytochrome bc1*. Biochim. Biophys. Acta 2010; 1797: 1820–1827.
- Sazanov LA. *A giant molecular proton pump: structure and mechanism of respiratory complex I*. Nat. Rev. Mol. Cell Biol. 2015; 16: 375–388.
- Schägger H. *Respiratory chain supercomplexes of mitochondria and bacteria*. Biochim. Biophys. Acta 2002; 1555: 154–159.
- Schägger H, de Coo R, Bauer MF, Hofmann S, Godinot C, Brandt U. *Significance of respirasomes for the assembly/stability of human respiratory chain complex I*. J. Biol. Chem. 2004; 279: 36349–36353.
- Schägger H, Pfeiffer K. *Supercomplexes in the respiratory chains of yeast and mammalian mitochondria*. EMBO J. 2000; 19: 1777–1783.
- Schägger H, Pfeiffer K. *The ratio of oxidative phosphorylation complexes I–V in bovine heart mitochondria and the composition of respiratory chain supercomplexes*. J. Biol. Chem. 2001; 276: 37861–37867.
- Schon EA, DiMauro S, Hirano M. *Human mitochondrial DNA: roles of inherited and somatic mutations*. Nat. Rev. Genet. 2012; 13: 878–890.
- Seelert H, Dencher NA. *ATP synthase superassemblies in animals and plants: two or more are better*. Biochim. Biophys. Acta 2011; 1807: 1185–1197.
- Shadel GS, Horvath TL. *Mitochondrial ROS Signaling in Organismal Homeostasis*. Cell 2015; 163: 560–569.
- Skehan P, Storeng R, Scudiero D, Monks A, McMahon J, Vistica D, et al. *New colorimetric cytotoxicity assay for anticancer-drug screening*. J. Natl. Cancer Inst. 1990; 82: 1107–1112.
- Skladal D, Halliday J, Thorburn DR. *Minimum birth prevalence of mitochondrial respiratory chain disorders in children*. Brain J. Neurol. 2003; 126: 1905–1912.
- Smith PM, Fox JL, Winge DR. *Biogenesis of the cytochrome bc(1) complex and role of assembly factors*. Biochim. Biophys. Acta 2012; 1817: 276–286.
- Song I-S, Kim H-K, Jeong S-H, Lee S-R, Kim N, Rhee BD, et al. *Mitochondrial Peroxiredoxin III is a Potential Target for Cancer Therapy*. Int. J. Mol. Sci. 2011; 12: 7163–7185.

- Soto IC, Fontanesi F, Liu J, Barrientos A. *Biogenesis and assembly of eukaryotic cytochrome c oxidase catalytic core*. *Biochim. Biophys. Acta* 2012; 1817: 883–897.
- Spiro AJ, Moore CL, Prineas JW, Strasberg PM, Rapin I. *A cytochrome-related inherited disorder of the nervous system and muscle*. *Arch. Neurol.* 1970; 23: 103–112.
- Stehling O, Wilbrecht C, Lill R. *Mitochondrial iron-sulfur protein biogenesis and human disease*. *Biochimie* 2014; 100: 61–77.
- Sun F, Huo X, Zhai Y, Wang A, Xu J, Su D, et al. *Crystal structure of mitochondrial respiratory membrane protein complex II*. *Cell* 2005; 121: 1043–1057.
- Suthammarak W, Somerlot BH, Opheim E, Sedensky M, Morgan PG. *Novel interactions between mitochondrial superoxide dismutases and the electron transport chain*. *Aging Cell* 2013; 12: 1132–1140.
- Sutovsky P. *Ubiquitin-dependent proteolysis in mammalian spermatogenesis, fertilization, and sperm quality control: killing three birds with one stone*. *Microsc. Res. Tech.* 2003; 61: 88–102.
- Szalárdy L, Zádori D, Klivényi P, Toldi J, Vécsei L. *Electron Transport Disturbances and Neurodegeneration: From Albert Szent-Györgyi's Concept (Szeged) till Novel Approaches to Boost Mitochondrial Bioenergetics*. *Oxid. Med. Cell. Longev.* 2015; 2015: 498401.
- Taiwo F. *Mechanism of tiron as scavenger of superoxide ions and free electrons*. *Spectroscopy* 2008; 22: 491–498.
- Tomitsuka E, Kita K, Esumi H. *Regulation of succinate-ubiquinone reductase and fumarate reductase activities in human complex II by phosphorylation of its flavoprotein subunit*. *Proc. Jpn. Acad. Ser. B Phys. Biol. Sci.* 2009; 85: 258–265.
- Trounce IA, Kim YL, Jun AS, Wallace DC. *Assessment of mitochondrial oxidative phosphorylation in patient muscle biopsies, lymphoblasts, and transmitochondrial cell lines*. *Methods Enzymol.* 1996; 264: 484–509.
- Tsukihara T, Aoyama H, Yamashita E, Tomizaki T, Yamaguchi H, Shinzawa-Itoh K, et al. *The whole structure of the 13-subunit oxidized cytochrome c oxidase at 2.8 Å*. *Science* 1996; 272: 1136–1144.
- Tucker EJ, Wanschers BFJ, Szklarczyk R, Mountford HS, Wijeyeratne XW, van den Brand MAM, et al. *Mutations in the UQCC1-interacting protein, UQCC2, cause human complex III deficiency associated with perturbed cytochrome b protein expression*. *PLoS Genet.* 2013; 9: e1004034.
- Tuppen HAL, Blakely EL, Turnbull DM, Taylor RW. *Mitochondrial DNA mutations and human disease*. *Biochim. Biophys. Acta* 2010; 1797: 113–128.
- Uhler JP, Falkenberg M. *Primer removal during mammalian mitochondrial DNA replication*. *DNA Repair* 2015; 34: 28–38.
- Van Vranken JG, Bricker DK, Dephoure N, Gygi SP, Cox JE, Thummel CS, et al. *SDHAF4 promotes mitochondrial succinate dehydrogenase activity and prevents neurodegeneration*. *Cell Metab.* 2014; 20: 241–252.
- Vartak R, Porras CA-M, Bai Y. *Respiratory supercomplexes: structure, function and assembly*. *Protein Cell* 2013; 4: 582–590.
- Velours J, Dautant A, Salin B, Sagot I, Brèthes D. *Mitochondrial F1F0-ATP synthase and organellar internal architecture*. *Int. J. Biochem. Cell Biol.* 2009; 41: 1783–1789.
- Vinogradov AD. *Catalytic properties of the mitochondrial NADH-ubiquinone oxidoreductase (complex I) and the pseudo-reversible active/inactive enzyme transition*. *Biochim. Biophys. Acta* 1998; 1364: 169–185.

- Vinothkumar KR, Zhu J, Hirst J. *Architecture of mammalian respiratory complex I*. Nature 2014a; 515: 80–84.
- Vinothkumar KR, Zhu J, Hirst J. *Architecture of mammalian respiratory complex I*. Nature 2014b; 515: 80–84.
- Vishal-Tandon M, Gupta B, Tandon R. *Free radicals/Reactive oxygen species*. JK Pract. 2005; 12: 143–148.
- Vukotic M, Oeljeklaus S, Wiese S, Vögtle FN, Meisinger C, Meyer HE, et al. *Rcf1 mediates cytochrome oxidase assembly and respirasome formation, revealing heterogeneity of the enzyme complex*. Cell Metab. 2012; 15: 336–347.
- Walker JE. *The ATP synthase: the understood, the uncertain and the unknown*. Biochem. Soc. Trans. 2013; 41: 1–16.
- Wallace DC. *Report of the committee on human mitochondrial DNA*. Cytogenet. Cell Genet. 1989; 51: 612–621.
- Wallace DC, Fan W. *Energetics, epigenetics, mitochondrial genetics*. Mitochondrion 2010; 10: 12–31.
- Wallace DC, Singh G, Lott MT, Hodge JA, Schurr TG, Lezza AM, et al. *Mitochondrial DNA mutation associated with Leber's hereditary optic neuropathy*. Science 1988; 242: 1427–1430.
- Wanschers BFJ, Szklarczyk R, van den Brand MAM, Jonckheere A, Suijskens J, Smeets R, et al. *A mutation in the human CBP4 ortholog UQCC3 impairs complex III assembly, activity and cytochrome b stability*. Hum. Mol. Genet. 2014; 23: 6356–6365.
- Weinberg SE, Sena LA, Chandel NS. *Mitochondria in the regulation of innate and adaptive immunity*. Immunity 2015; 42: 406–417.
- Wibrand F, Ravn K, Schwartz M, Rosenberg T, Horn N, Vissing J. *Multisystem disorder associated with a missense mutation in the mitochondrial cytochrome b gene*. Ann. Neurol. 2001; 50: 540–543.
- Williams SL, Valnot I, Rustin P, Taanman J-W. *Cytochrome c oxidase subassemblies in fibroblast cultures from patients carrying mutations in COX10, SCO1, or SURF1*. J. Biol. Chem. 2004; 279: 7462–7469.
- Wittig I, Karas M, Schägger H. *High resolution clear native electrophoresis for in-gel functional assays and fluorescence studies of membrane protein complexes*. Mol. Cell. Proteomics MCP 2007; 6: 1215–1225.
- Wittig I, Schägger H. *Features and applications of blue-native and clear-native electrophoresis*. Proteomics 2008; 8: 3974–3990.
- Xia D, Esser L, Tang W-K, Zhou F, Zhou Y, Yu L, et al. *Structural analysis of cytochrome bc1 complexes: implications to the mechanism of function*. Biochim. Biophys. Acta 2013; 1827: 1278–1294.
- Xia D, Yu CA, Kim H, Xia JZ, Kachurin AM, Zhang L, et al. *Crystal structure of the cytochrome bc1 complex from bovine heart mitochondria*. Science 1997; 277: 60–66.
- Yamashita T, Voth GA. *Insights into the mechanism of proton transport in cytochrome c oxidase*. J. Am. Chem. Soc. 2012; 134: 1147–1152.
- Yasukawa T, Reyes A, Cluett TJ, Yang M-Y, Bowmaker M, Jacobs HT, et al. *Replication of vertebrate mitochondrial DNA entails transient ribonucleotide incorporation throughout the lagging strand*. EMBO J. 2006; 25: 5358–5371.
- Yoshikawa S, Muramoto K, Shinzawa-Itoh K. *Reaction mechanism of mammalian mitochondrial cytochrome c oxidase*. Adv. Exp. Med. Biol. 2012; 748: 215–236.

- Yoshikawa S, Shimada A. *Reaction Mechanism of Cytochrome c Oxidase*. Chem. Rev. 2015; 115: 1936–1989.
- Yusoff AAM, Ahmad F, Idris Z, Jaafar H, Abdullah JM. *Understanding Mitochondrial DNA in Brain Tumorigenesis*. In: Lichtor T, editor(s). *Molecular Considerations and Evolving Surgical Management Issues in the Treatment of Patients with a Brain Tumor*. InTech; 2015.
- Zara V, Conte L, Trumpower BL. *Identification and characterization of cytochrome bc(1) subcomplexes in mitochondria from yeast with single and double deletions of genes encoding cytochrome bc(1) subunits*. FEBS J. 2007; 274: 4526–4539.
- Zara V, Conte L, Trumpower BL. *Biogenesis of the yeast cytochrome bc1 complex*. Biochim. Biophys. Acta 2009a; 1793: 89–96.
- Zara V, Conte L, Trumpower BL. *Evidence that the assembly of the yeast cytochrome bc1 complex involves the formation of a large core structure in the inner mitochondrial membrane*. FEBS J. 2009b; 276: 1900–1914.
- Zickermann V, Wirth C, Nasiri H, Siegmund K, Schwalbe H, Hunte C, et al. *Structural biology. Mechanistic insight from the crystal structure of mitochondrial complex I*. Science 2015; 347: 44–49.